The Reciprocal Sliding Wear Behavior of SiC Particulate Reinforced Aluminum Composite

by

Zhencheng Feng

A Thesis

Submitted to the University of Manitoba

in fulfillment of the

thesis requirement for the degree of

MASTER OF SCIENCE

in

Mechanical and Industrial Engineering

Winnipeg, Manitoba, Canada

National Library
of Canada

Acquisitions and
Bibliographic Services Branch

395 Wellington Street
Ottawa, Ontario
K1A 0N4

Bibliothèque nationale
du Canada

Direction des acquisitions et
des services bibliographiques

395, rue Wellington
Ottawa (Ontario)
K1A 0N4

Your file Votre référence

Our file Notre référence

ISBN 0-612-13120-3

Canada

Name _____

Dissertation Abstracts International is arranged by broad, general subject categories. Please select the one subject which most nearly describes the content of your dissertation. Enter the corresponding four-digit code in the spaces provided.

Materials Science

SUBJECT TERM

0794

SUBJECT CODE

U·M·I

Subject Categories

THE HUMANITIES AND SOCIAL SCIENCES

COMMUNICATIONS AND THE ARTS

- Architecture 0729
- Art History 0377
- Cinema 0900
- Dance 0378
- Fine Arts 0357
- Information Science 0723
- Journalism 0391
- Library Science 0399
- Mass Communications 0708
- Music 0413
- Speech Communication 0459
- Theater 0465

EDUCATION

- General 0515
- Administration 0514
- Adult and Continuing 0516
- Agricultural 0517
- Art 0273
- Bilingual and Multicultural 0282
- Business 0688
- Community College 0275
- Curriculum and Instruction 0727
- Early Childhood 0518
- Elementary 0524
- Finance 0277
- Guidance and Counseling 0519
- Health 0680
- Higher 0745
- History of 0520
- Home Economics 0278
- Industrial 0521
- Language and Literature 0279
- Mathematics 0280
- Music 0522
- Philosophy of 0998
- Physical 0523
- Psychology 0525
- Reading 0535
- Religious 0527
- Sciences 0714
- Secondary 0533
- Social Sciences 0534
- Sociology of 0340
- Special 0529
- Teacher Training 0530
- Technology 0710
- Tests and Measurements 0288
- Vocational 0747

LANGUAGE, LITERATURE AND LINGUISTICS

- Language
  - General 0679
  - Ancient 0289
  - Linguistics 0290
  - Modern 0291
- Literature
  - General 0401
  - Classical 0294
  - Comparative 0295
  - Medieval 0297
  - Modern 0298
  - African 0316
  - American 0591
  - Asian 0305
  - Canadian (English) 0352
  - Canadian (French) 0355
  - English 0593
  - Germanic 0311
  - Latin American 0312
  - Middle Eastern 0315
  - Romance 0313
  - Slavic and East European 0314

PHILOSOPHY, RELIGION AND THEOLOGY

- Philosophy 0422
- Religion
  - General 0318
  - Biblical Studies 0321
  - Clergy 0319
  - History of 0320
  - Philosophy of 0322
- Theology 0469

SOCIAL SCIENCES

- American Studies 0323
- Anthropology
  - Archaeology 0324
  - Cultural 0326
  - Physical 0327
- Business Administration
  - General 0310
  - Accounting 0272
  - Banking 0770
  - Management 0454
  - Marketing 0338
- Canadian Studies 0385
- Economics
  - General 0501
  - Agricultural 0503
  - Commerce-Business 0505
  - Finance 0508
  - History 0509
  - Labor 0510
  - Theory 0511
- Folklore 0358
- Geography 0366
- Gerontology 0351
- History
  - General 0578
  - Ancient 0579
  - Medieval 0581
  - Modern 0582
  - Black 0328
  - African 0331
  - Asia, Australia and Oceania 0332
  - Canadian 0334
  - European 0335
  - Latin American 0336
  - Middle Eastern 0333
  - United States 0337
- History of Science 0585
- Law 0398
- Political Science
  - General 0615
  - International Law and Relations 0616
  - Public Administration 0617
- Recreation 0814
- Social Work 0452
- Sociology
  - General 0626
  - Criminology and Penology ... 0627
  - Demography 0938
  - Ethnic and Racial Studies 0631
  - Individual and Family Studies 0628
  - Industrial and Labor Relations 0629
  - Public and Social Welfare 0630
  - Social Structure and Development 0700
  - Theory and Methods 0344
- Transportation 0709
- Urban and Regional Planning 0999
- Women's Studies 0453

THE SCIENCES AND ENGINEERING

BIOLOGICAL SCIENCES

- Agriculture
  - General 0473
  - Agronomy 0285
  - Animal Culture and Nutrition 0475
  - Animal Pathology 0476
  - Food Science and Technology 0359
  - Forestry and Wildlife 0478
  - Plant Culture 0479
  - Plant Pathology 0480
  - Plant Physiology 0817
  - Range Management 0777
  - Wood Technology 0746
- Biology
  - General 0306
  - Anatomy 0287
  - Biostatistics 0308
  - Botany 0309
  - Cell 0379
  - Ecology 0329
  - Entomology 0353
  - Genetics 0369
  - Limnology 0793
  - Microbiology 0410
  - Molecular 0307
  - Neuroscience 0317
  - Oceanography 0416
  - Physiology 0433
  - Radiation 0821
  - Veterinary Science 0778
  - Zoology 0472
- Biophysics
  - General 0786
  - Medical 0760

EARTH SCIENCES

- Biogeochemistry 0425
- Geochemistry 0996
- Geodesy 0370
- Geology 0372
- Geophysics 0373
- Hydrology 0388
- Mineralogy 0411
- Paleobotany 0345
- Paleoecology 0426
- Paleontology 0418
- Paleozoology 0985
- Palynology 0427
- Physical Geography 0368
- Physical Oceanography 0415

HEALTH AND ENVIRONMENTAL SCIENCES

- Environmental Sciences 0768
- Health Sciences
  - General 0566
  - Audiology 0300
  - Chemotherapy 0992
  - Dentistry 0567
  - Education 0350
  - Hospital Management 0769
  - Human Development 0758
  - Immunology 0982
  - Medicine and Surgery 0564
  - Mental Health 0347
  - Nursing 0569
  - Nutrition 0570
  - Obstetrics and Gynecology .. 0380
  - Occupational Health and Therapy 0354
  - Ophthalmology 0381
  - Pathology 0571
  - Pharmacology 0419
  - Pharmacy 0572
  - Physical Therapy 0382
  - Public Health 0573
  - Radiology 0574
  - Recreation 0575
  - Speech Pathology 0460
  - Toxicology 0383
- Home Economics 0386

PHYSICAL SCIENCES

Pure Sciences

- Chemistry
  - General 0485
  - Agricultural 0749
  - Analytical 0486
  - Biochemistry 0487
  - Inorganic 0488
  - Nuclear 0738
  - Organic 0490
  - Pharmaceutical 0491
  - Physical 0494
  - Polymer 0495
  - Radiation 0754
- Mathematics 0405
- Physics
  - General 0605
  - Acoustics 0986
  - Astronomy and Astrophysics 0606
  - Atmospheric Science 0608
  - Atomic 0748
  - Electronics and Electricity 0607
  - Elementary Particles and High Energy 0798
  - Fluid and Plasma 0759
  - Molecular 0609
  - Nuclear 0610
  - Optics 0752
  - Radiation 0756
  - Solid State 0611
- Statistics 0463

Applied Sciences

- Applied Mechanics 0346
- Computer Science 0984
- Engineering
  - General 0537
  - Aerospace 0538
  - Agricultural 0539
  - Automotive 0540
  - Biomedical 0541
  - Chemical 0542
  - Civil 0543
  - Electronics and Electrical 0544
  - Heat and Thermodynamics ... 0348
  - Hydraulic 0545
  - Industrial 0546
  - Marine 0547
  - Materials Science 0794
  - Mechanical 0548
  - Metallurgy 0743
  - Mining 0551
  - Nuclear 0552
  - Packaging 0549
  - Petroleum 0765
  - Sanitary and Municipal 0554
  - System Science 0790
- Geotechnology 0428
- Operations Research 0796
- Plastics Technology 0795
- Textile Technology 0994

PSYCHOLOGY

- General 0621
- Behavioral 0384
- Clinical 0622
- Developmental 0620
- Experimental 0623
- Industrial 0624
- Personality 0625
- Physiological 0989
- Psychobiology 0349
- Psychometrics 0632
- Social 0451

THE RECIPROCAL SLIDING WEAR BEHAVIOR OF SiC PARTICULATE REINFORCED ALUMINUM COMPOSITE

BY

ZHENGCHENG FENG

A Thesis submitted to the Faculty of Graduate Studies of the University of Manitoba in partial fulfillment of the requirements of the degree of

MASTER OF SCIENCE

ABSTRACT

The behavior of SiC particles and the wear mechanisms of SiC particulate reinforced A356 aluminum composite in sliding against a steel counterface were studied for both dry and lubricated reciprocal sliding wear conditions. In dry sliding wear experiments, a load of 9.8N and a constant sliding frequency of 2×120 strokes per min with a 25mm stroke length were used. In lubricated wear tests, the applied load was changed in the range of 9.8N to 78.4N at the constant sliding frequency 2×120 strokes per min. The curves of normalized wear rate versus contact stress were plotted from the weight loss data for both the dry and the lubricated wear process. Optical and scanning electron microscopic studies were performed for the examination of wear surface morphology, cross sections and longitudinal sections of the wear track, and wear debris.

Two wear regimes were identified in the dry reciprocal sliding wear tests. At low contact stresses (<3MPa), abrasive microgrooving was the dominant mechanism for the wear of the composite and the slider. At high contact stresses (>5MPa), a surface mixed layer (SML) was formed underneath the wear track. In this regime, the major mechanism responsible for the material loss of the composite was the delamination of this SML. A transition zone between these two regimes existed at the contact stress level of 3~5MPa. In lubricated sliding wear experiments, two wear regimes were again noted, a mild wear regime corresponding to low contact stresses (<30MPa) and a severe wear regime at high contact stresses (>100MPa). It was found that the application of lubrication oil (10W30) effectively reduced wear and that the contact stress was a main factor in affecting the SiC particle behavior and the wear mechanisms of this composite.

ACKNOWLEDGMENTS

The author wishes to sincerely thank Dr. K. N. Tandon for proposing this work and for his supervision and consistent encouragement throughout the preparation of this thesis.

Special thanks are given to my beloved wife, Margaret Gao, for her consistent support and assistance throughout this long project.

The author is also grateful to Dr. You Wang for his helpful discussions and suggestions. All the experiments in this thesis were conducted in the metallurgical laboratory in the University of Manitoba. The technical assistance from tow technicians in the laboratory, John Van Dorp and Don Mardis, is also gratefully acknowledged.

Thanks are also given to Dr. J. R. Cahoon and Dr. D. Polyzois for their valuable suggestions in the editing of this thesis and the proper usage in English.

TABLE OF CONTENTS

LIST OF FIGURES

LIST OF TABLES

CHAPTER 1 INTRODUCTION

Aluminum-silicon based composites have been used increasingly in the automobile industry because of their high strength-to-weight ratio, good castability, and high temperature strength over unreinforced alloys. The potential applications of these composites may be found in many components where tribological properties of the material are important, such as brake rotors, cylinder heads and pistons. Several studies related to this field have been conducted during the past decade. Unfortunately, almost all of these investigations were performed by either pin-on-disk or block-on-ring testing machines where the composite material experienced only unidirectional sliding wear, and very few of these were completed on a reciprocal sliding wear machine where the same material may behave differently from that in unidirectional wear process. In fact, an understanding of the reciprocal wear behavior of these composites is important considering that a number of industrial applications, such as engine cylinders, pistons etc., involve reciprocal sliding wear.

It has been noticed that the research work done by M. A. Martinez et al. on the reciprocal dry sliding wear process was mainly about the macroscopic behavior of the composites in terms of weight loss, specific wear rate and external damage to the surface. The behavior of SiC particles and the wear mechanism in these composites have not been studied systematically with respect to the change in microstructure during the wear process. As for the lubricated sliding wear process, no detailed investigation has been reported thus far.

The principal objective of this present work was to characterize microstructurally an important commercial SiC particle reinforced aluminum composite material, to study the behavior of reinforcing SiC particles during sliding wear, and to determine the wear mechanisms in both dry and lubricated sliding against steel counterfaces. Consequently, physical models which describe the wear mechanisms were proposed and a comparison

between dry and lubricated wear with respect to weight loss and SiC particle behavior was made in order to understand more fully the influence of SiC particles on the wear mechanism with a change in wear conditions.

In the present research program, all of the experiments were conducted on A356-20% SiC particle composite sliding against 52100 steel balls under various sliding cycles and loads. Both dry and lubricated wear conditions were used for tests. The change in the surface morphology of both the composite and the steel balls was fully examined by a scanning electron microscope (SEM). Moreover, collected wear debris and cross and longitudinal sections of the wear track were examined using an optical microscope and a SEM. The near-surface features in the composite after wear were also analyzed. The SiC size distribution was investigated using an image analyzer before and after sliding wear.

CHAPTER 2 LITERATURE REVIEW

2.1 Introduction

Wear behavior of SiC particulate reinforced aluminum composites, especially the unidirectional sliding wear of this type of material has been extensively investigated with respect to weight loss, specific wear rate, surface morphology, subsurface microstructure and the effects of various testing parameters to understand the wear mechanism. However, very few studies related to the reciprocal wear characteristics of these composites have been conducted. In order to understand fully the wear performance of SiC particulate reinforced metal matrix composites, a comprehensive review of the background knowledge about both wear and the composites is necessary before this research work was conducted.

This literature review will cover four aspects: firstly, a general review about wear processes; secondly, a presentation of the fabrication methods for particulate reinforced metal matrix composites and their tribological applications in industries; thirdly, a review of the tribological behavior of these composites with the emphasis on their sliding wear behavior against steel counterface; and finally, a presentation of the various mechanisms of wear in particulate reinforced metal matrix composites, including abrasive wear and sliding wear.

2.2 Overview of Various Wear Processes

2.2.1 Wear Definition

Wear is one of the most commonly-encountered industrial problems causing major expense and leading to the replacement and maintenance of components and assemblies. It is a good engineering practice to solve wear problems and prolong the life of components.

Wear is generally defined as the progressive loss of substance from the operating surface of a body occurring as a result of relative motion at the surface [1, 2]. In consideration of the situation that surface material may be displaced but not removed, wear is also regarded as "displacement or removal of material as a result of tribological processes [3].

2.2.2 Wear Classification

There are different approaches to the classification of wear. It is outside the scope of the present investigation to cover every classification in this review. However, there are two main methods in the classification of wear which have been widely accepted. They are listed in accordance with wear mechanism, and types of surface damage.

2.2.2.1 Classified by wear mechanism

(1) Traditional Regimes of Wear

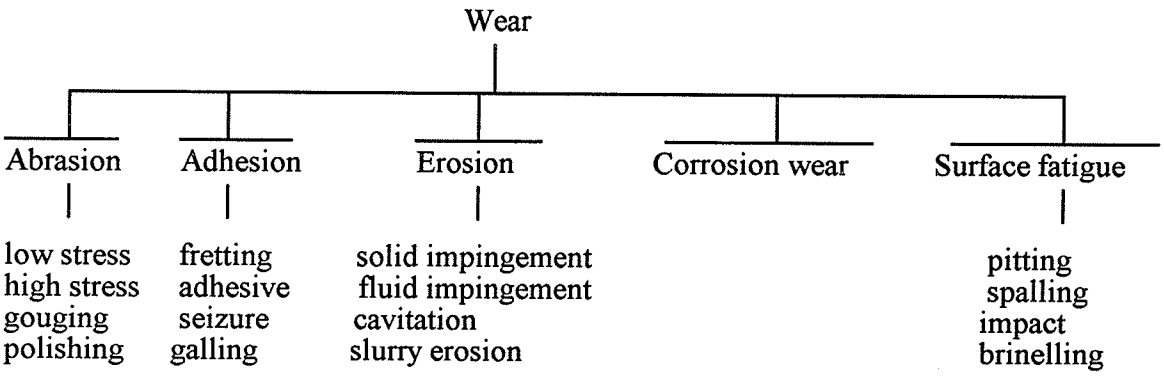

Fig 2.1 Traditional regime in the classification of wear [4, 5]

The scheme presented in Fig 2.1 is the most conventional scheme. As shown in Fig 2.1, there are five common mechanisms in describing wear processes: abrasion, adhesion, erosion, corrosion wear, and surface fatigue. Moreover, each title can be further divided into several categories. The most frequently encountered categories in industry will be examined in more detail in the following sections:

Abrasive wear

Abrasive wear is due to hard particles or hard protuberances that are forced against and moved along a solid surface [6]. In this case, when two surface asperities interact, the harder asperity might plough or cut through the softer one instead of both of them deforming or adhering. Thus, this type of surface is characterized by a scored, grooved or machined appearance.

Abrasion can be further categorized according to types of contact such as two body and three body wear. If an abrasive slides along a surface, it is two body wear; if an abrasive is caught between one surface and another, it is termed three body wear. Abrasion can also be categorized as low stress, high stress and gouging. Low stress abrasion is referred to as the situation when the abrasive remains intact. High stress abrasion occurs when abrasive particles are being crushed. Gouging abrasion exists when a relatively large abrasive cuts the material being concerned.

Adhesive wear

From a microscopic point of view, metal surfaces are far from smooth and many asperities exist on the surface. It may be assumed that any two surfaces loaded against each other contact only in a number of asperities. If two surfaces slide against each other and the total load is only born by some very small asperities between them, the contact stress is high enough to cause plastic deformation. Adhesion will take place and adhesive junctions will form. These junctions will break and new junctions will form when sliding continues. The breakage of the junction will be accompanied by metal transfer. So, adhesion is likely to occur when materials used for wear couple have structural and chemical similarities and when the wear couple have clean surfaces with no oxidizing conditions [4, 7].

Other definitions of adhesive wear also exist. In a wear process, if no abrasive substances are found, and if the wear rate does not follow the principles of oxidation, adhesive wear is said to occur [8].

Corrosive wear

Corrosive wear is defined as the removal of materials in which both corrosion and wear mechanisms are involved. This combination effect can induce greater material loss than the additive effects of each process alone.

In early wear classifications, oxidation wear is also included in the 'corrosive' wear regime [4]. This process is generally observed in unlubricated conditions of sliding. At a certain high temperature, a clean metal surface will react with its environment and form contamination films. In most cases, these films only loosely adhere to the metal surface and can be easily removed by the wear process, leaving exposed new surfaces. This process will repeat as wear process continues. These oxides will further serve as debris and enhance the abrasive wear since most metal oxides are harder than the metal itself.

Surface fatigue

During a wear process, if wear surfaces experience a cyclic load, such as repeated sliding, rolling or impacting, in general, the maximum stress is developed at a small distance below the surface. Therefore, when the wear process continues under stress cycles, fatigue cracks will normally initiate below the surface and parallel to the surface, resulting in the removal of relatively large pieces of particles [2]. These particles will rapidly deteriorate the wear surface and bring about three-body abrasion. Surface fatigue can occur either in dry adhesive wear or in lubricated systems where there is no asperity contact but the stress can be transferred to the near surface through a lubricant film.

Surface fatigue is similar to the fatigue process of bulk material but there are two major differences. Firstly, the variation in fatigue life in surface fatigue is much greater as compared with bulk fatigue. Secondly, for some materials, there exists a fatigue limit stress for the bulk material below which the material will have an infinite life. For surface fatigue, no such limit apparently exists.

Fretting

Fretting is not really a separate mechanism of wear in some classifications [2]. It is treated differently because of its special circumstances. Fretting is the small amplitude oscillatory movement between two contact surfaces [8]. Such movement will produce a form of adhesive wear and create oxide debris. This debris will then cause a second stage of abrasive wear; hence the term "fretting wear".

(2) Recent Regimes of Wear

A more recent classification of wear based on wear mechanism was illustrated on tribomaps by giving the boundaries of different wear processes [9, 10]. As shown in Fig. 2.2, there exist four broad classes of wear mechanisms: (1) Seizure, (2) Melt wear, (3) Oxidation - dominated wear, and (4) Plasticity-dominated wear.

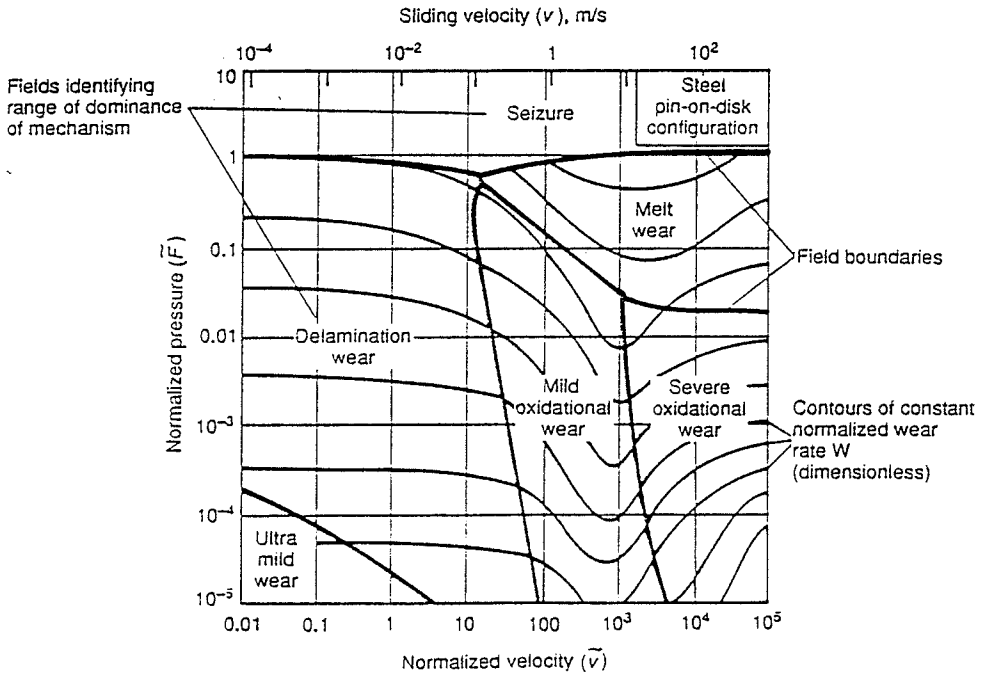

Fig 2.2 Empirical wear mechanism map for steel (pin-on-disk configurations) [9]

The normalized values of wear rate, load, and sliding velocity are defined by

$$\overline{W} = W / A_n \tag{2-1}$$

$$\overline{F} = F / A_n \cdot H_0 \tag{2-2}$$

$$\overline{V} = \frac{v r_0}{a} \tag{2-3}$$

In the above equations, A_n is the nominal contact area of wearing surface, H_0 is the room-temperature hardness, a is the thermal diffusivity, r_0 is the radius of the circular contact area, $\overline{W}$ is the volume lost per unit area of surface, per unit distance slid, $\overline{F}$ is the nominal pressure divided by the surface hardness and $\overline{V}$ is the sliding velocity divided by the velocity of heat flow.

Seizure

Seizure can be further classified into friction seizure and galling seizure [11]. Friction seizure occurs when the sliding motion causes the non-availability of sufficient driving force to overcome the friction force. Galling seizure is marked by a sharp rise in wear and extensive surface damage with respect to a small increase in external variables. Seizure may be accompanied by gross surface welding.

Melt Wear

At high sliding velocities, such as 10-1000m/s, the coefficient of friction drops to very low values because a film of liquid metal forms at the sliding interface. This is the signature of melt wear. The normal load is borne by this liquid layer through a hydrodynamic mechanism [12].

Oxidation - dominated wear

If steel surfaces slide at a speed above 1m/s, the wear debris will consist mainly of iron oxides [13]. The formation of oxide - debris is associated with a drop in wear rate when the sliding velocity increases to a certain value and local oxidation occurs. The oxide

is, for most of the time, cold and brittle, and is called mild - oxidational wear. At even higher velocities, the oxide is thicker, more continuous, hotter and more plastic. This type of wear is termed severe - oxidational wear.

Plasticity - dominated wear: adhesion and delamination

Surface oxidation is negligible as sliding velocities below 0.1m/s[14]. In this case the result of the frictional force is to deform the metal surface, shearing it in the sliding direction, thus it is the plasticity of a material that dominates its wear process. The removal of slivers must come from the nucleation and propagation of cracks which allow separation of the wear fragments from its parent surface. Three models have been proposed to account for the nucleation and growth of these cracks: the Adhesion-model, the Delamination-model, and the Fatigue crack propagation model. In the models based on adhesion [15, 16, 17], some touching asperities stick together along the tribosurface. They are sheared off tips of the softer asperities during the sliding process, and left adhering to the harder surface, from which they later become detached, forming a wear fragment. For delamination-models, cracks nucleate from the voids blow wear surface, which are produced by unidirectional shearing of the metal during sliding. When a crack is large enough it will break out resulting in the formation of a flake-like wear particle. If the load applied as a cyclic character, fatigue crack will develop [18].

2.2.2.2 Classification by types of surface damage

During the last few years, some investigators have tried to classify wear processes in a broader sense based on the types of surface damage rather than the traditional by wear mechanism [8]. This classification is shown in Fig 2.3. As shown in Fig 2.3, all the types of damage will affect the behavior of the surface layer. Even though loss of material is only one type of surface damage, it is the most frequently encountered and the most important problem in tribology. Normally, the wear on a component or material is a combination of two or more types of the damage in Fig 2.3. The combined effects may

interact mutually to increase the effects of one another or may lead to a net reduction of the individual effects [19].

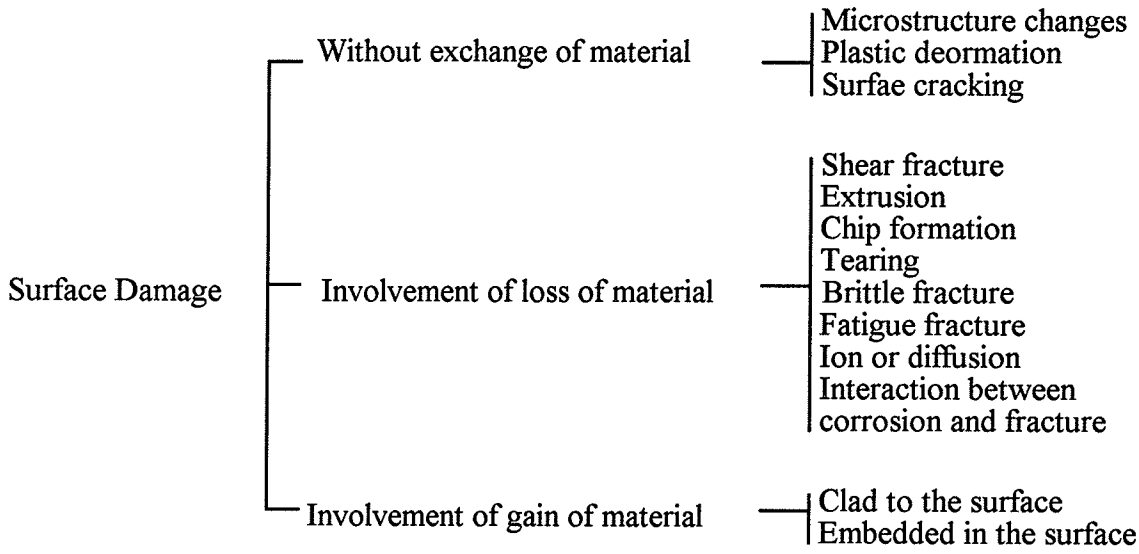

Fig 2.3 Types of surface damage [9]

2.2.3 Principal Factors Influencing Wear

In order to control the wear process and to minimize weight loss, it is important to know the basic factors which influence wear. The factors influencing the wear process are summarized below, except for the effect of lubrication:

2.2.3.1 Hardness

Increasing hardness, especially hot hardness, generally reduces the wear of materials. 'Hot hardness' means that the material can retain its hardness at high temperature. 'Hot hardness' is a significant characteristic of a material in decreasing wear since all wear processes result in a local temperature raise. But this principle is not correct all the time. There are come exceptions, such as the effect of hardness on surface fatigue and erosion processes. Fig 2.4 Shows the effect of materials hardness on the abrasive wear resistance [20].

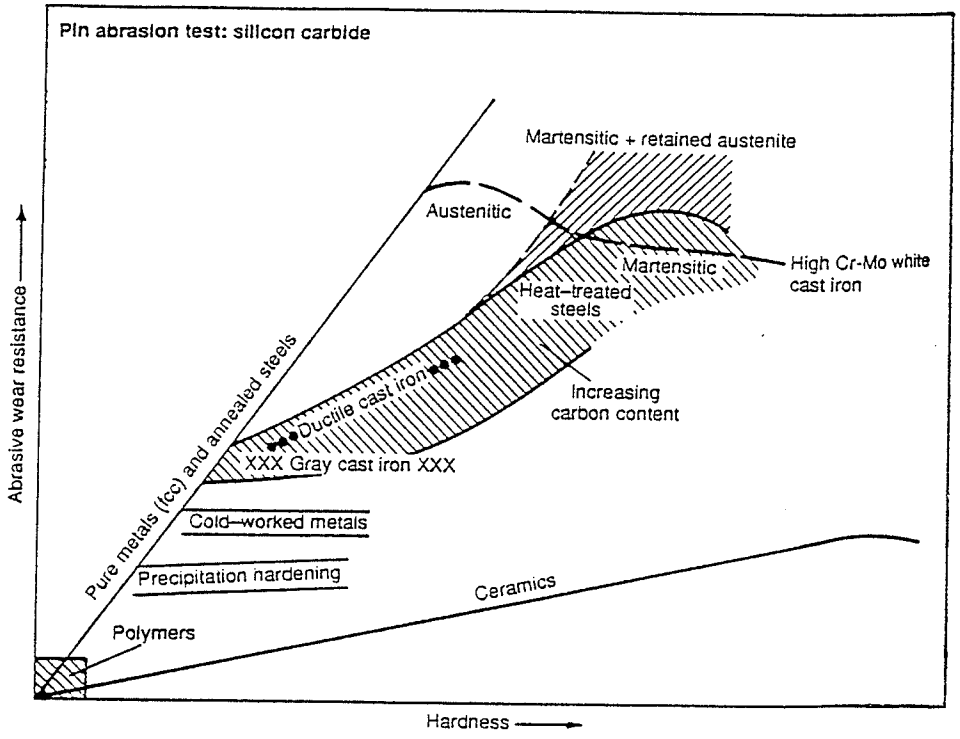

Fig 2.4 Two-body abrasion resistance (1/volume wear rate) for various materials plotted against bulk hardness [20]

2.2.3.2 Operational parameters

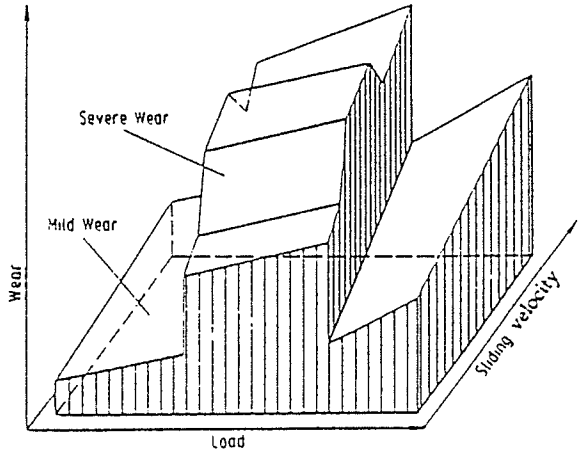

Fig 2.5 Wear intensity of steels in dry sliding as a function of load and sliding velocity (logarithmic scales) [8]

Load, wear speed and temperature are three main process factors affecting wear[2,4]. There is a general trend that wear rate increases with the increase of load. But for adhesive wear, there exists a stepwise transition between mild wear and severe wear which reverses the above trend (Fig 2.5)[8]. Wear speed can affect wear rate significantly. However, there is no straight forward relationship between these two. With the increase in temperature, the materials involved at the local contact region will become softer, which will lead to a consequent acceleration in the wear process.

2.2.3.3 Surface roughness

Surface roughness has a significant influence on the wear process. For abrasive wear, the initial roughness might bring about very severe surface damage and then be gradually reduced. But this is not always true. A very smooth surface at the beginning may become roughened afterwards [2].

2.2.3.4 Crystal structure

The crystal structure of most metals falls in the regimes of BCC, FCC or HCP. HCP is generally the most wear resistant structure among these three, since it only deforms along its basal plane. However, in the boundary lubricant condition, it is the oxide film attaching to the surface of the bulk material that partly determines the wear resistance by forming a protection layer which restricts the extent of metal to metal contact. Different oxide films will provide different characteristics for resisting wear [4,8].

2.2.3.5 Mutual solubility

Here, mutual solubility refers as to both the physical and the chemical similarities between two metals in contact. Wear is generally greater where the mutual solubility is high and less where mutual solubility is low [4].

2.2.3.6 Lubricated conditions

In order to reduce direct physical interactions between relatively moving surfaces, a film of material (the lubricant film) has been used to separate the surfaces

moving relative to each other. The effect of the presence of this lubricant film on the wear process can be expressed by the Stribeck curve (Fig 2.6) [21]. In this curve, the friction coefficient of lubricated moving surfaces is a function of the lubricant viscosity, the velocity and the normal load.

I: Thick film lubrication. In this regime, the mating surfaces are completely separated by a thick film. because of no direct contact between the rigid surfaces, wear can not take place.

II: Mixed lubrication. In this regime, the applied load is carried partly by the lubricant film and partly by the contacting asperities.

III: Boundary lubrication. In this regime, the applied load is carried almost entirely by the asperity contacts and the bulk properties of the lubricant becomes less important. Instead, it is the physical-chemical interaction of the solid interface with the lubricant that determines the wear characteristics of the materials.

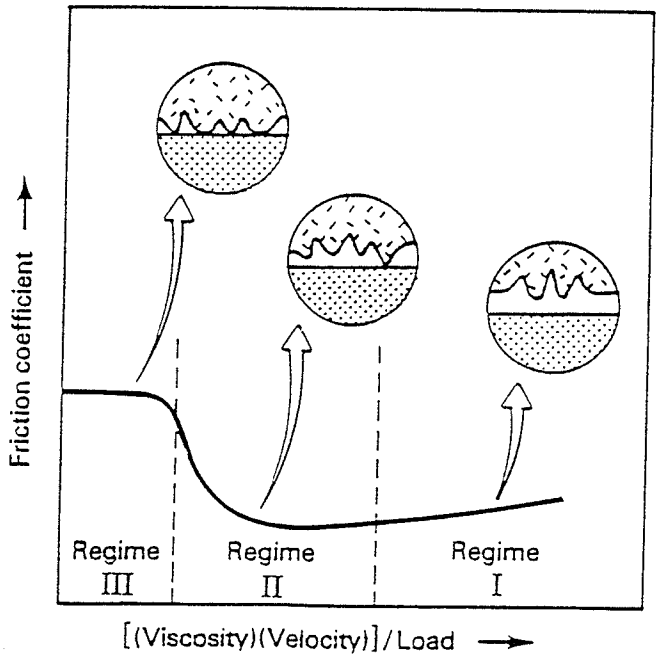

Fig 2.6 Stribeck curve and lubrication regimes

2.2.4 Testing Methods for Wear

The testing methods for wear fall into three categories: service trial, service equipment testing in a laboratory, and wear testing on a laboratory rig. A service trial is the ideal performance test, but factors, such as the duration of trial, lack of control and inadequate monitoring, will limit the application of a service trial. Thus, a simulation in a laboratory by fabricating the practical service equipment or components is used instead of a service trial. Even though this method has the advantage of a very high level of control and monitoring, it is often expensive. Therefore, in most cases, laboratory rigs are used to simulate the service conditions. In the following sections, a description of the wear testing methods in laboratory rig simulations will be described.

All laboratory wear tests can be classified into two sub-categories, standard tests and wear tests for special purposes. Some standardized laboratory test methods have been established for evaluation of material wear. These tests are: pin-on-block test, ASTM G99 [22], cross cylinders test, ASTM G83 [23]; pin or block-on-ring test ASTM G77 [24]. These tests are mostly used for comparing the wear resistance of different materials for selection purposes. In order to evaluate or predict the wear properties of a material in a specific application, a number of non-standardized tests have also been developed [25-28].

There are two factors that influence the selection of a wear test method, the wear mode, and the objective of the test. In general, a wear test is performed to investigate one of the following missions [5]: fundamental understanding, determination of the effect of variables, characterization of materials and lubricants, and selection of materials for a specific application. In the selection of a wear testing method, the first step is to perform a wear monitoring and diagnosis to figure out the dominant wear mechanism. Practical wear systems might be classified as different wear processes, such as sliding wear, erosion wear, chemically enhance loss of material or the combination of more than two mechanisms. Then the selection or the construction of the wear test apparatus should be done in the way that the services conditions are simulated as closely as possible [2]. Once the wear

monitoring or diagnosis is performed, a decision should be made to either design a new test rig or use a standard rig. The advantage of a specially designed rig is that it usually permits a closer simulation of the actual service conditions. Its disadvantage is its relatively high cost and the restricted range of situations for the application of the test results. The use of a standard test apparatus usually results in a lower degree of simulation of the actual service conditions, but at a lower cost.

Another standard wear test that should be mentioned is the Round-Robin Test [29, 30]. The intention is used to determine the precision, repeatability and the reproducibility of a test method in ASTM E691 by an inter laboratory study. VAMAS (Versailles Project on Advanced Materials and Standards) round-robin sliding wear tests were performed at 31 institutions in seven countries. A ball-on-disk test configuration was chosen as the test system. The test results illustrated that the reproductivity of friction and wear measurements are comparable with that of other engineering quantities.

2.3 Metal Matrix Composites

Metal matrix composites (MMC) have received a great deal of attention in tribological applications because of their superior mechanical properties. Non-metallic materials added to the metal can be in the form of whiskers or particles. Since particulate-reinforced MMC cost less and are isotropic in physical and mechanical properties, they have found the most tribological applications [31]. Therefore, particulate-reinforced MMC will be primarily reviewed.

2.3.1 Types of non-metallic particles

As shown in Table 2.1, various types of non metallic particles have been injected to produce MMC each with different metal matrices [32]. According to their hardness, these particles can be classified into two categories; hard particles with hardness 4-30

GPa, and soft particles with hardness below 4GPa. The particles are arbitrarily classified in this way because metal matrix composites containing hard particles will generally behave differently from those containing soft particles with respect to tribological properties.

Table 2.1 Density and hardness of various non-metallic particles [32]

Particle type	Hardness (GPa)	Density (g/cm^3)
TiC	20-30	4.93
SiC	24.5-29	3.22
Al_2O_3	18-26	3.97
WC	24	15.63
TiN	20.61	5.22
Si_3N_4	16-20	3.44
VC	16-18	5.77
TiO_2	12.7	4.26
$ZrSiO_4$	11	4.56
ZrO_2	6.5-10	5.89
SiO_2	8	2.65
MgO	...	3.55-3.68
Glass	4	2.48-2.54
Mica	0.3	2.7-2.8
Talc	...	2.2.58-2.83
MoS_2	...	4.62-4.8
Graphite	0.25	2.09-2.23
PTFE	<0.2	2.13

2.3.2 Synthesis of MMC

There are several different processes used in the production of MMC with high volume fractions of reinforcement for wear resistance. The optimum method depends upon the economic factors and the nature of the matrix and the reinforcement particles [32]. The fabrication techniques include casting methods, such as melt-stir casting [33, 34], squeeze casting [35, 36] centrifugal casting [37], direct infiltration [38], composting [39], atomizing, gas injection [40-41], mechanical alloying and powder metallurgy [42, 43]. Some inexpensive liquid metallurgy techniques have been used widely in recent years, including stir casting, squeeze casting and pressure infiltration. The fabrication techniques in the fabrication of MMC can also be classified in accordance to the nature of the phase reactions. They include solid-state transformations, liquid-liquid reactions, liquid-solid reactions, gas-liquid reactions, gas-solid reactions and mechanical mixing. The casting methods can also be classified into two groups; non reactive casting and reactive casting [31]. In non reactive casting, the particles are added to the melt of the matrix (Duralcan used this method), and this can produce quite economical aluminum-matrix composites. During reactive casting, the reinforcing phase is formed by the reaction within the melt [42].

A recent classification of casting methods for MMC is shown in Fig 2.7 [43]. The composites which have been fabricated are listed in Table 2.2

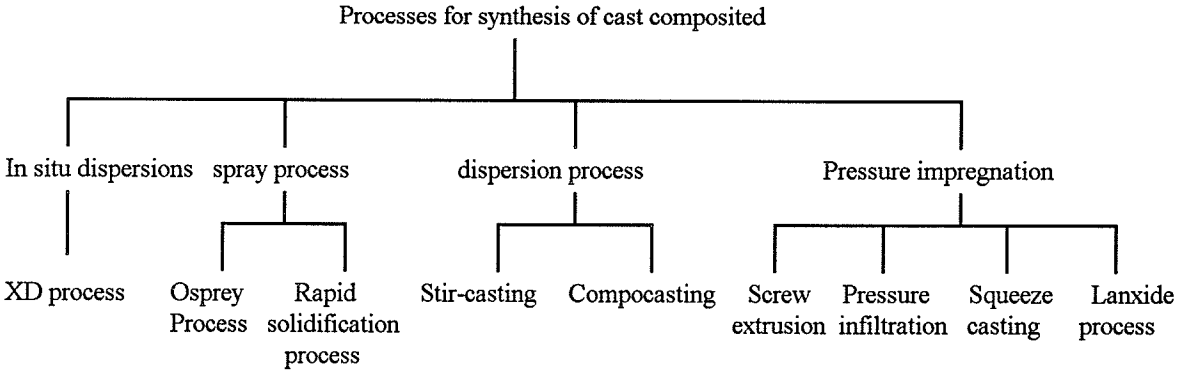

Fig 2.7 Different casting routes for synthesis of cast metal-matrix composites [43]

Table 2.2 Synthesis of cast composites [43]

Period	Location	Composite system	Technique used
1965	Inco., USA	Al/gr	Particle coating and gas injection
1968	IITK, India	Al/Al_2O_3	Magnesium inoculation and stir-casting
1974	IISc, India	Al/SiC; Al/mica	Magnesium inoculationand stir-casting
1975	MIT, USA	Al/Al_2O_3	Magnesium inoculation and compocasting
1978	Hitachi, Janpan	Al/gr	pressure casting
1979	RRL, India	Al/TiO_2; Al/ZrO_2; Al flyash	Magnesium inoculating and stir-casting
1979	USSR	Al/gr	Stir-casting
1983	Marin Matietta, USA	Al/TiC	XD process
1983	Dupont-Toyota	Al/Al_2O_3	Pressure infiltration
1984	RRL, India	Al/microballons	Stir-casting
1984	Norsk, Hydro, Norway	Al/SiC	Stir-casting
1985	Iraq	Al/MgO-coated Al_2O_3	Stir-casting
1986	MIT, USA	Al/SiC	Pressure infiltration
1986	DURAL USA	Al/SiC; Al/Al_2O_3	Stir-casting under reduced pressure
1987	Martin Marietta	TiAl, Ti_3Al/TiB_2, $NiAl/TiB_2$	XD process
1987	MIT, USA	Fe/TiC	In situ synthesis
1987	Comalco, Australia	Al/coated Al_2O_3	Stir-casting
1988	Lanxide Corporation, USA	Al/Al_2O_3; Al/SiC	Pressureless infiltration
1988	Grenoble, France	Al/SiC	Stir-casting
1988	Drexel Univ., USA	Al/TiC	In situ synthesis
1989	Univ. of Wisconsin, Milwaukee, WI	Cu/gr	Stir-casting and compocasting
1989	Honda, Japan	Al/Al_2O_3-C	Pressure casting

Even though all the processes in Fig 2.7 appear to have potential applications in industry for the production of MMC, only the stir-casting method has been used on a regular production scale at Duralcan, USA, and Comalco, Australia. The composite ingots of this type are now commercially available. Metal matrix composites have yet to be used on a regular basis for industrial application despite the great attention that has been paid by researchers and the high priority of their development given by different governments [43]. Two reasons are believed to be responsible for this delay. First, conventional alloy producers are not active in this field because they have the perception that the development of composites may threaten their own established market. The second is the early over optimistic promises concerning properties and the later disappointment of the results. There are three types of industries that are promoting the development of metal matrix composites: manufactures of reinforcing materials, industries involved in producing components and some small companies interested in specific inventions.

To the present time, the focus of research concerning MMC has been in developing different casting methods and several routes are available for their fabrication. However, it is far from clear as to which method should be preferred. It has also been suggested that attention should be paid to heat treatment, bulk deformation and non-destructive testing of the detects in composites [43].

For composite materials, there are several types of defects that have a significant effect on their mechanical properties. These include porosity, interfacial reactions and particle degradation. The existence of porosity has an adverse effect on the mechanical properties of metal matrix composites. The porosity in cast composites can be classified into two types, those at the boundary of matrix and dispersoids, and those away from dispersoids. The first type porosity can promote the disbonding of particles from the matrix, so these are more undesirable particles. Segregation may be produced either in the slurry or during solidification and particle segregation could be over on either a microscopic or a macroscopic scale. The solute rich regions are generally composed of

brittle interdendritic structures. Thus, the segregation of dispersoids into these regions can induce the disbonding of particles from the matrix at lower strains and subsequently damage the mechanical properties. The presence of an interfacial reaction layer often impairs the load-carrying capacity of a composite because of the disbonding of particles from the matrix at lower loads.

2.4 Tribological Application of MMC

Even though the industrial application of these metal matrix composites has yet to begin on a regular basis, some components or parts have been produced out of MMC (as seen in Table 2.3 [43]) for anti-wear purposes, and MMC are increasingly being introduced to tribological application, especially in the automotive industry. As shown in Table 2.3, the matrix metal is often aluminum, copper or magnesium alloy. Most of the applications of these composites are related to the improvement of wear resistance or for reducing weight such as engine pistons, brake rotors and liners, electrical contact strips and engine blocks. Recently, aluminum engine blocks have been produced out of fiber reinforced MMC (12 Vol. % Al_2O_3 + 9 Vol. % graphite) in an integrally cast MMC liner. Experimental results showed that the wear rates of the MMC-lined bore are similar to those for cast iron liners, resulting in 20% weight reduction from that of aluminum block with cast iron liners [44]. These applications in a wear-resistant field to reduce weight generated considerable interest in some industries, including the automotive and aerospace industries. Other applications in the field of satellites, antennae and sporting goods such as bicycle frames, golf clubs and boats [45].

Table 2.3 List of some composite components with proven potential [43]

Composite [a]	Components	Benefits	Manufacturers
Al-SiC(p)	Piston Brake rotor, caliper, liner Prop. shaft	Reduced weight, high strength and wear resistance	Duralcan, Martin Marietta, Lanxide
Al-SiC(w)	Connecting rod	Reduction of weight and high specific stiffness	GKN, Duralcan
Mg-SiC(p)	Sprockets, pulleys and covers	Reduce weight high strength and stiffness	Dow Chemical
Al-Al_2O_3(sf)	Piston ring Piston crown (combustion bowl)	Wear resistance, high running temperature Reduced reciprocating mass, high creep and fatigue resistance	Toyota T&N, JPL, Mahle etc.
Al-Al_2O_3(lf)	Connecting rod	Reduced reciprocating mass, improved strength and stiffness	Dupont Chrysler
Cu-graphite	Electrical contact strips, electronics packaging bearings	Low friction and wear, low CTE	Hitachi Ltd
Al-graphite	Cylinder liner, piston, bearings	Reduced friction, wear and weight	Associated Eng., CSIR
Al-TiC(p)	Piston, connecting rod	Reduced weight and wear	Martin Marietta
Al-fibre flax	Piston	Reduced weight and wear	Zollner
Al-Al_2O_3(f)-C(f)	Engine block	Reduced weight, improved strength and wear resistance	Honda

[a] p, particle; w, whiskers; sf, short fibers; fl, long fibers.

2.5 Tribological Properties of MMC

2.5.1 Wear in Dry Condition

2.5.1.1 Friction and abrasive wear

The abrasive wear and friction tests for particle metal matrix composites are generally classified into two types, low stress tests and high stress tests. Low stress tests, such as ASTM standards G-65 and B-611, are rubber wheel abrasion tests in which quartz abrasive particles (generally rounded sand SiO_2, SiC particles or crushed quartz) are fed between a rotating rubber wheel and the specimen. The feeding particles do not break. Some researchers have measured wear rates of hard particle composites by this method [46-48]. In high stress tests, a pin-on-drum of pin-on-disk apparatus (Al_2O_3 abrasive particles bonded to an aloxite cloth sheet) is used, where the abrading particles break. Several investigators have used high stress type test machine in studying wear properties of particle metal matrix composites [49, 50].

The volume fraction, hardness, shape and size of reinforced particles are very important factors in determining abrasive wear behavior of a MMC. It was found that the coefficient of friction is a function of the volume fraction of the particles. The coefficient of friction decreases with the increase in volume fraction of hard particles [49]. The friction coefficient of ceramic-ceramic contact, which is usually much higher than that of metal-metal, is generally 0.25 or less [50]. Since the increase in the volume fraction of ceramic particles will contribute more ceramic-ceramic contact, the friction coefficient of the composite can be thus effectively lowered.

Fig 2.8 shows the relationship between specific wear rate and particle volume fraction for aluminum alloy matrix reinforced by various types of particles [51]. It is indicated that the harder particles result in lower specific wear rate for a given particle volume fraction. The specific wear rate generally decreases with the increase of particle volume fraction. It seems that there is a common acknowledgment for the improvement of

wear resistance by adding particles to metal matrix. The low-stress abrasive wear rate of two aluminum alloys the alloys decreased by a factor of five by adding 35 Vol. % zircon and 20 vol. % Al_2O_3 particles [48, 51, 52], and the low-stress abrasive wear rates of these composites are comparable to 1045 steel. Another low stress test[53] also indicated that the wear resistance of the composite - 2014 Al-20wt%SiC is about two times higher than that of the peak-aged 2024 alloy. The experimental results show that the abrasive wear of metal-matrix composites, as in monolithic materials, involves ploughing, scouring and plastic deformation of matrix induced by moving abrading particles. At the same time, the plastically deformed matrix might cause the smearing over of the SiC particles of the composite. The interaction of the dispersed particles in the composite with abrading particles can cause their mutual fragmentation [54]. By studying the effects of different abrasive particles on the abrasive wear of engineering materials, it is concluded that alumna is more aggressive than silica sand [55].

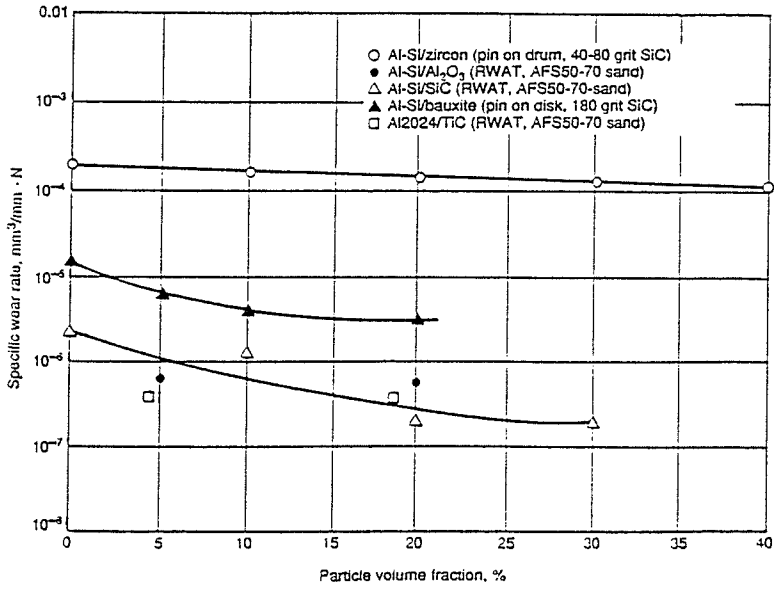

Fig 2.8 Specific abrasive wear rate as a function of particle volume fraction in aluminum alloy composites [51]

2.5.1.2 Friction and sliding wear

(1) Sliding friction coefficient

The presence of reinforced particles has a remarkable effect on the wear coefficient of metal matrix composites. In wearing against steel counterfaces, non-metallic particles generally reduced friction coefficients [31]. The influence of the addition of second phase particles on the coefficients of friction were systematically discussed in [51]. Fig. 2.9 shows the value of wear coefficients of various particles with different volume fraction. It was arbitrarily divided into three regions [52, 56-60]: Region 1 - for composites containing hard particles (μ=0.3-0.35); Region 2 - for composites containing particles of intermediate hardness (μ=0.25-0.4); Region 3 - for composites containing soft particles (μ=0.1-0.30). Most of the matrices shown in Fig. 2.9 are aluminum alloys. In sliding against a hard steel counterface, the friction coefficients of Al/Si alloys containing different silicon content are in the range of μ=0.45-0.6 [61]. The friction coefficients of the matrix alloys are obviously reduced by dispersing non-metallic particles. But beyond this, no clear relation between the coefficient of sliding friction and the particles content can be found [33]. From Fig 2.9 it seems that the higher hardness of the particles, the greater the friction coefficients. Silicon carbide and alumina belong to the group of hard particles. Even though these hard particles cause low adhesion to a metallic counterface, they will induce more severe plastic deformation due to asperity-asperity interaction, and consequently result in a greater increase in friction coefficients than for other types of particles. Graphite and MoS_2 are in range 3 with low friction coefficients. The comparatively low friction coefficients in region 3 are induced by the formation of a solid lubricating film on the mating surface which comes from the soft solid lubricating particles.

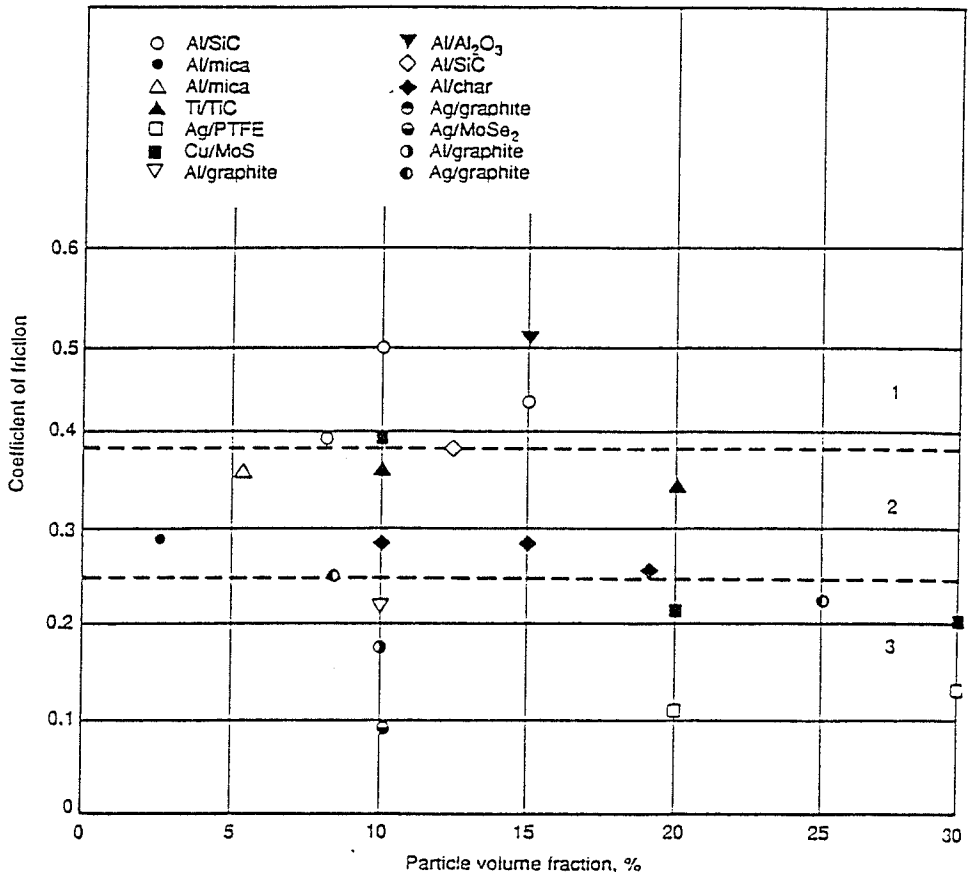

Fig 2.9 Coefficient of sliding friction as a function of particle volume fraction in metal-matrix composites sliding against a steel counterface (except those with a silver matrix) [52, 56-60]

The sliding wear behavior of the aluminum alloy matrix and other matrices containing graphite particles has been systematically studied by several investigators [62, 65]. The coefficients of friction are summarized in Fig 2.10 which shows that the coefficient friction is reduced significantly in MMC as compared to that in plain matrix alloys. When the amount of graphite exceeds 20vol.% in the metal matrix composites, the coefficient of friction becomes almost constant and beyond that (20% graphite) it virtually becomes independent of the matrix alloy and the graphite content. This constant coefficient of friction is about 0.2. The elemental graphite has a friction coefficient of 0.18.

Thus, it seems that the mating surfaces are smeared with graphite, and a coefficient of friction close to that of pure graphite is observed.

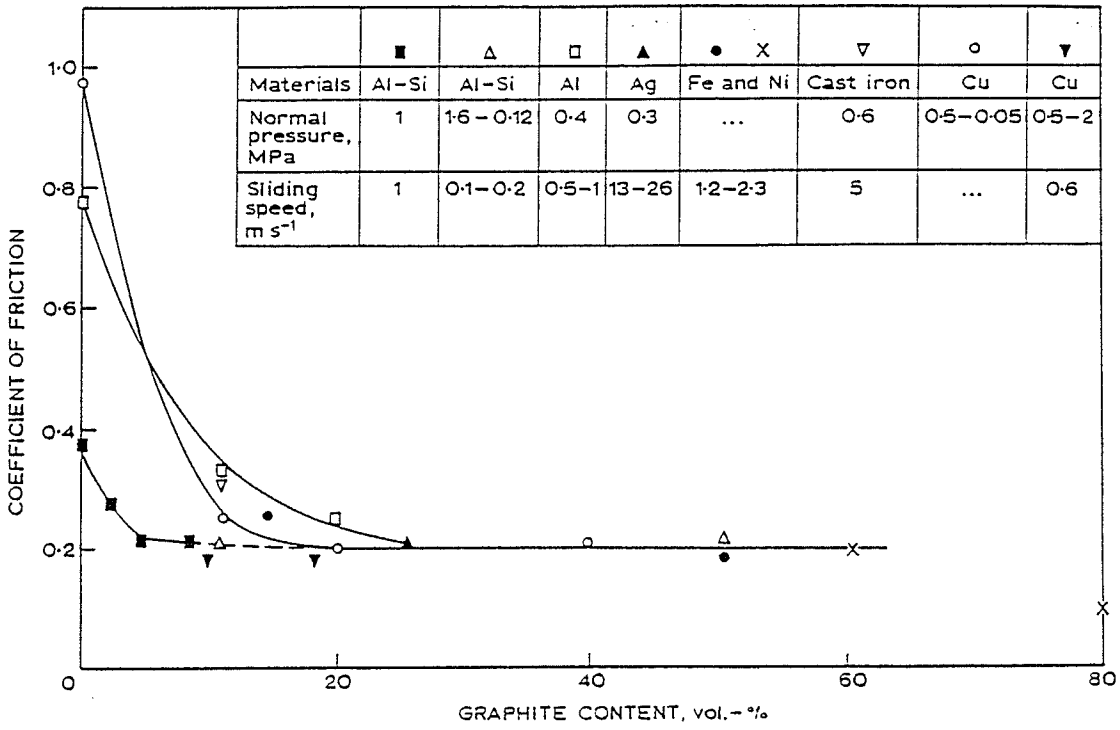

	■	△	□	▲	● X	▽	○	▼
Materials	Al–Si	Al–Si	Al	Ag	Fe and Ni	Cast iron	Cu	Cu
Normal pressure, MPa	1	1·6 – 0·12	0·4	0·3	...	0·6	0·5–0·05	0·5–2
Sliding speed, m s^{-1}	1	0·1–0·2	0·5–1	13–26	1·2–2·3	5	...	0·6

Fig 2.10 Variation of coefficient of friction with graphite content for composites with different base alloys [62, 65]

The coefficient of friction of the composites containing soft particles is also affected by particles size. For Cu-20WS_2 composites, the value of friction coefficient in sliding decreased from 0.4 to 0.2 when the size of WS_2 increased from 0.1 to 0.2 μm. However, the effect of particle size on sliding coefficient for composites containing hard particles is not clear.[23].

(2) Weight loss and wear rate

For the effect of addition of non-metallic particles on the weight (volume) loss or wear rate, experimental results vary with different investigators [33, 53, 56, 66, 67], and, sometimes, they are even contradicted. Both 2024 aluminum alloy and the composite 2014 aluminum alloy reinforced by 20wt%SiC particle blocks were tested. Similar wear rates were obtained through the sliding wear tests for the materials. No significant improvement in wear resistance was noted for the composite. However, most investigations indicated that the incorporation of SiC particles could effectively enhance the wear resistance [8, 33, 68]. Also, with pin-on-disk sliding wear machines, and at the same sliding velocity as in [53], very different test results were obtained by F. M. Hosking et al. [33]. For a given sliding distance the weight loss was reduced by introduction of hard non-metallic particles, and furthermore, the weight loss decreased with increasing weight percent and size of Al_2O_3 particles. Experimental results also indicated that the SiC particles (Vickers hardness of 2600) were more effective than the Al_2O_3 particles (Vickers hardness of 1800) in resisting wear. The wear volume and specific wear rate for Al-7Si/20vol.% SiC composite, Al-20Si and Al-12Si alloys were also examined in reciprocal sliding wear test at ambient temperature [68]. Improved wear resistance of the composite over the plain alloys was clearly demonstrated.

The addition of graphite in an aluminum matrix not only reduces the friction coefficient for the composites but also significantly improves their wear resistance [62,67,69]. The presence of graphite particles in aluminum alloys was found to reduce the sliding wear and friction coefficient even under dry conditions, because the graphite in the composite gets transferred onto the tribosurfaces, and the hexagonal layered structure of graphite which can easily shear along the basal plane serves as a solid lubricant..

Particle size also has an effect on specific wear rate of a composite. The increase in particle size generally improves the wear resistance of composites containing hard or soft particles [50,67]. The same trend was also reported for the composites of aluminum

alloys containing graphite [51]. But, if the particle size was smaller than 20μm, no significant effect was noted by the change in particle size.

(3) Effect of testing parameters

Load

Load is the most active factor in influencing the sliding wear behavior of a composite. Several studies have been reported to substantiate this [33,56,62]. In general, wear rate increases when the normal load increases for hard particle reinforced composites. But the extent of the effect changes with the change of normal load [70]. Wear loss for a composite of A356-20%SiC against 52100 bearing steel was studied by a block-on-ring wear jig. At low loads below 10N (region I in Fig 2.11), the wear rate of the composite was an order of magnitude lower than that of the unreinforced alloy. But, at an "intermediate" load between 10-95N (region II), there was almost no difference in wear rates between SiC reinforced and the unreinforced alloys. As the normal load increased above 98N, the wear rate of the unreinforced A356 accelerated by about two orders of magnitude. However, the wear rate of SiC reinforced composites only increased slightly. These results indicated the significant influence of applied normal load on wear rate and possibly on the wear mechanism of the composite.

For the composite containing soft particles, the trend in the change of wear rate as a function of normal load becomes more complicated than that of the composite containing hard particles. For the composite with high volume fraction of soft particles, such as Cu-30Ta base soft particle, the wear rate first decreases, up to a limiting value of contact pressure, and then increases [51]. Fig 2.12 shows the change of wear volume, in a copper- graphite composite, with contact pressure [71]. The wear volume of this composite increases with the increase in pressure, and a critical pressure exists when wear changes from "mild" to "severe" wear. Similar results have been obtained for other composites containing less amount of soft particles [72].

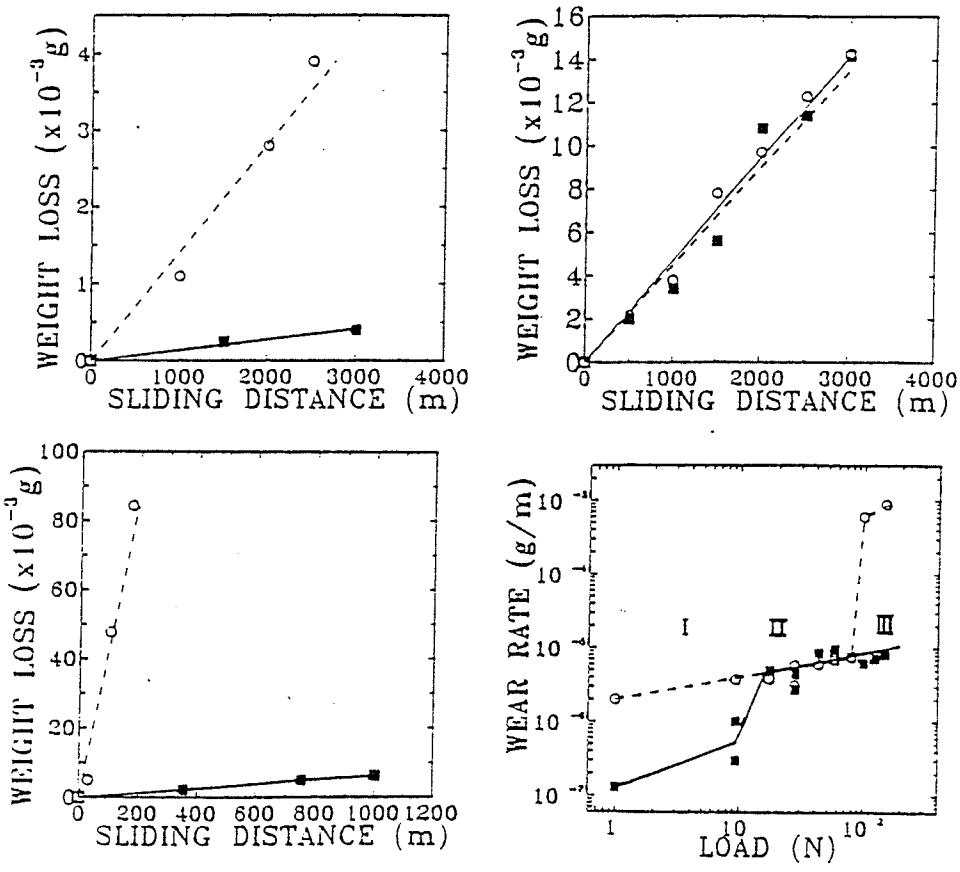

Fig 2.11 Weight loss versus sliding distance curves for unreinforced A356 (o) and A356-20%SiC (▪). a) Load = 0.9N; b) Load = 17N; c) Load = 98N; d) Log Wear rate versus Log Load diagram for unreinforced A356 (o) and A356-20%SiC(▪)[70]

The effect of normal load on friction was also investigated for the composite Al-1.5 Pct Mg/SiC [73,74]. It was found that friction coefficient decreases as the normal load increases.

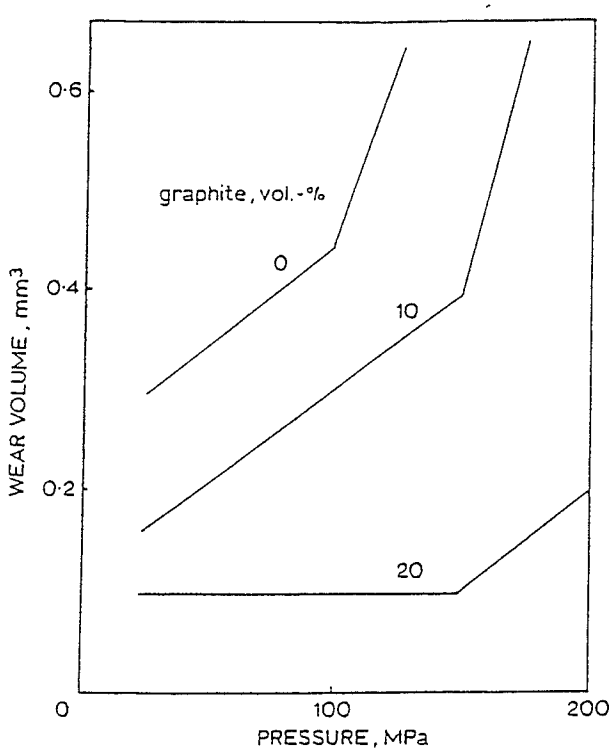

Fig 2.12 Variation of wear volume with pressure (normal) for copper-graphite particle composites containing 0-20 vol. % graphite [71]

Sliding velocity

The effect of sliding velocity on volume-loss and specific wear rate of unreinforced and reinforced 7079 aluminum alloy with 20 vol. % SiC particles have been investigated by [75]. At sliding velocities below $1.2ms^{-1}$, the incorporation of SiC particles did not affect the wear resistance, and the unreinforced and reinforced alloys exhibited similar wear rates. At sliding velocities greater than $1.2ms^{-1}$, the wear rate of the composite was about an order of magnitude lower than that of unreinforced matrix. For the unreinforced matrix, the specific wear rate increased with an increase in the sliding speed, but for the reinforced material the specific wear rate decreased with an increase in sliding velocity. The steady state coefficient of friction was also related to sliding velocity.

Similar to the relationship of wear rate-sliding velocity, the reinforced composite showed a continuous decrease in friction coefficient with an increase in sliding velocity, while the unreinforced alloy exhibited a minimum at $0.72ms^{-1}$ followed by a dramatic increase at $1.2ms^{-1}$. Similar experimental results were also obtained in aluminum alloy composites containing 10% glass when the sliding velocity was increased from 0.1 to $3ms^{-1}$ and by the wear test of an Al-12Si-50Al_2O_3 composite as sliding velocity increased from 3 to $8ms^{-1}$ [76]. However, for soft particles, the effect of sliding velocity on wear rate is more complex [76,77]. At low content of graphite-5%, the wear rate decreased with the sliding speed. When graphite fraction was increased to above 15%, there was no significant effect of sliding speed on the wear rate.

Temperature

High temperature wear can be often found in many industrial applications. It is surprising that not many publications about the effect of temperature on the wear behavior of metal matrix composites are available. The wear properties of an Al-Si/SiC composite were studied by a reciprocal sliding process in a temperature range of 25-200°C [68]. It was reported that the coefficients of friction and specific wear rate for Al-7Si/SiC composite and Al-20Si alloy increased with an increase in temperature. A transition temperature was evident for the materials from mild wear to severe wear. The transition temperature was found to be 110°C for Al-20Si alloy and 150°C for the composite. This difference was attributed to the thermal stability provided by SiC reinforcement. However, no detailed microstructural studies were carried out to study the behavior of particles during the wear processes.

2.5.2 Wear in Lubricated Condition

Little investigation has been performed on the sliding wear behavior of MMC containing hard particles under lubricated conditions. By using a lubricant, such as SAE 10W30 motor oil, metal-metal contact area and wear rates were significantly reduced, but no detailed and systematic description about the wear behavior of these composites has been given [53]. The effect of lubricant on the wear properties of composites containing graphite particles has been studies by some researchers. Variation of wear volume with sliding distance was compared for Al-Si alloy composite containing various graphite contents in dry sliding and under lubrication with turbine oil [67]. Experimental results have shown that the load for lubricated sliding had to be increased considerably before getting a significant amount of wear. It was also observed that the graphite film formed can help to spread the lubricant oil much more rapidly than that in the alloys without graphite [78,79].

2.6 Wear Mechanisms of MMC

2.6.1 Dry Sliding Wear of MMC Containing Hard Particles

There are mainly three mechanisms that have been proposed for the sliding wear of metal matrix composites containing hard particles: (a) subsurface delamination; (b) grinding of the sliding surface by the formation of a transfer layer; and, (c) adhesion.

(1) Subsurface delamination

Almost all of the wear tests from which delamination theory was proposed were performed on unidirectional block-on-ring or pin-on-disk sliding wear machines [53,54,70,80]. In this regime, plastic deformation flow on the contact surfaces plays a vital role in determining the wear of the composite. During the wear of Al-Si alloys,

delamination occurs via cracks which originate from silicon particles in the deformed zone and which propagate to the surface. The critical depth for the location of subsurface cracks is determined by the competition between the hydrostatic pressure and the plastic strain. Subsurface delamination was also observed in a reciprocal sliding wear process at a high temperature (200°C) for Al-7Si/SiC composite against a 52100 ball-bearing [68].

(2) Grinding of the sliding surface by formation of a transfer layer

Contrary to the subsurface delamination model in which the separation of hard particles from the matrix plays an important role, some researchers have shown that the disbonding of particles is not a dominant mechanism of sliding wear. Instead, formation of a transfer layer induces the grinding of the sliding surface. The transfer layer on the sliding surface has been found by many investigators [56,76,81]. During the sliding wear of a 2024-20%SiC aluminum base composite against a steel counterface on a pin-on-disk test, three different stages of wear have been reported [81]: firstly, formation of steel filings on the pin from microcutting of the steel counterface by SiC particles; secondly, packing of the filing on the sliding pin surface between particles; and finally, gross pin surface deformation with loss of SiC particles. Therefore, under a steady-state wear, a transfer layer- (mixture of iron debris, SiC fragments and aluminum matrix debris) forms on the sliding surface.

(3) Adhesive wear model

In this model, the wear coefficient of composites can be expressed by the following equation:

$$K_C = K_m f_m + K_p f_p \tag{2-4}$$

Where K_m and K_p are the wear coefficient of the matrix and the particle respectively, and f is their volume fraction. This equation is obtained from the assumption that each phase in

the composite wears out independently [82,83,84]. Since K_p is usually much smaller than K_m, therefore,

$$K_C \approx K_m f_m = K_m(1-f_p) \tag{2-5}$$

A modification of this equation includes the effect of particle hardness is taken into consideration. The above equation then becomes:

$$K_C = -\alpha f_p + K_m \tag{2-6}$$

Where α is a coefficient factor and can be obtained from the slope of wear curves.

There are a number of other models developed for the wear mechanism of sliding wear. Such as abrasive wear assisted by oxidation [33], surface-fatigue-related surface cracking and subsurface-cracking-assisted adhesive transfer [75]. Moreover, experimental results show that testing parameters have significant effect on wear mechanism, such as sliding velocity, applied normal load and temperature as discussed previously in section 2.5.1.

2.6.2 Sliding Wear in MMC Containing Soft Particles

A representative composite in this category is a metal-matrix-graphite particle composite. Before sliding, the area fraction of tribosurface occupied by graphite approximately equals to the original volume fraction in the composite. However, as sliding proceeds, the graphite will be squeezed out of the composite and spread out along the tribosurface in the form of a of solid lubricant film. Thus the friction coefficient of the composite depends on the extent of film formation on the interface [84].

$$f_c = (1 - A_g) f_m + A_g f_g \tag{2-7}$$

Where f_m and f_g are the friction coefficients of the matrix and the contact area covered by graphite film, A_g is the area fraction of the interface covered by graphite film. and

$$f_m = f_{am} + f_{dm} \tag{2-8}$$

$$f_g = \frac{s_g}{p} + \alpha \tag{2-9}$$

Where f_{am} and f_{dm} are contributions to the coefficients of friction of the matrix f_m, due to the process of adhesion and deformation respectively. S_g is the shear strength of graphite, p is the applied normal pressure. α is a constant of graphite film. After the formation of a graphite lubricant film, wear process continues with the wear of both the film and the matrix. A balance can be reached between the formation of the graphite film and the rate of its wear, and this leads to a dynamic steady state characterized by a steady value of friction. So, there is a transient period from original metal-metal asperity interaction to the film formation which can prevent such metal to metal contact. If the composite contains high amounts of graphite, large area of the counterface will be covered by a thick graphite film, and delamination wear may take place within the film if the thickness of this film exceeds a critical value. The softer asperities on graphite can be easily fractured by asperity interaction and a smooth surface would be generated. Consequently, asperity-asperity type of contact changes to asperity-plane contact. The accumulation of dislocation under the surface will cause subsurface cracking followed by delamination[64]. Similar results have been obtained in composites containing MoS_2 [49, 85].

2.6.3 Abrasive Wear in MMC Containing Hard Particles

For two-body abrasive wear, delamination mode was believed to be the dominant mechanism. A copper-base hard-particle composite was studied, and a delamination model was proposed [86] (as seen in Fig 2.16). In this model, cracks initiate due to the disbonding of hard particles from the matrix and propagate by the coalescence of the voids

resulting from the disbonding process. According to this model, wear resistance also depends on fracture toughness of the matrix, in addition to the composite strength.

For a three-body abrasive wear, it was reported that the abrasive particles will break down and embed in the matrix of the composite[55]. Moreover, the reinforced hard particles in a composite bear the load and resist scratching under low loads, but fracture into small pieces at high loads. The wear process is characterized by plastic deformation of the matrix, the smearing of this deformation layer over SiC particles of the composite and fracture of SiC particles in the composite [87, 88]. Micromachining is thought to be the dominant mechanism of wear during the abrasion wear of these composites.

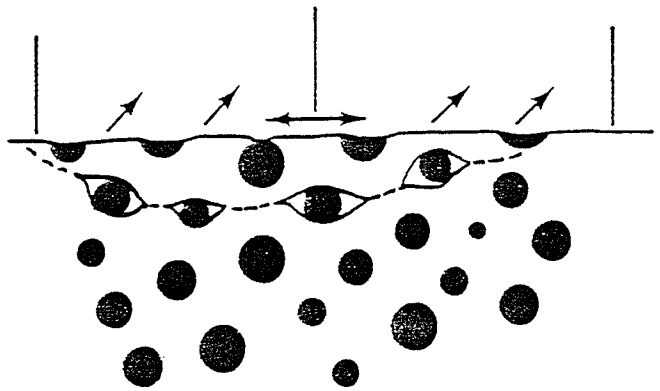

Fig 2.13 Schematic diagram showing the delamination process in abrasive wear of metal-matrix composites containing hard particles[86]

CHAPTER 3 EXPERIMENTAL PROCEDURE

3.1 Material

Since the wear tests in this research are of a ball-on-block type, there are two kinds of materials involved. 52100 steel ball was used as the slider. It has a microstructure of tempered martensite with a hardness of HRC 60. The diameter of the steel ball is 10mm.

Aluminum silicon alloy composite-A356 + 20%vol. SiC particles in the as cast condition supplied by Canmet was used as the block material. This composite was produced by a remelting method followed by permanent mold casting. It was received in the form of a 15cm×30cm×3cm cast plate.

3.2 Specimen Preparation

3.2.1 Wear Test Samples

A cutter with a slow-speed diamond blade saw was used in cutting the reciprocal sliding wear test samples from the cast plate. A coolant was applied during the whole cutting process to prevent overheating. Samples in the form of 50mm×20mm×6mm blocks were obtained. Before polishing, the wheels used were carefully cleaned. A new cloth was used at the beginning of the polishing operation. Rough polishing was done on SiC paper, starting with 120 grit and finishing with 600 grit. Water was used as the coolant. Fine polishing was done on a wheel pasted with diamond short-nap synthetic rayon cloth (Microcloth), beginning with 3μm and finishing at 0.25μm. In each step of the fine polishing, the wheel was properly lubricated with kerosene. At initial stages, slow to medium wheel speed and heavy pressure were used. This stage lasted about 5 minutes. After initial polishing, the diamond paste was renewed, the wheel speed increased and the specimen pressure decreased. The polishing continued with high wheel speed and light

pressure for about 10min or until microscopic examination showed that all grinding scratched had been removed. In between each step, the specimen was cleaned to remove the residual dirt from its surface. After final polishing, the thickness of the specimen was about 5mm. Reciprocal wear tracks were made on the 50mm×20mm sides of the specimen.

3.2.2 Optical Metallography and Hardness Test Specimens

To characterize the bulk cast composite, hardness tests and examination of microstructure were performed on three sections (as shown in Fig 3.1)-S_1, S_2 and S_3, in order to get a microstructure in all three dimensions of this composite material. To make an optical metallorgraphy specimen, the bulk cast composite was sectioned in a similar way to the wear test specimen. The section was then mounted in bakelite and mechanically polished using silicon carbide paper to 6μm, diamond paste and aluminum oxide powder to a final surface finish of 0.05μm. Etching was performed with Keller's Reagent (2ml HF (48%) + 3ml HCl (Conc) + 5ml HNO_3 (Conc) + 195 ml H_2O).

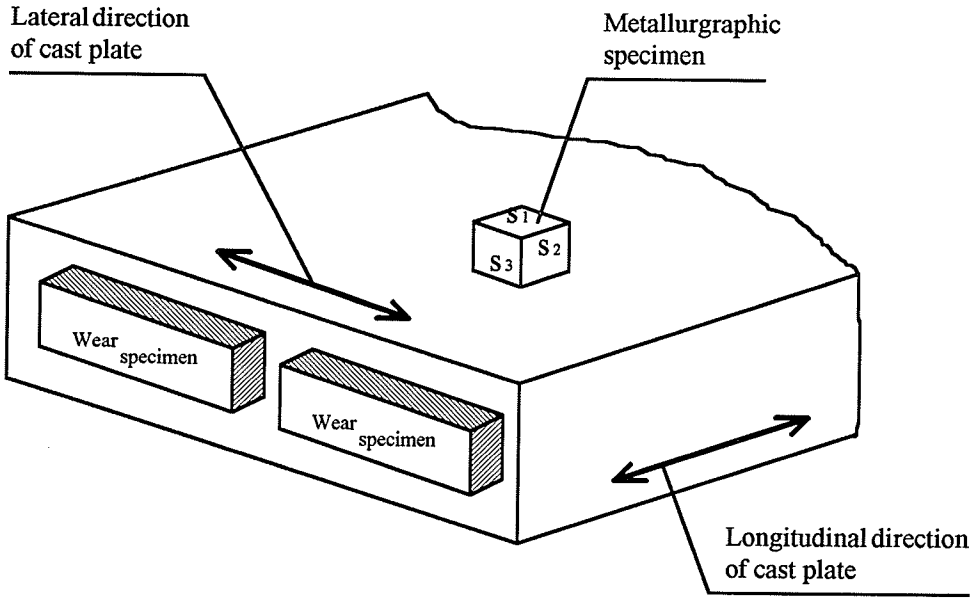

Fig 3.1 Locations of wear specimens and optical metallurgraphy specimen in bulk composite material

Hardness tests were performed on the optical metallurgraphy specimens. The optical microscopy and the scanning electron microscopy were performed on same specimen.

3.2.3 Scanning Electron Microscopy Specimens

Scanning electron microscopy specimens were required for studying the surface morphology of wear tracks, cross-sections, longitudinal sections of wear tracks, and wear debris. These samples were cut from selected wear samples of the composite block specimens (as shown in Fig 3.2).

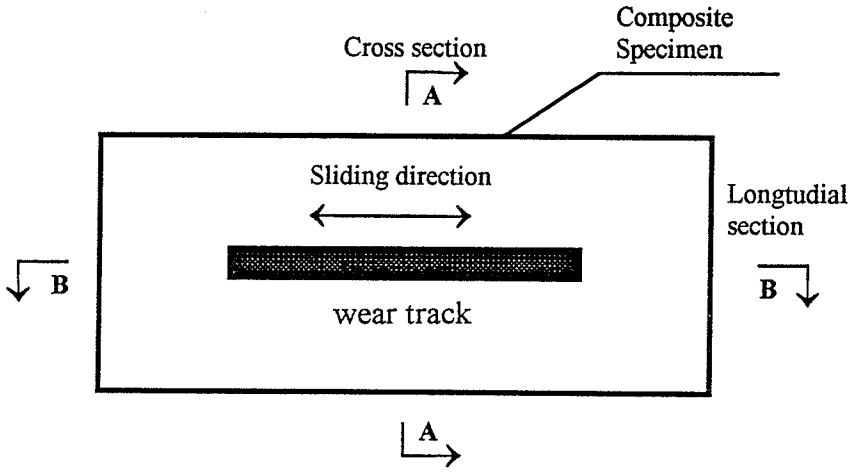

Fig 3.2 Scanning electron microscopy specimens

For cross sections, slices perpendicular to the wear direction were taken from the wear tracks. For longitudinal sections, slices parallel to the wear direction and running through the centers of the track were produced. Sectioning was done by a slow-speed diamond blade saw. To prevent the surface layer on the wear track from falling apart from the base, an electroless coating of nickel was applied to the specimens by Edgemet before mounting specimens in bakelite. The operating procedure for Edgemet is shown in Table

3.1. Specimens were then mounted in bakelite and polished to 0.05 μm finish following the same procedure as used for optical metallography specimens.

Table 3.1 Operation parameters for Edgement

Step	Purpose	Bath composition	Comments	Approx. time
1	Cleaning	Acetone	Use gentle agitation	2 min.
2	Cleaning	One-half pound of sodium hydroxide (NaOH) in 1 qt. water	Save and re-use. Hold specimen with clamp	2 min.
3	Cleaning	Pre-clean, full strength	Save and re-use	20 sec.
4	Application of EDGEMET	Equal parts of Solution A and Solution B - Minimum amount 75 ml of each	Use at approx. 185 °F - Use only once	2 hours

After the wear tests, bulk specimens were cleaned in a ultrasonic vibrator to remove loose debris and residual lubricant on the track surfaces for SEM examination. In addition to the cleaning in acetone, the lubricated composite specimen and sliders were also cleaned in trichloroethane.

Wear debris was collected and then glued to a flat and clean copper plate by conductive carbon paint for SEM observation.

3.3 Wear Testing

3.3.1 Reciprocal Wear Test Rig

The operating parameters of this wear test rig are shown in Table 3.2.

Table 3.2 Wear test rig operating parameters

Parameters	Value
Cycles per minute	0~415
Stroke length (mm)	30
Sliding distance per cycle (mm)	2×30
Angle to ground	10°
Atmosphere	Laboratory air
Humidity (%)	38~40

All of the wear tests were performed on a custom-fabricated wear test rig [89] which was originally built to simulate the reciprocal sliding condition in a internal combustion engine. Both unlubricated and lubricated reciprocal sliding wear can be done with various applied loads. The wear test rig is illustrated in Fig 3.3.

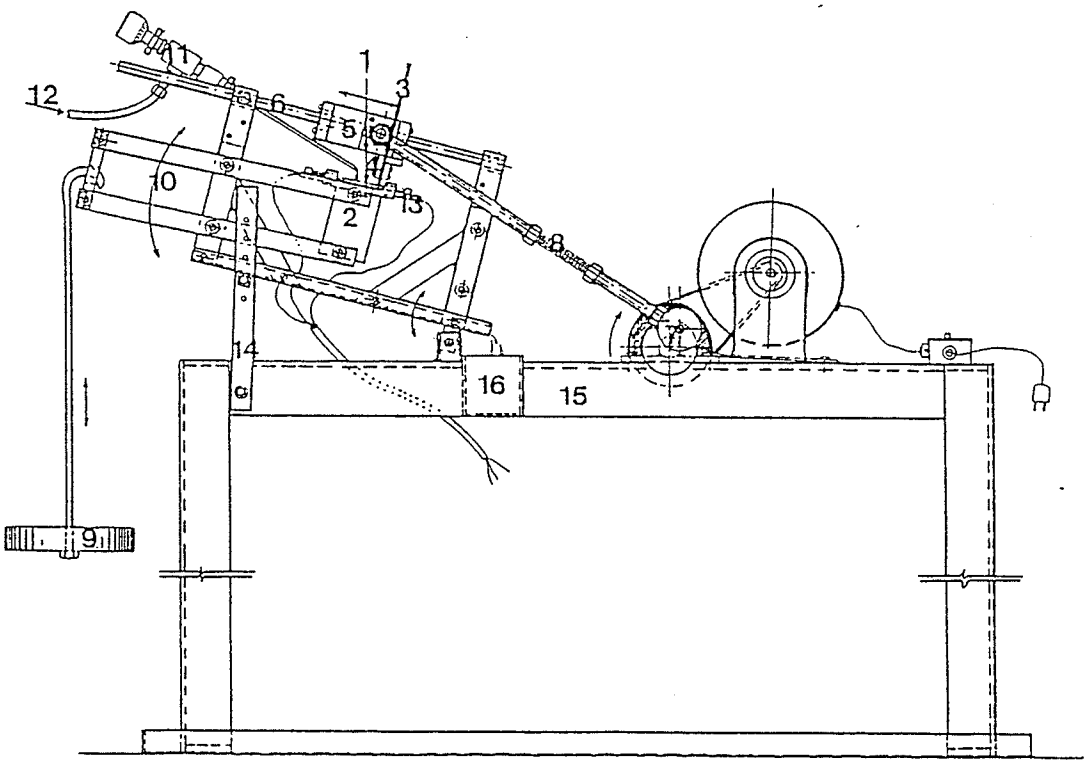

Fig 3.3 Wear test rig

(1) Specimen, (2) Specimen holder, (3) Bearing steel ball, (4) Ball holder

(5) Slider, (6) Two shafts, (7) Driving motor, (8) Connecting rod

(9) Applied load, (10) Parallel arm - linkage mechanism

(11) Needle value controlling lubricant drop rate

(12) Rope connected to lubricant reservoir, (13) Heater

(14) Support bars, (15) Frame, (16) Reservoir collecting used oil.

3.3.2 Dry Wear Test Parameters

The operating parameters for the unlubricated wear test in this research are shown in Table 3.3. For each wear test, a new slider (ball) was used. Two or three tracks were made on each side of a specimen. The distance between each two tracks was about 3mm so that they did not interact with each other. Before each new wear track was produced, the whole block specimen was cleaned in the procedure as described earlier in this chapter. No debris was left from the former tracks on the specimen surface to interfere with the following wear tests on the same surface.

Table 3.3 Dry sliding wear testing parameters

Parameter	Value
Normal load	9.8N
Number of sliding cycles	10, 50, 100, 500, 1000, 2000, 3000, 5000, 10,000, 20,000, 50,000
Frequency	2×120 strokes/min.
Length of stroke	25mm
Surrounding atmosphere	laboratory air
Temperature	room temperature in the Lab
Humidity	38 - 40%

3.3.3 Lubricated Sliding Wear Test Parameters

The testing parameters for lubricated wear tests are listed in Table 3.4. Higher loads compared to dry tests were applied. The lubrication rate was adjusted by the oil valve as shown in Fig 3.3. Before sliding, the whole surface of the block specimens were covered with the lubricant.

Table 3.4 Lubricated wear testing parameters

Parameter	Value
Normal load	9.8N, 19.6N, 39.2N, 78.4N
Number of sliding cycles	100, 1000, 5000, 10,000, 100,000, 500,000
Frequency	2×120 strokes/min.
Length of stroke	25mm
lubricant drop rate	0.005ml/min
Surrounding atmosphere	laboratory air
Temperature	room temperature in the Lab
Humidity	38 - 40%

3.4 Weight Loss Measurement and Microstructural Examination

3.4.1 Weight Loss Measurement

Weight loss of a worn specimen corresponding to a wear track is defined as the weight difference of the specimen before and after the wear track is produced. All weight losses were obtained by weighing on a electronic scale (Fisher Meter H18) to an accuracy of 0.1mg. The scale was calibrated with a standard sample before each measurement was made.

3.4.2 Optical Microscopy and Microhardness Test

Optical microscopy was performed to characterize the microstructure of the bulk casting composite. Factors such as the appearance of aluminum silicon matrix in the composite, aluminum silicon eutectic structures and silicon carbide particles were considered. The cross sections and longitudinal sections of wear tracks were also examined especially for the redistribution of silicon carbide particles and the deformation

in the matrix. The width and depth of wear tracks were measured by optical microscopy with an affiliated lens. The optical microscopy was done on a Nicon-Epiphot-TME optical microscope at magnifications from 50× to 1000×. A 35mm photographic system was used in recording images.

3.4.3 Scanning Electron Microscopy

Scanning electron microscopy with its enhanced magnification, resolution and greater depth of focus was used extensively in studying wear scars, debris, and near-surface microstructure on both cross and longitudinal sections. It was the most important tool in studying the SiC particles behavior and wear mechanism in this research. Specimen preparation for SEM was described in 3.2.4. In this research, all scanning electron microscopy was performed using a Jeol J×A-840 scanning microscope normally with an acceleration voltage of 15.0KV. Lower acceleration voltages, such as 8.0KV, were used when studying silicon carbide particles at high magnifications because silicon carbide particles are not electrically conductive and discharging often occurs. SEM images were recorded on a polarized film 55 (with negative) or polarized film 52 (without negative).

3.4.4 Energy Dispersive X-ray Analysis

Energy dispersive X-ray analysis was used to investigate material transfer either from the composite to the slider or from the slider to the composite. It was also applied in the examination of silicon carbide particle redistribution on both wear track surfaces and the near-surface region on cross sections. Micro-area chemical compositions were obtained by the spot mode operation of energy dispersive system. Element distributions were determined using X-ray mapping (IPP operation mode). EDS results were recorded by taking pictures directly from the screen for X-ray mapping or by printing out the chemical composition and diffraction spectrum on a printer. The data or images were also stored on a floppy disk.

3.5 Quantitative Metallography

Quantitative metallography was used to statistically analyze the SiC particle size and distribution in the A356-20%vol. SiC particle composite before and after wear tests.

Image analysis was performed using a LEITZ/TASIC automatic image analyzer. The image analysis was not performed directly on the metallographic sample but on the X-ray mapping image of the element Si to improve the contrast between SiC particle and the matrix. The images were first recorded on 667-Polaroid photographs from the EDS monitor which were then used for image analysis. TIP (TAS Instruction by Pen) operation was used to perform the global diameter-distribution. The analysis results were outputted in the form of a histogram and display of values by an Epson printer. Five to six bulk areas were chosen to get an average value for each wear condition.

3.6 Wear Surface Profile Examination

A wear surface profile is referred to as the configuration of the cross-section of a wear track. A surface profile measuring device, Surtronic 3P, was used to produce this. By studying the wear surface profile of a wear track, the pattern of plastic deformation and wear mechanism of the SiC particle composites might be related to the sliding cycles and applied load.

3.7 Calculation of the contact Stress

The contact stress between the composite specimen and the slider is the applied normal load divided by the contact area. During a wear test, the normal load was unchanged, but the contact area which was measured by the optical microscope kept changing. So the contact stress changed with different sliding cycles. The changing contact area would in turn lead to the change in contact stress.

CHAPTER 4 EXPERIMENTAL RESULTS AND DISCUSSION

4.1 Characterization of A356-20% SiC Particle Composite

4.1.1 Microstructure of the Composite before Wear

In a received state, the cast A356-20% SiC particle composite was examined using both optical microscopy and scanning electron microscopy. Since silicon carbide particles are much harder than the aluminum-silicon alloy matrix, SEM which has a greater depth of focus can give a better image of the composite surface. As shown in Fig 3.1, three perpendicular planes in the cast MMC plate were examined. It was found that there was no difference in the microstructures on these planes. The cast composite is essentially isotropic in microstructure. The SEM image of the cast bulk composite is shown in Fig 4.1, which is an unetched polished surface (polished to 0.25μm). Clusters of SiC particles are revealed. It can be seen that SiC particles do not distribute uniformly on the whole polished surface. It seems that silicon carbide particles tend to locate in some preferable sites. Another observation made was that the locations with silicon carbide particles were less polished, but the locations without silicon carbide particles were polished deeper. Fig 4.2 is the composite sample after a deep etching with Keller's regent. Apart from the silicon carbide particles, a net-work structure - Al/Si eutectoid has shown up. It can be seen that silicon carbide particles concentrate in the intercellular regions of eutectic structure. During the solidification process of casting, aluminum silicon solid solution (α phase) solidified first, and the residual liquid at about 577°C transformed to Al/Si eutectoid. The SiC particles were rejected by the solidification meniscus and pushed to the intercellular regions. The distribution of SiC particles thus got clustered along the converging dendrites [90]. Solidification rate is important in determination of the cell size. Models for the particle entrapment have been developed by some investigators [90, 91].

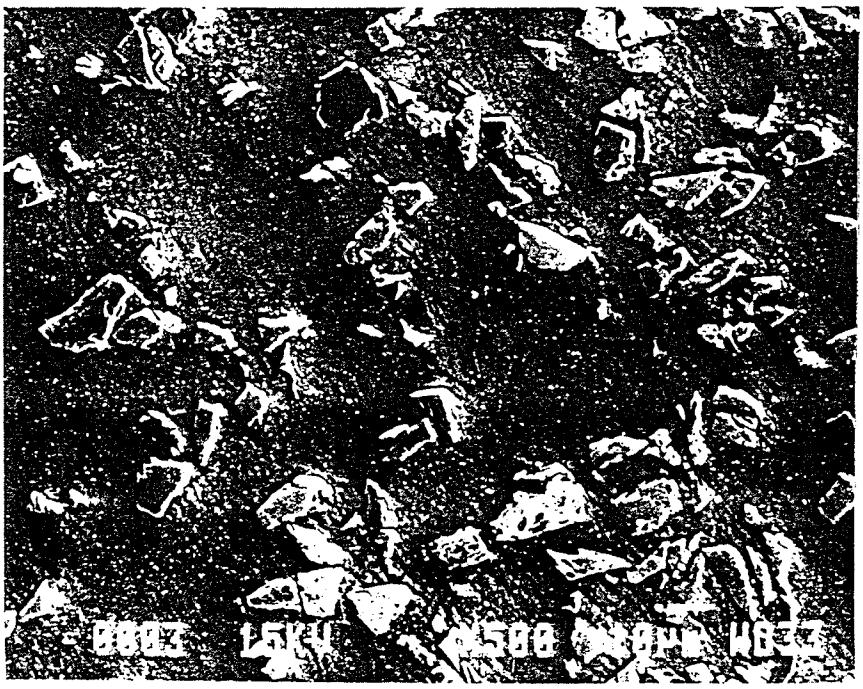

Fig 4.1 Polished surface of A356-20%vol. SiC particle composite

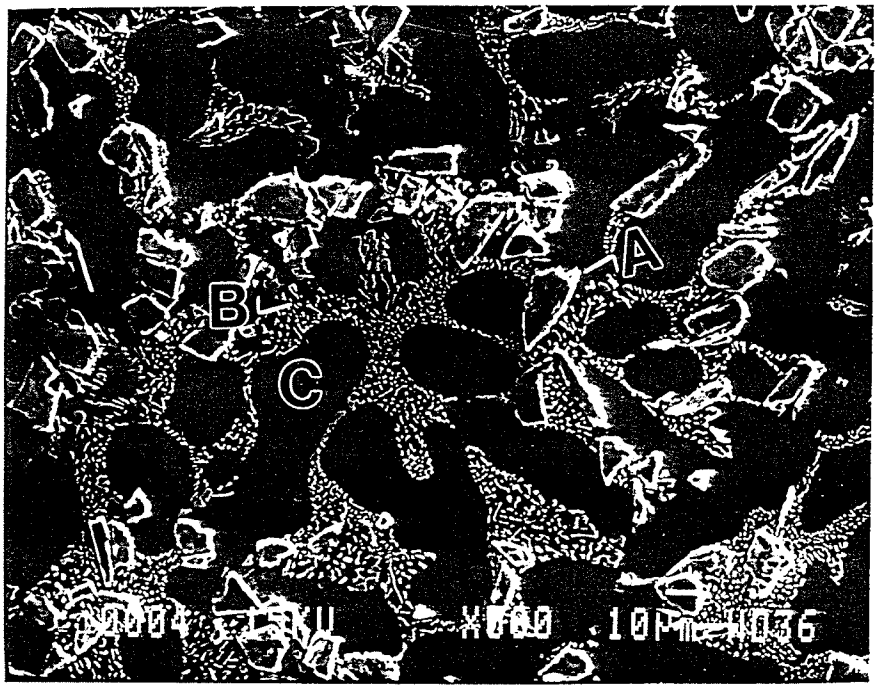

Fig 4.2 Etched surface of A356-20% vol. SiC particle composite (Etchant-Keller's Regent)
(A - SiC particle B - eutectoid C - α-Al)

4.1.2 Hardness Tests

Micro-hardness (DPH) tests and Vickers's hardness tests were performed for the measurement of hardness values of different phases in the composite and the bulk hardness of the composite respectively. The results are listed in Table 4.1. It is evident that the SiC particles have the highest hardness, aluminum-rich phase (α-solid solution) the lowest hardness, and the Al-Si eutectic net work has an the "intermediate" value. The hardness of the bulk composite is in between that of the α solid solution and the Al-Si eutectic. Since the diagonal of the indentation in the Vickers's hardness test is about 300-400 μm, which is much greater than the dimension of the SiC particles, the hardness value obtained should represent the average hardness of the bulk material. Each reading in Table 4.1 is the average of ten measurements.

Table 4.1 Hardness of SiC particulate reinforced A356 Al-Si alloy

Phase name		α solid solution	Al-Si eutectic	SiCp	Al/Si+SiC
Micro (DPH) Hardness	load=25g	71.9	143	>460	----
Vickers's Hardness	load=10kg	----	----	----	93.6

4.1.3 SiC Particle Size and Distribution

The measurement of SiC particle size and the investigation of their distribution were performed using an image analyzer. It is difficult to analyze silicon carbide particles either from the metallographic sample or optical microscopy image and SEM image due to their poor contrast. In order to solve this problem, the EDS technique was used. A SEM image of the bulk composite was first obtained (Fig 4.2 (a)), then the X-ray mapping of the element aluminum and silicon was done by EDS from the same area. A low

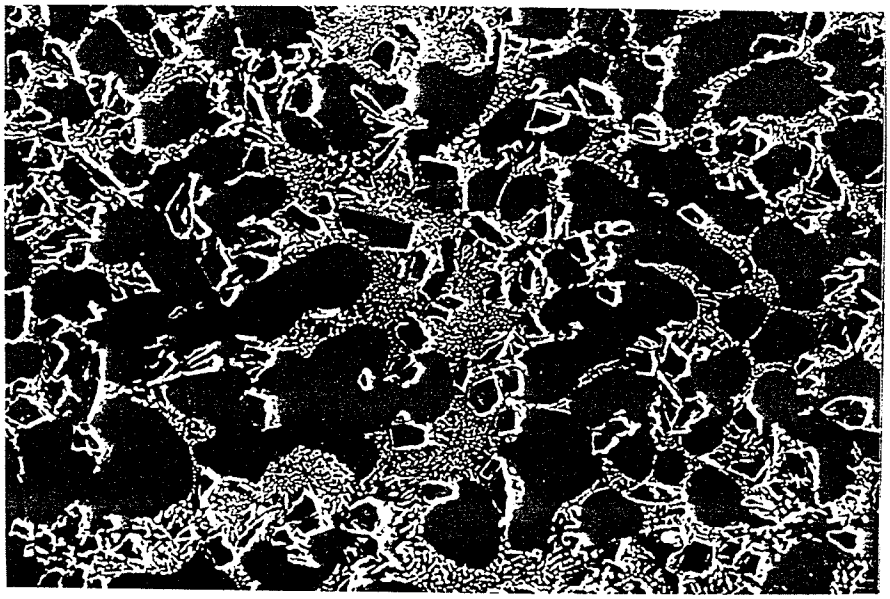

(a)

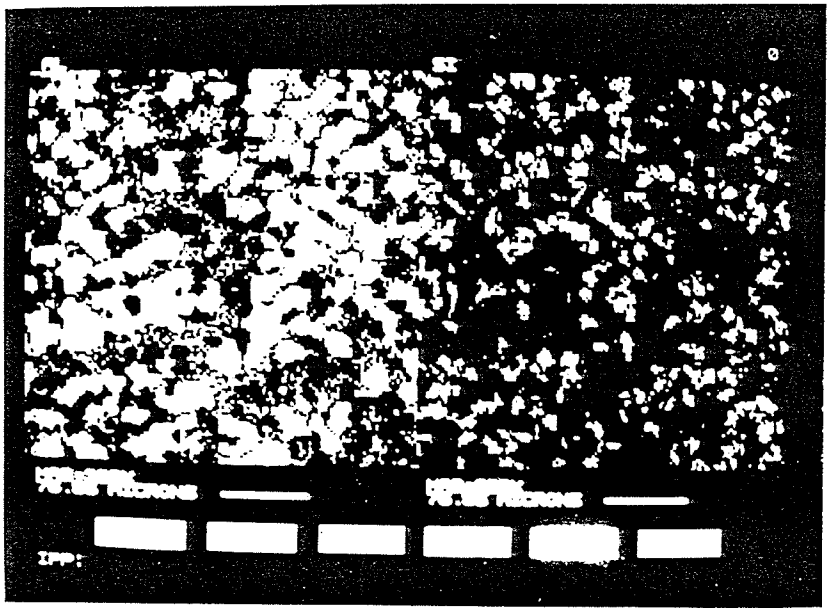

(b)

Fig 4.3 Microstructure of A356-20%vol. SiC particle composite

(a) SEM image (b) X-ray mapping of Al (left) and Si (right)

magnification. SEM image and the corresponding EDS images of X-ray maps of Al and Si are shown in Fig 4.3. In the X-ray mapping image of element aluminum, the brightest areas are α solid solution. All the SiC particles shown in Fig 4.3 (a) appear as totally dark in Fig 4.3 (b). The areas of aluminum silicon eutectic net-work are darker than the α solid solution but brighter than SiC particles. In the X-ray mapping image of the element silicon, only the image of SiC particles is shown. Very good contrast between SiC particles and the matrix was thus obtained. Therefore, X-ray mapping image of silicon can be used to analyze SiC particle size and distribution.

The results of image analysis are shown in Fig 4.4. The average size of the SiC particles in the composite is 9.7μm.

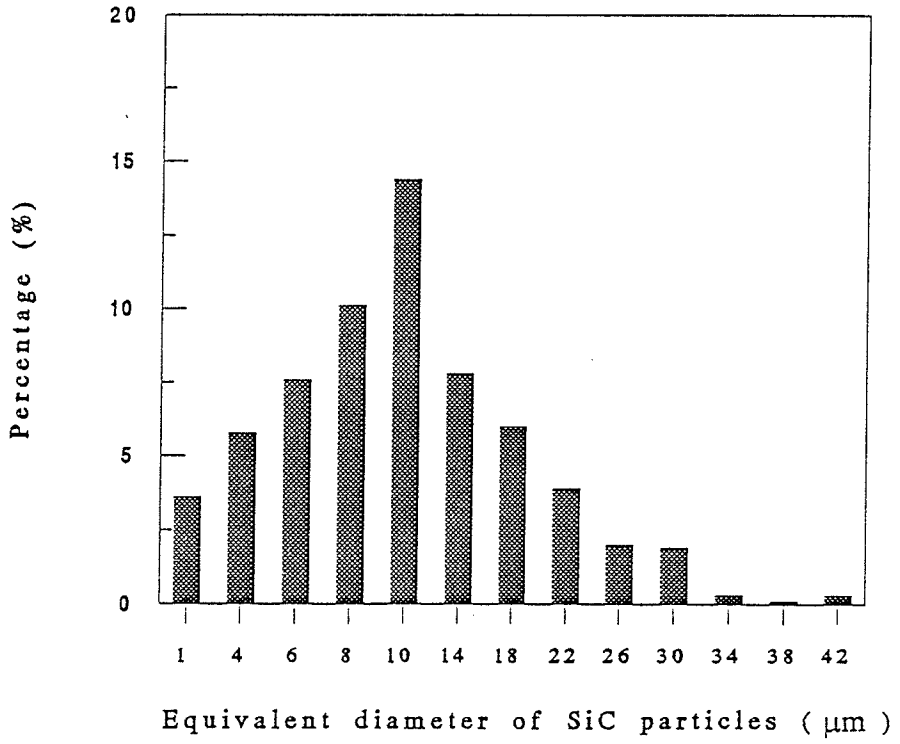

Fig 4.4 SiC particle size distribution

4.2 Reciprocal Dry Sliding Wear Tests

4.2.1 Change in Weight Loss with Sliding Cycles

To obtain the weight losses on a worn composite specimen and a ball, both of them were weighted before and after the wear test by a electronic scale. An average of three readings was obtained at each sliding cycle.

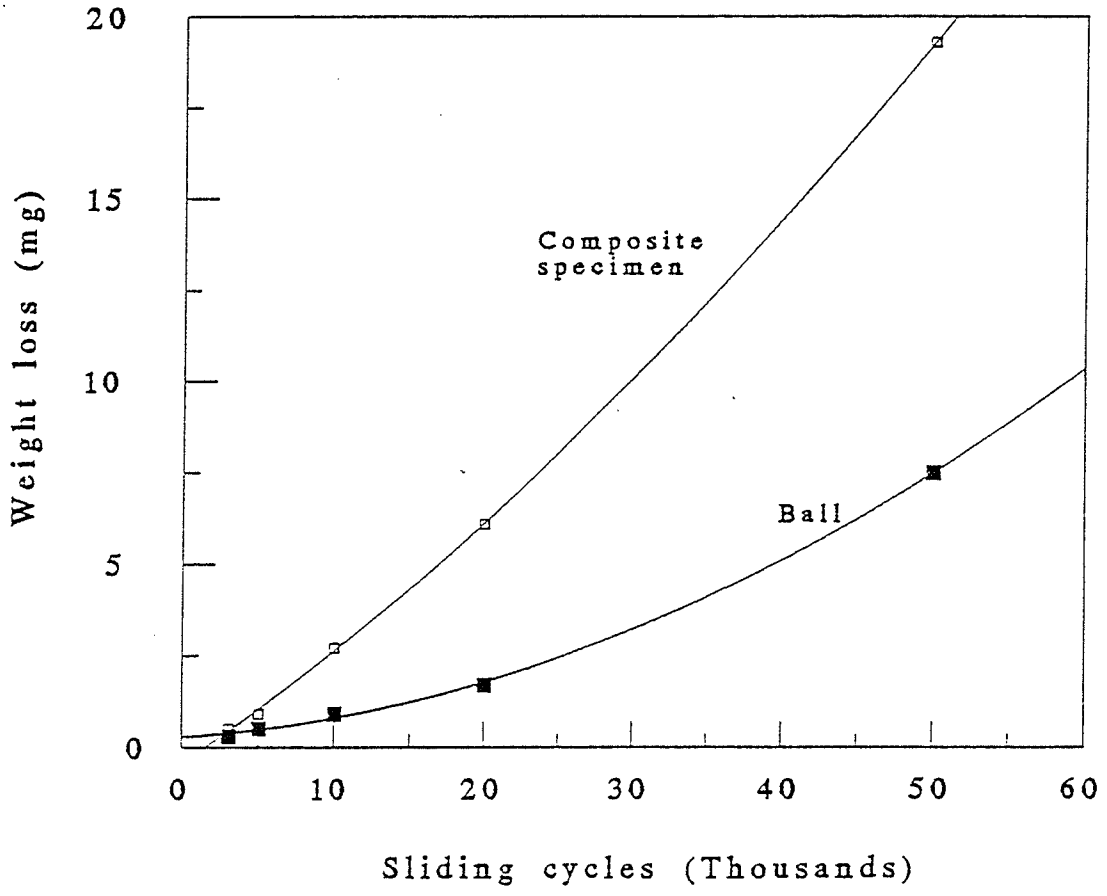

Fig 4.5 Effect of sliding cycles on weight loss (load~9.8N)

Fig 4.5 shows the change in weight loss with the increase in wear cycles for both of the composite specimens and the bearing steel balls. Under a constant load (9.8N), in general, the weight loss increases when the number of wear cycles becomes larger. At a given cycle, the weight loss of the composite specimen is one or two times greater than that of bearing steel ball. Moreover, the slope of the weight loss curve for the composite specimens is also greater than that of the sliders.

When a wear test started, the process went on smoothly at initial stage (number of cycles < 100). Then, more noise together with vibration was produced. This process was found to occur at wear cycles of 500-5,000. As wear cycles exceeded 20,000, the sliding wear process became smooth again and the noise level became lower as well.

4.2.2 Change of Wear Track Profile with Wear Cycles

At a constant applied load of 9.8N, wear cycle ranged from 100 to 50,000. The surface profiles of these wear tracks are shown in Fig 4.6. After sliding 100 cycles, only a little rough scar was seen, the wear track was very shallow and not much composite material had been worn away. From 100 to 3000 cycles, the track depth increased rapidly. At the same time, plastic deformation and material loss was involved. The surface profile, including both depth and width of the track, did not change very much when wear cycles increased from 3000 to 5000. From 5000 and 10,000 cycles, plastic deformation and accumulation of material at the sides still existed. Moreover, both the width and depth of the wear track increased. The bottoms of the wear tracks were not flat when sliding cycles were below 10,000. However, starting approximately from 10,000, the track bottom became more flat and there was less plastic flow of material to the sides. As wear cycles increased to 50,000, the track bottom became totally flat and very little plastic deformation could be observed. At this time, the wear track almost doubled its size, and its width and depth remained the same in the value about 4.5μm.

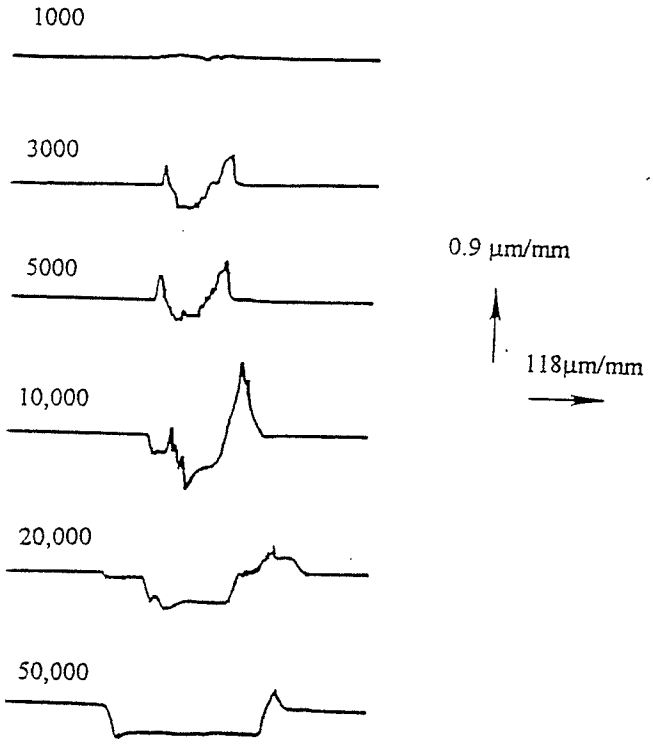

Fig 4.6 Profile of dry wear tracks after different sliding cycles (load-9.8N)

4.2.3 Microscopic Study of Wear Track Morphology

4.2.3.1 Surface morphology of normal wear track

Under a constant applied normal load at 9.8 N, track appearance in its normal part (not including the ends) was investigated with the change in wear cycles. It was found that track appearance varied significantly when sliding cycles increased from 10 to 50,000. The whole process can be divided into the different regions as discussed below.

0-100 sliding cycles

Fig 4.7 shows the typical track appearance during the initial period of sliding wear. The track was examined after 10 strokes of sliding. The matrix was formed to be plastically deformed. Nearly the whole track was covered by the deformed matrix, and no exposed SiC particles were observed on the surface of the wear track. Some of the SiC particles covered by the plastically deformed matrix continued to stay at the original location and worked against the further deformation of bulk material (Marked U). Some SiC particles, (marked V), wrapped by deformed matrix, moved in the direction *b* and stopped at this point because of the build-up of deformed matrix in front of it; leaving behind a groove in the matrix (Fig 4.7 b).

As sliding cycles increased to 50, almost the whole track was covered by the evenly deformed matrix (Fig 4.8). Local scoring or grooving was effectively reduced and SiC particles were smeared over by the deformed matrix. Neither the bare SiC particles in original size nor the fragmented SiC particles were observed on the surface. X-ray mapping (Fig 4.8 b) of aluminum and silicon showed that most of the smeared SiC particles still kept their original dimensions underneath a very thin layer of deformed matrix (Marked P). This suggested that the SiC particles were not crushed and fragmented.

Both Fig 4.7 and Fig 4.8 showed no significant plastic flow at the edges of wear tracks. The wear track on ball is illustrated in Fig 4.9 (a) and (b), corresponding to 10 sliding wear cycles. Most part of the track was covered by a thick layer of the deformed matrix, Al-Si, transferred from the block composite specimen, especially on the front side and back side in the direction of wear. Pure abrasive wear also took place on the wear track.

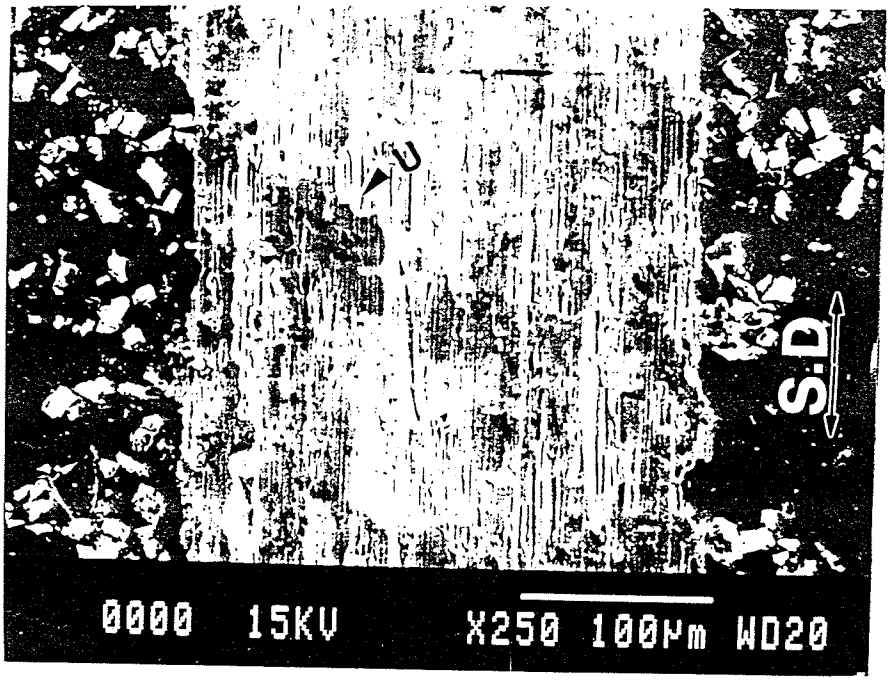

(a)

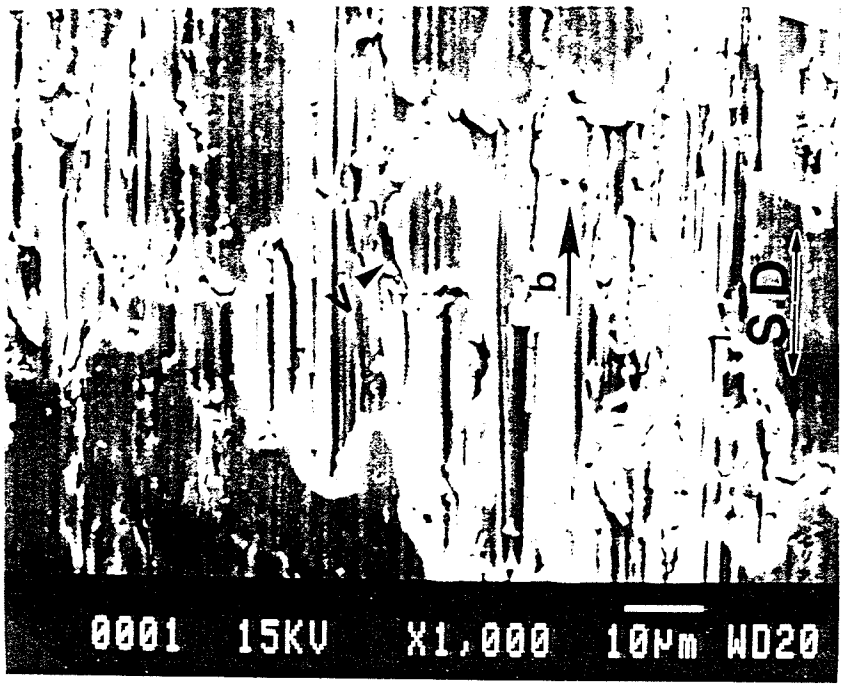

(b)

Fig 4.7 Wear surface of the composite after 10 strokes dry sliding wear

(a) ×250 (Marked U-smeared SiC particle)

(b) ×1000 (Marked V-wrapped and moved SiC particle)

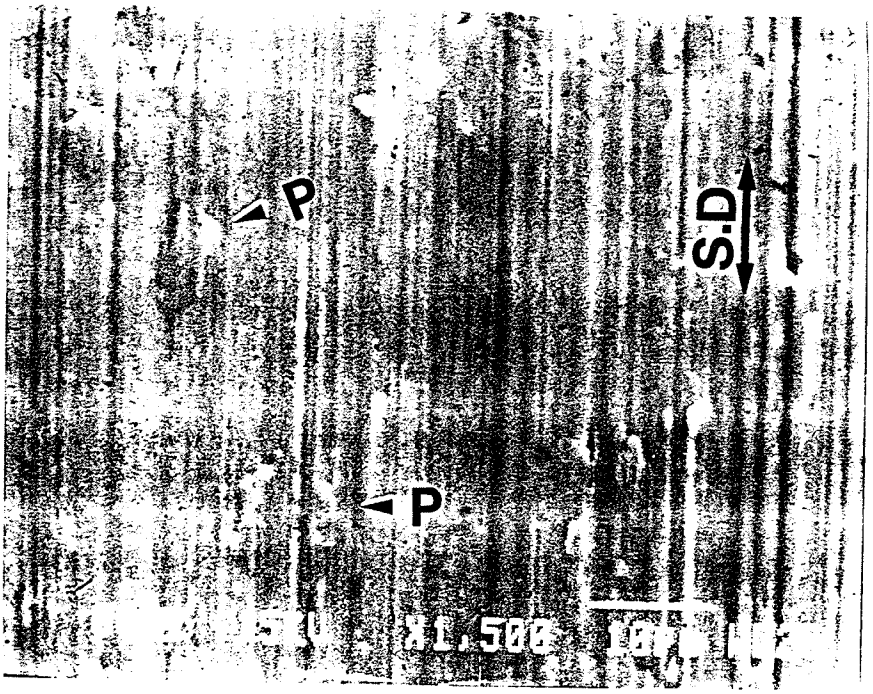

(a)

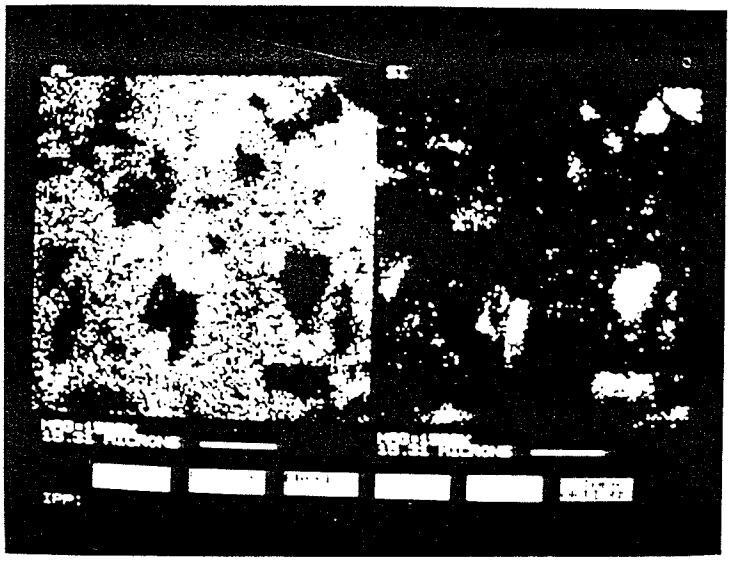

(b)

Fig 4.8 Wear surface of the composite after 50 strokes dry sliding wear

(a) SEM image ×1500 (Marked P-smeared SiC particles in integrity)

(b) X-ray mapping of Al and Si

(a)

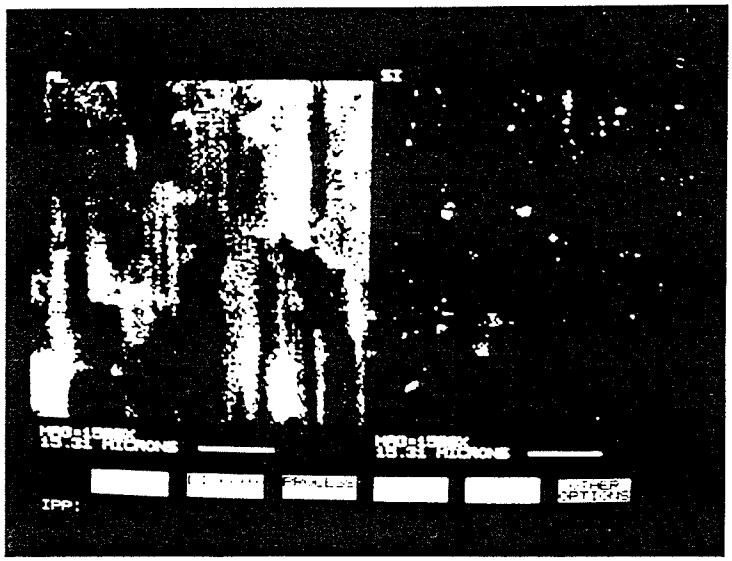

(b)

Fig 4.9 Surface of the steel ball after 10 strokes dry sliding wear

(a) SEM image (b) X-ray mapping of Al (left) and Si (right)

100-5000 sliding cycles

When sliding cycles increased above 100, severe plastic flow of the matrix could be observed at the edges (marked Q) of wear tracks and inside the tracks (Fig 4.10 (a)). The deformed matrix was squeezed by the slider (ball) and flakes were thus produced (marked P). The greater the number of sliding cycles, the more plastic flow was produced. The wear surface was also characterized by a large number of abrasive wear grooves along the wear direction (Fig 10(b)). Almost no surface cracks were observed after a sliding of 1000 cycles. However, as shown in Fig 4.11 (b, c), many fatigue cracks occurred on the wear surface at the sliding cycle of 3000, which were perpendicular to the wear direction.

Fig 4.11 (d) shows the result of X-ray mapping of the area corresponding to Fig. 4.11 (c). Comparing with the X-ray mapping results for the wear cycle of 50, some SiC particles are noted to be fractured and re-distributed. The wear surface is covered with a mixed layer of Al-Si/SiC particles which have fragmented. There appears to be a relationship between the location of these cracks and the sites of SiC particles. Fig. 4.11 (b) indicates that these fatigue cracks have propagated and subsequently induced delamination of the surface layer.

The wear track on the ball surface about 1000 strokes is illustrated by Fig 4.12 (a). Most part of the wear scar is covered by the transferred composite material from the block specimen. Plastic flow lines of the matrix along the sliding direction have occurred on this wear surface (Fig 4.12 (b)). As the number of strokes increased, the wear scar grew larger and the area covered by the transferred matrix became relatively smaller. Abrasion by SiC particles on the surface of steel balls and abrasive wear were noted (Fig 4.12 (b)). Ploughing and scouring by the abrading SiC particles on steel ball surface could also be observed (Fig 4.12 (c)).

Local delamination or spalling started to appear at about 4000-5000 strokes, and tended to increase with the increasing number of strokes (Fig 4.13). During these stroke

cycles, the surface of the composite was featured by the mixture of abrasive wear and delamination which appeared to have occurred at the sides of Al-Si eutectic/SiC colonies.

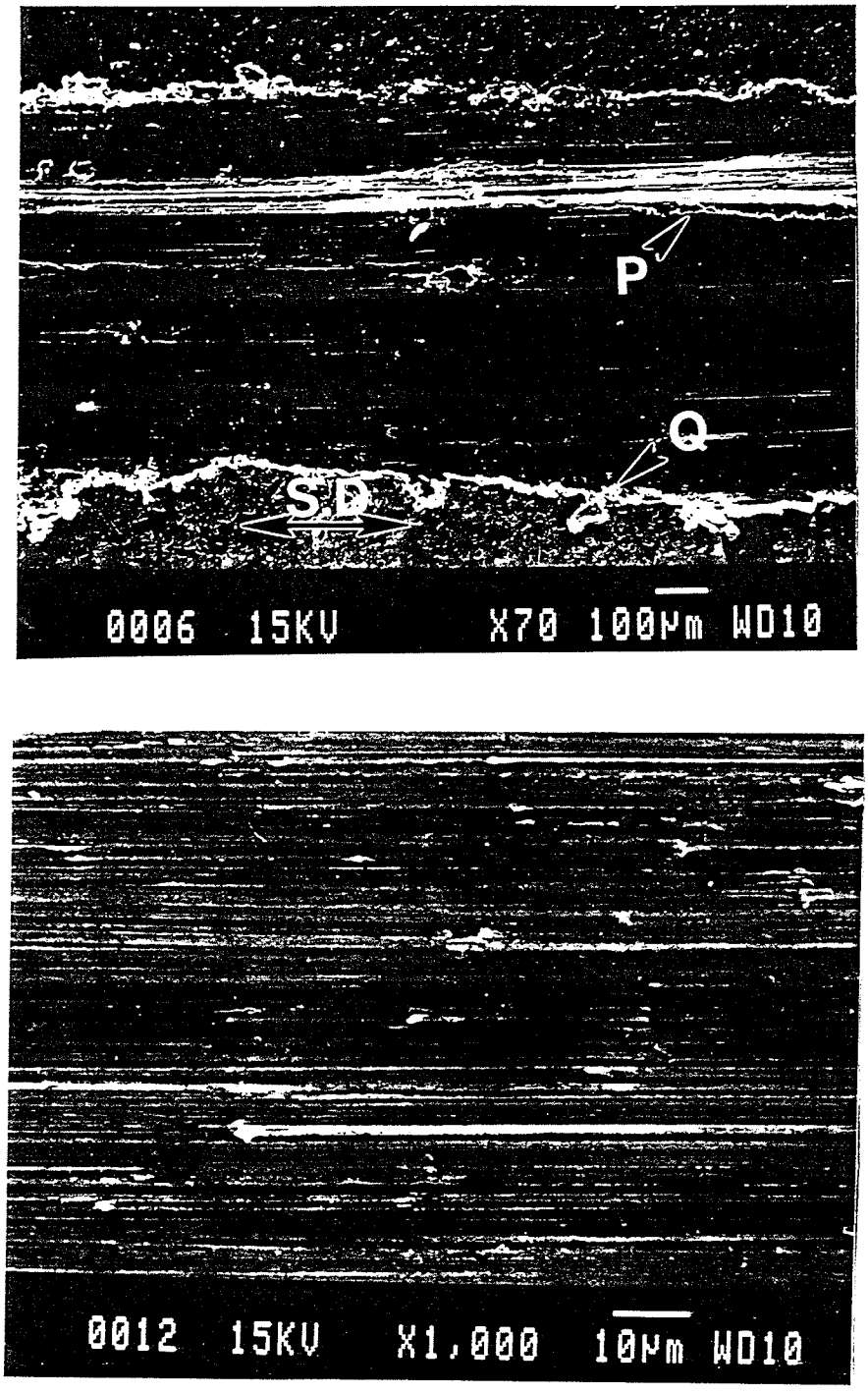

(a)

(b)

Fig 4.10 Wear surface of the composite after 1000 strokes dry sliding wear
(a) ×70 (b) ×1000

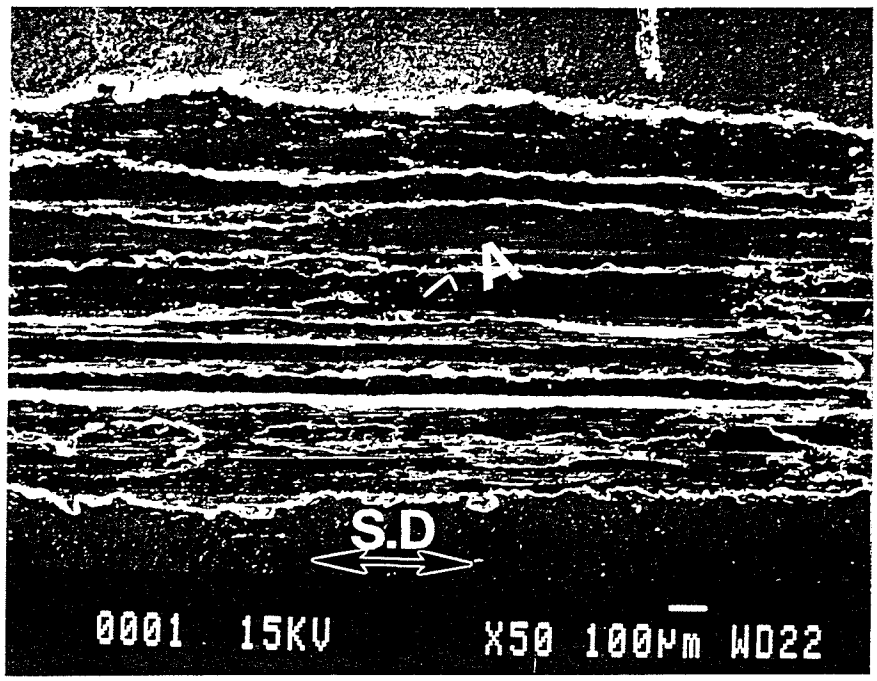

(a)

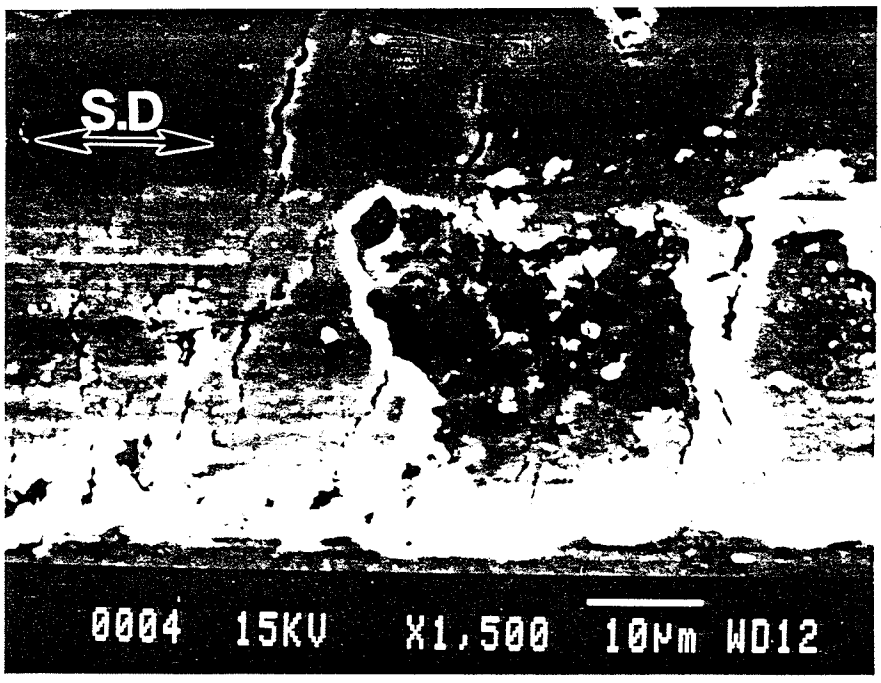

(b)

(See next page for figure caption)

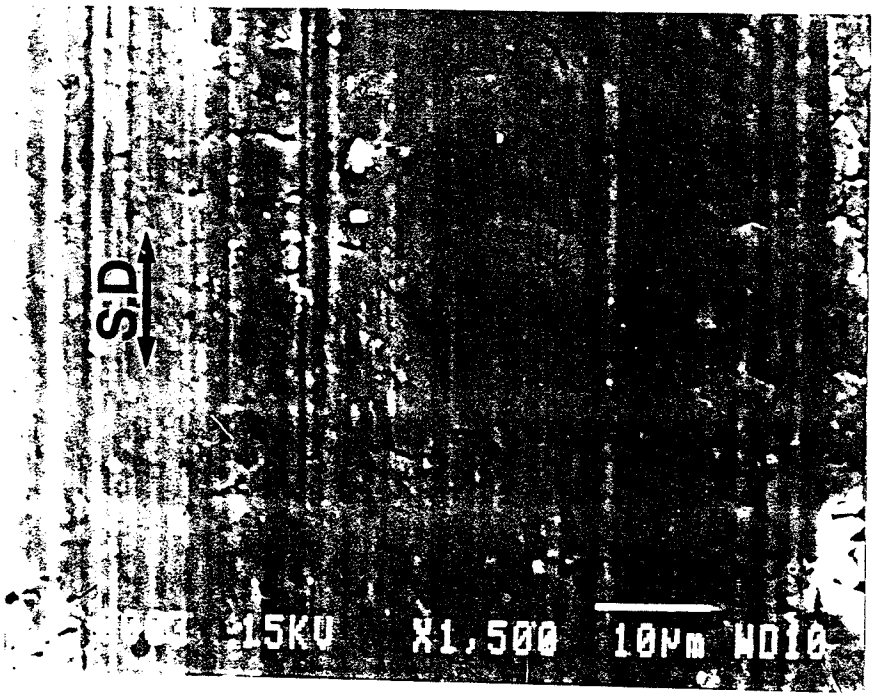

(c)

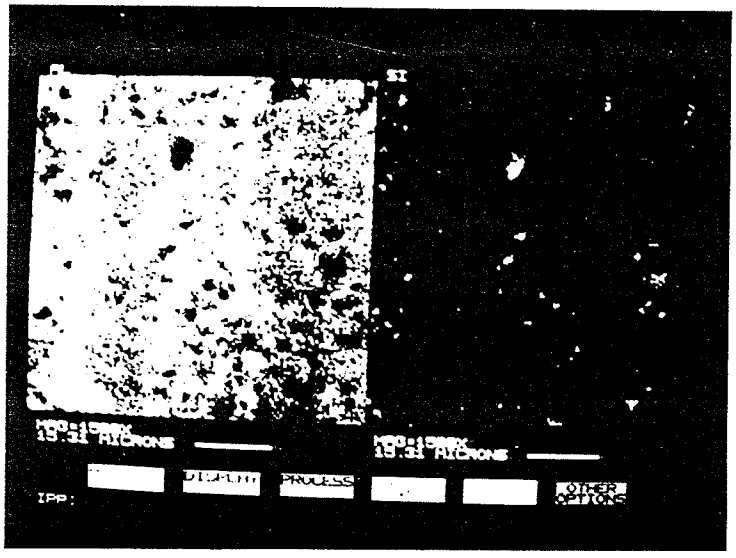

(d)

Fig 4.11 Wear surface of the composite after 3000 strokes dry sliding wear

(a) General view (b) Fatigue cracks and delamination (Area A in (a))

(c) Abrasive microgrooving

(d) X-ray mapping of Al (left) and Si (right) for the area shown in (c)

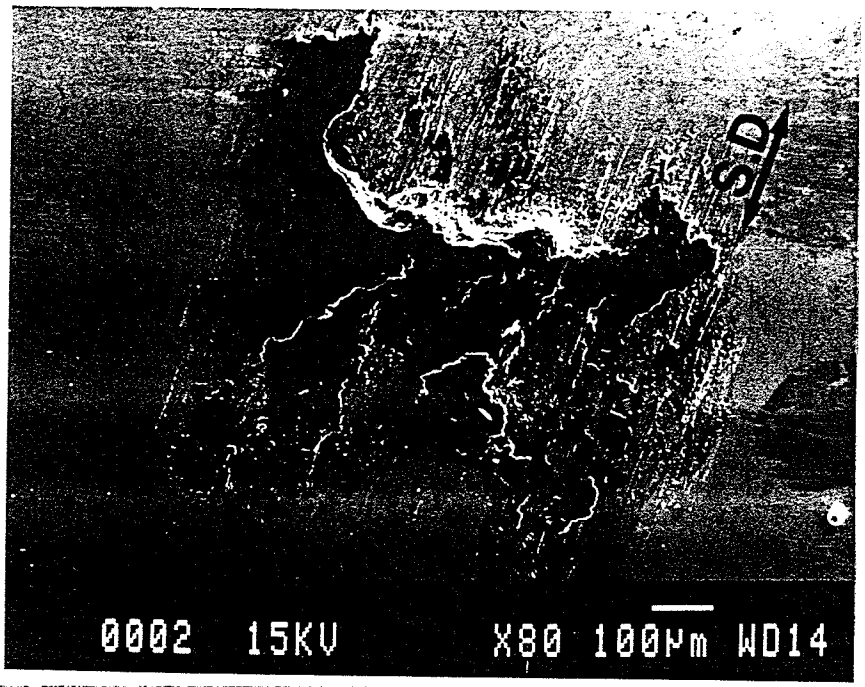

(a)

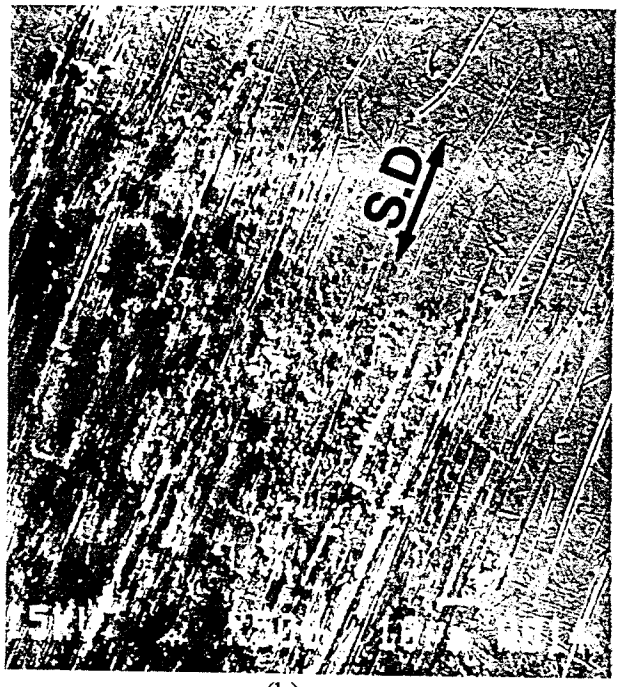

(b)

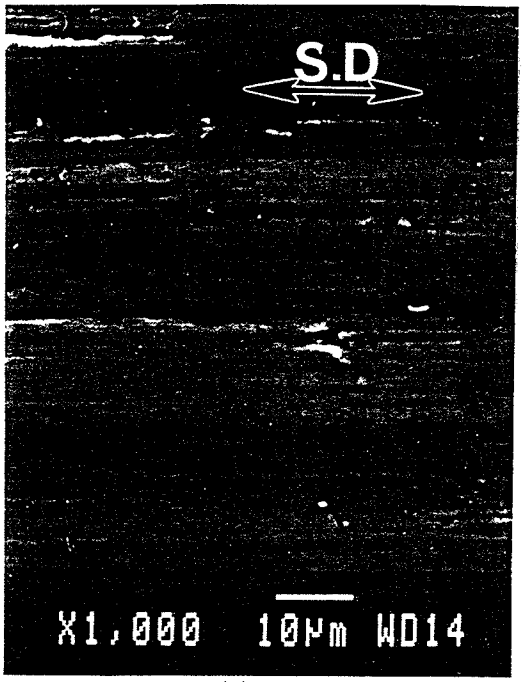

(c)

Fig 4.12 Wear surface of the steel ball after 1000 strokes dry sliding wear

(a) General view (b) Abrading and ploughing on ball

(c) Microgrooving on the transferred material

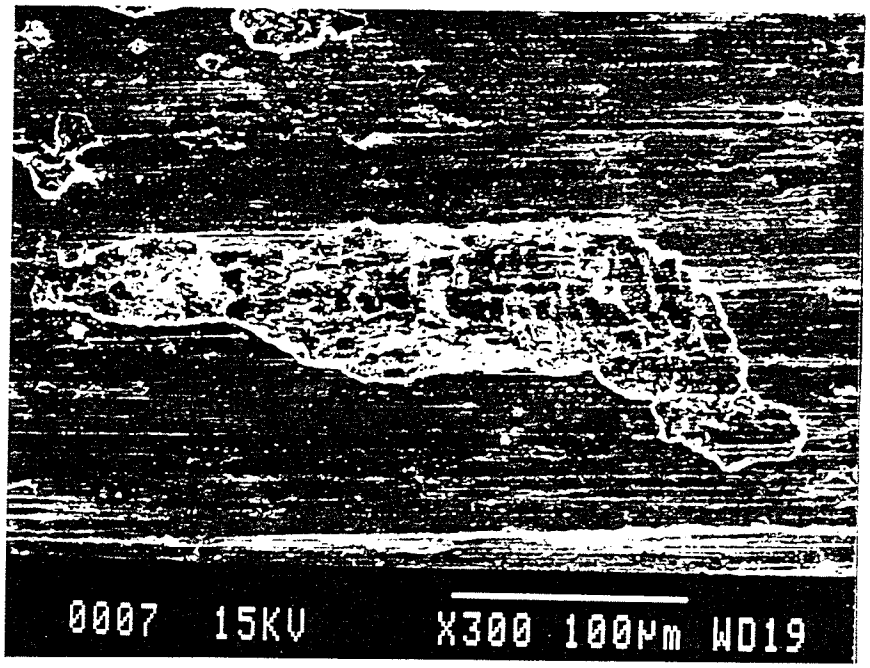

Fig 4.13 Wear surface of the composite after 5000 cycles dry sliding wear

20,000-50,000 sliding cycles

Above 20,000 sliding strokes, as shown in Fig 4.14, the morphology of these wear tracks shows two characteristics: cavities (marked A in Fig 4.14 (a)) and abrasive wear (marked B). Fragmented and rounded SiC particles were found in these cavities where delamination has occurred. Nearly half of the wear surface of the composite specimen is covered by cavities. Fragmented and rounded SiC particles were observed in these cavities (Fig 4.14 (b)). Abrasive wear only took place in the area with Al-Si solid solutions. (Fig 4.14 (c)). The wear track surface appeared smoother compared to that during small number of strokes.

The balls after the sliding of 20,000 to 50,000 strokes, experienced purely abrasive wear. Fig 4.15 shows an abrasive polished wear surface on the steel slider after wear 50,000 strokes. The whole surface is dominated by abrasive, marked A in Fig 4.15 (b), and the scouring, (marked B), made by the cross movement of SiC particles. No

exposed SiC particles could be observed on this surface, but small SiC particles wrapped by Al/Si matrix are present (Fig 4.15 (c)).

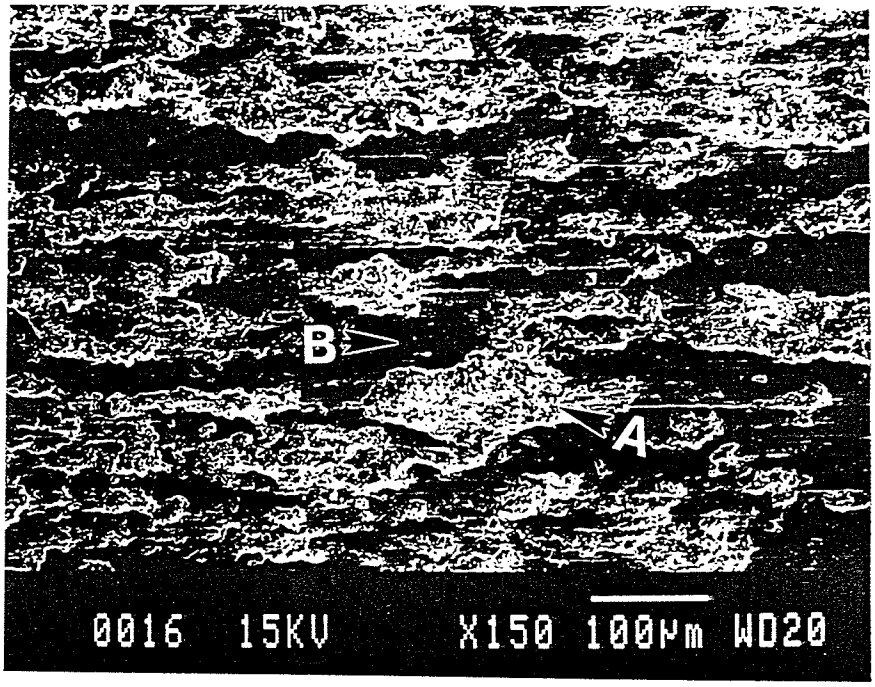

(a)

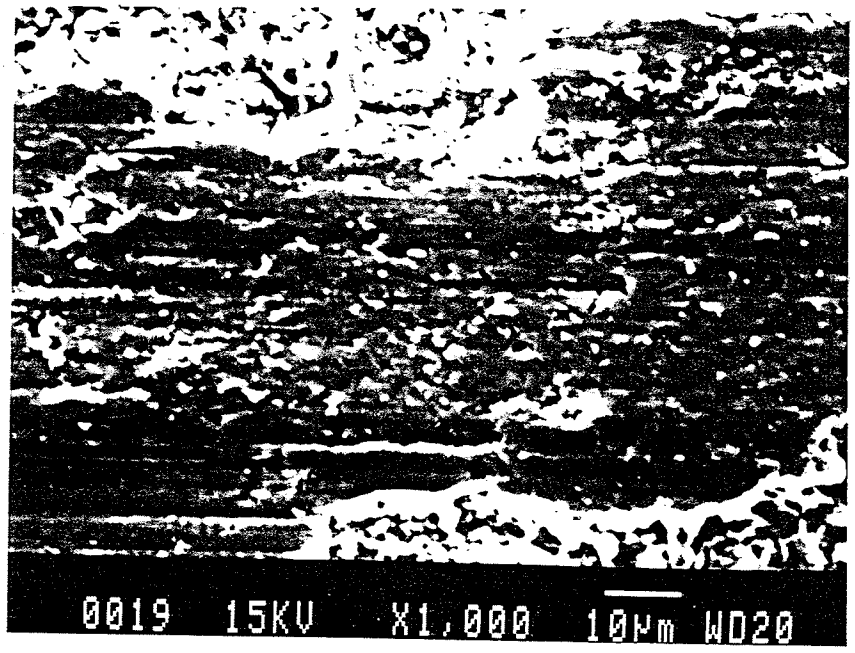

(b)

(See next page for figure caption)

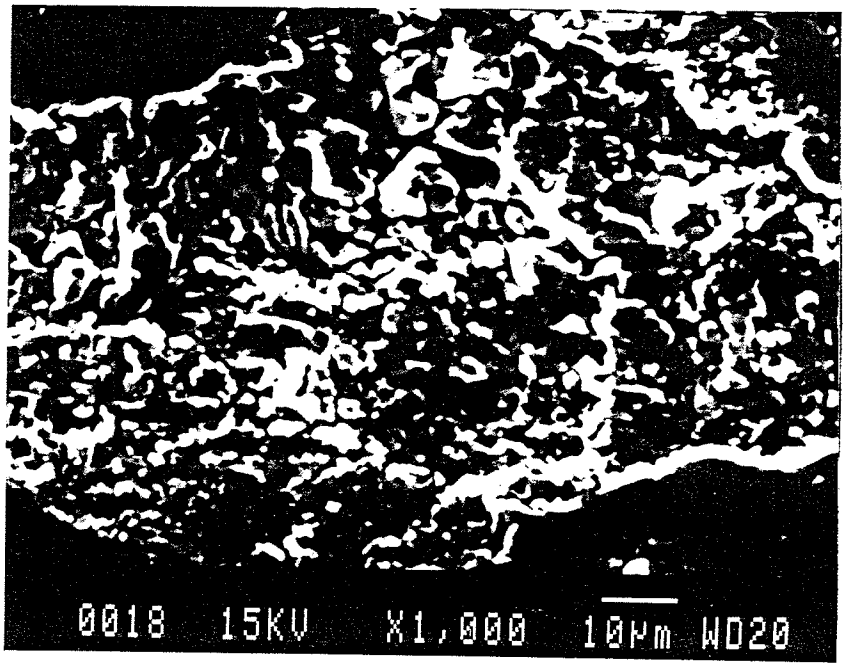

(c)

Fig 4.14 Surface of the composite after 50,000 strokes dry sliding wear
(a) SEM image ×150 (Marked B-abrasive wear, Marked A-cavity)
(b) Abrasive wear surface (c) Rounded SiC particles in cavities

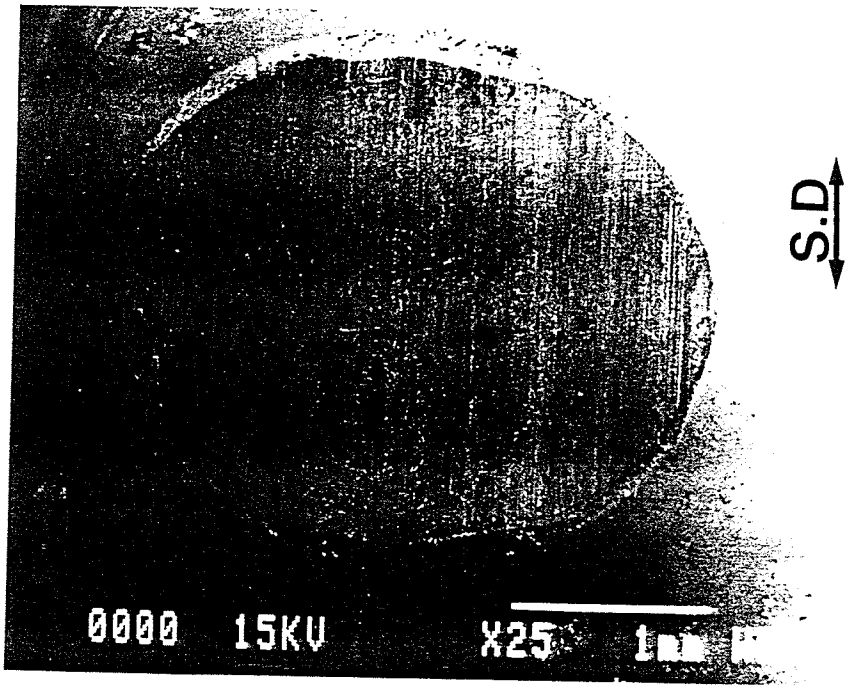

(a)

(See next page for figure caption)

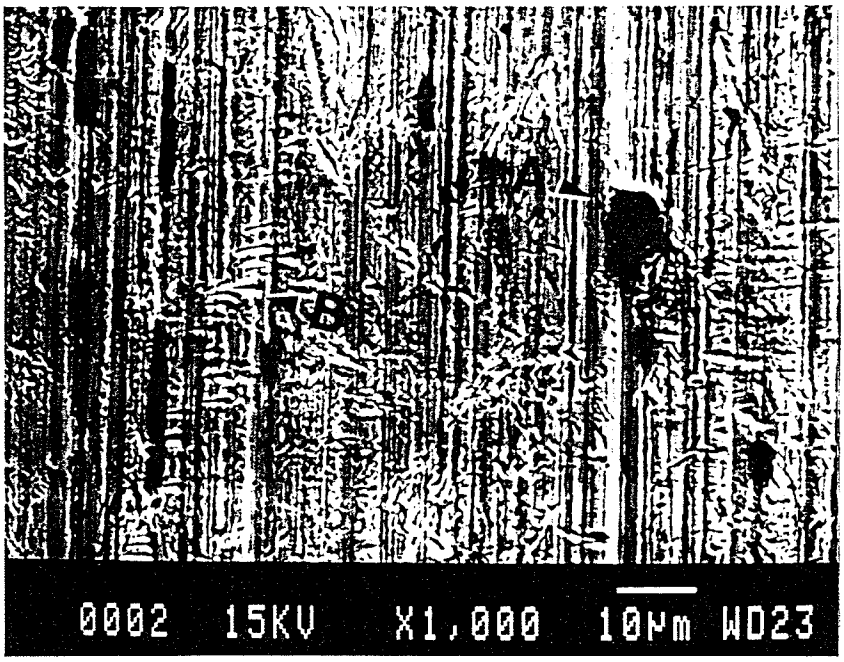

(b)

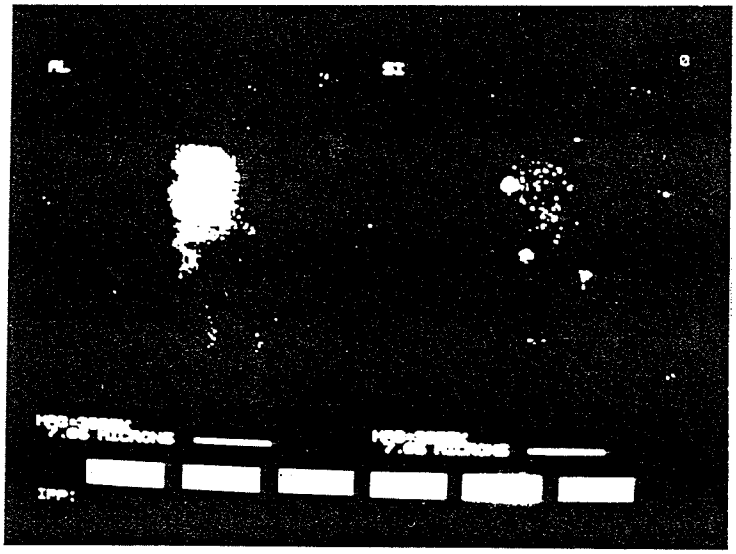

(c)

Fig 4.15 Surface appearance of the wear scar on steel ball after 50,000 strokes of unlubricated wear

(a) SEM image ×25 (b) Ploughing (marked A) and cross-abrading (marked B)
(c) X-ray mapping of (b)

4.2.3.2 Cross section of the wear tracks on the composite specimens

Cross sections of the wear tracks on the composite specimen were cut by using a precise diamond saw as described in Chapter 3. Before wear, there was no fragmentation of SiC particles and deformation layer present along the cutting surface (Fig 4.16(a)). After a wear of 500 strokes, the track surface became rougher than that in non-worn surface, and a layer of deformed matrix and fragmented SiC particles was produced (Fig 4.16 (b)). The thickness of this layer was about 5-15μm. Further increase in the number of sliding cycles resulted in an increase in the depth of this layer, defined as SML (surface mixed layer) here after in this thesis. At a constant load of 9.8N, the depth of SML reached its maximum value at about 3000 stokes (Fig 4.16 (e)). SML totally disappeared when sliding cycles increased to 20,000 (Fig 4.16 (g)). The microscopic features of SML will be described in details in section 4.2.4.

The microscopy of the longitudinal section of the composite specimen after 50,000 strokes wear was performed using a SEM (Fig 4.17). In the region of α-solid solution no fractured small particles were collected (marked m). As shown in Fig 4.14 (c), the bulk material in this area experienced abrasive wear. These abrasives mainly came from the crushed SiC and matrix particles. The region marked n, is a cross section of the cavity which is similar to the cavity shown in 4.14 (b) where delamination may have occurred. The depth of these cavities is approximately 3-5μm. The SiC particle has been fractured and fragmented into small particles and many of them have been retained in this cavity. Moreover, it can be seen that the SiC particles are well grounded and rounded. EDS analysis indicated that some of the particles in these cavities are SiC particles (gray particles) and some of them are silicon particles from the eutectic dendrite (white particles).

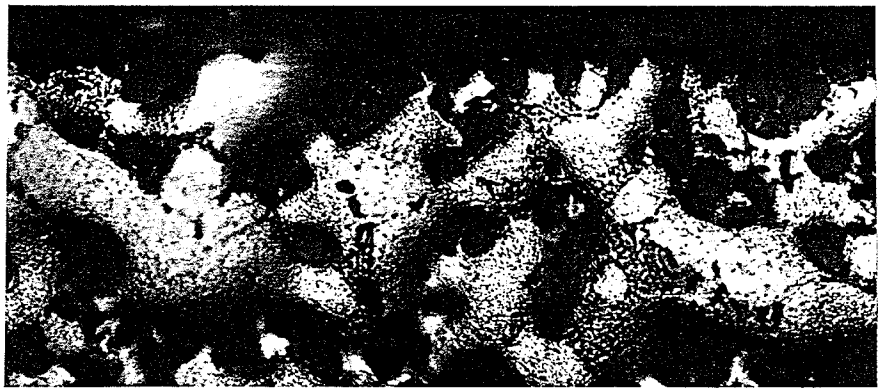

(a)

(b)

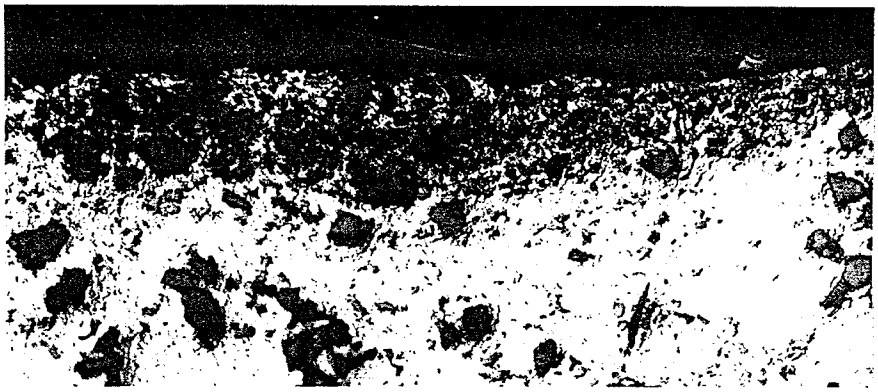

(c)

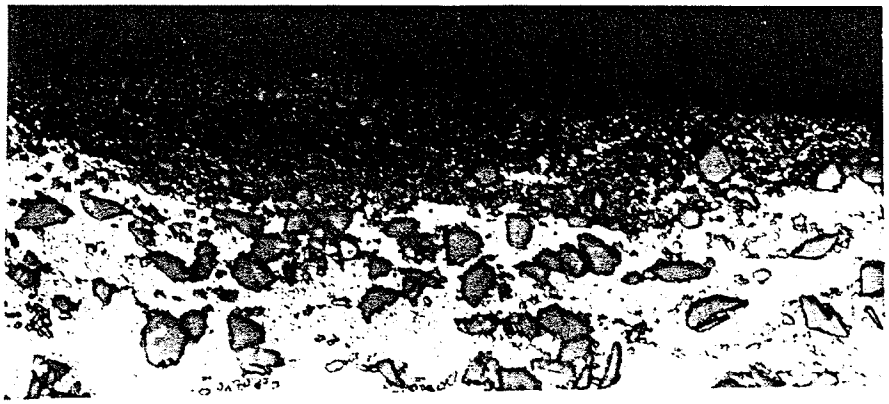

(d)

(See next page for figure caption)

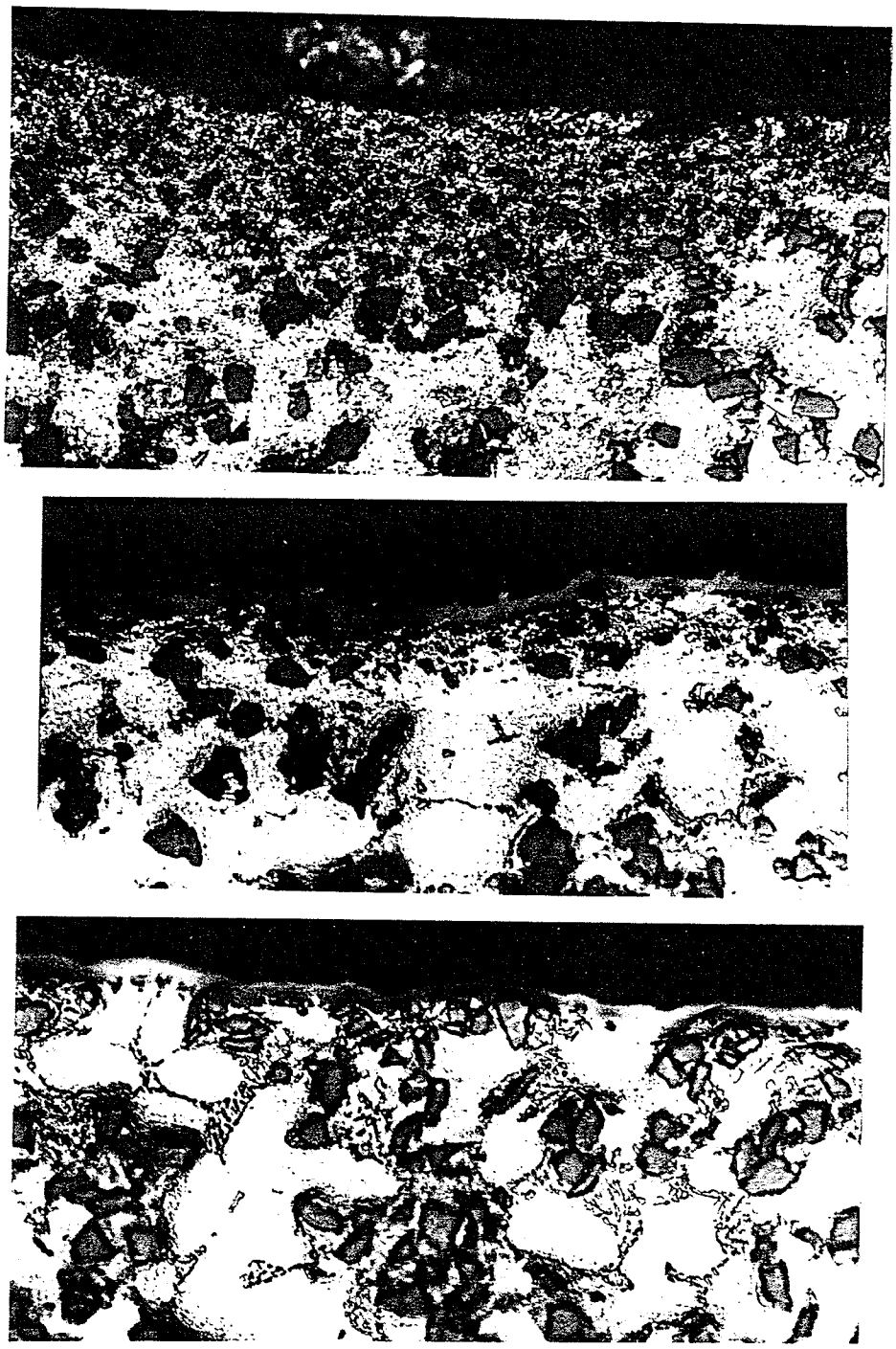

(e)

(f)

(g)

Fig 4.16 Cross section of the polished surface before and after wear in different sliding cycles on composite specimen (×400)

(a) Polished surface before wear (b) 500 strokes (c) 1000 strokes

(d) 2000 strokes (e) 3000 strokes (f) 5000 strokes (g) 20,000 strokes

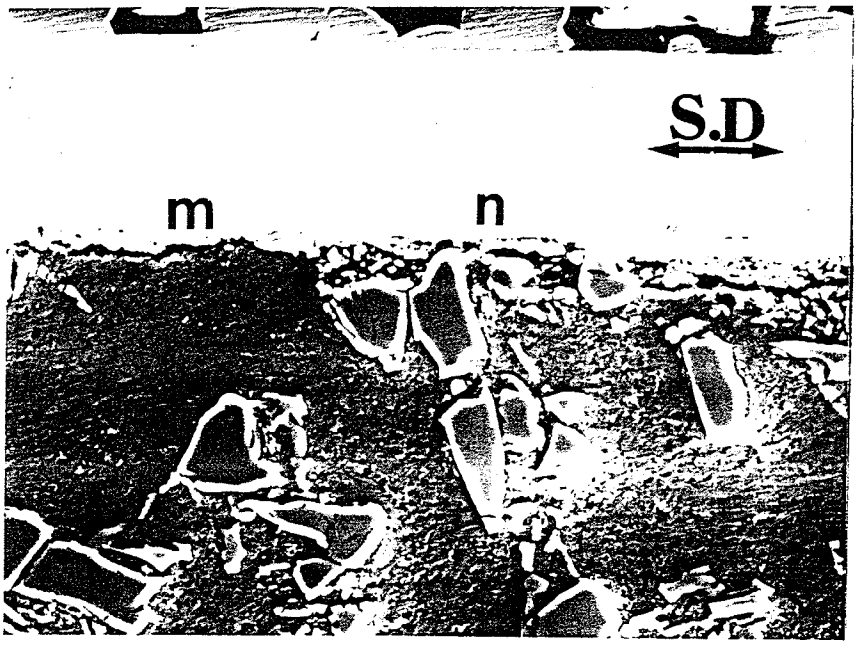

Fig 4.17 SEM image of the longitudinal section of the dry wear track after sliding 50,000 cycles

A relationship seems to exist between the location of these cavities and the position of Al-Si eutectic networks. The cavities only developed from these eutectic networks and no cavities were found to form on top of the bulk material where α solid solution exists. Possibly, the Si particles in the eutectic phase assisted the fragmentation of the matrix and/or SiC particles during the reciprocal wear.

4.2.3.3 The morphology of track ends in dry sliding wear test

(1) Sliding speed and contact stress for dry wear test

Fig 4.18 is a diagram for the sliding wear process. The slider (ball) moving speed can be expressed by the following equation,

$$Vs = \omega \times r \times \sin \omega t$$

Where Vs is the sliding speed, ω is the angle speed, r is the radius of the motor wheel to which the connecting rod is attached ,and t is the time. The stroke length is 25mm, therefore the radius r becomes 12.5mm.

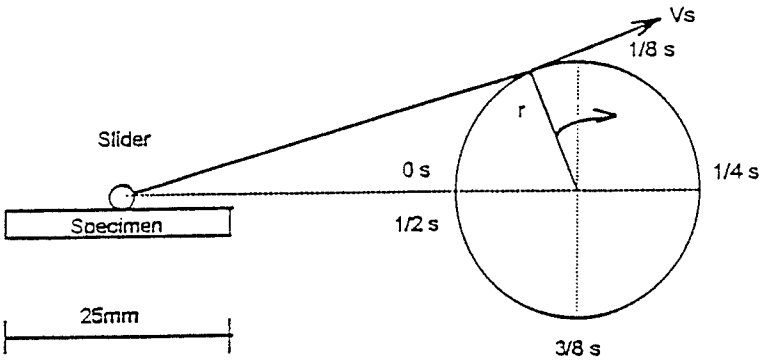

(a)

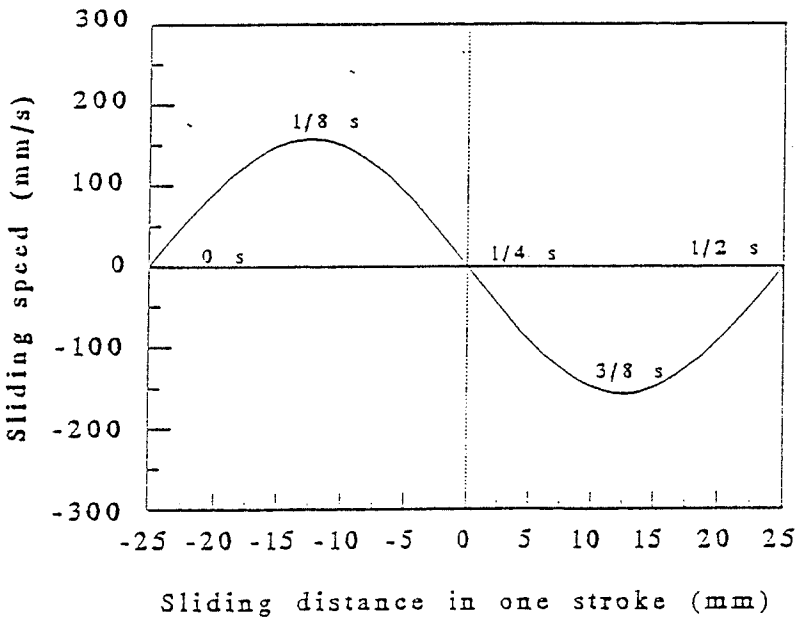

(b)

Fig 4.18 Sliding speed distribution in the reciprocal sliding wear test
(a) Diagram for the sliding wear (b) Sliding speed distribution

As indicated by Fig 4.18, the maximum speed occurs in the middle of a stroke, which is 157mm/s; The minimum speed occurs at the ends of the track, which is zero. Initially, the contact stress is high due to very small contact area. However, a higher number of wear cycles will give rise to a larger contact area between the mating surfaces, which will in turn lead to a decrease in contact stress, even though the applied load is kept constant.

(2) Wear surface morphology of track ends

For clarity of description, this section will be discussed in three parts according to different level of wear cycles.

Low number of wear cycles (< 100).

During wear at low number of cycles, contact area was low and stress was high. The sliding process went smoothly and almost no wear debris was produced. Weighing specimens after wear showed no weight loss. Fig 4.19 shows the end morphology at 50 wear cycles. It is featured by localized plastic flow of the matrix and micro-ploughing or scouring by loose SiC particles. At this stage the contact area between the slider and the composite specimen is very small, contact stress is high enough to fragment some SiC particles and force them to move and make a groove.

Around each SiC particle mating the ball surface, the matrix appeared to be fragmented or fatigued. This was expected since the reciprocating action of the slider not only loosens the SiC particle but fatigues the matrix around the particle. While the middle part of the track exhibited some plastic flow and more contact between the ball and MMC surface, the end sections of the track did not undergo such a plastic deformation. Only micro ploughing by some SiC particles and scratching was visible. It should be noted that the slider (ball) velocity near the middle of track is much higher than the end, causing the SiC particles and the matrix around it to be subjected to a much higher strain rate

compared to the ends of the track. This high strain rate causes SiC protrusions/particles to fracture easily, the matrix to disbond and separate easily, creates more debris and its compaction to the track surface. Furthermore, the difference in the rise in temperature between the 'normal part' and the end during sliding wear should be taken into consideration. It was suggested that the effect of frictional temperature on wear should not neglected when the sliding velocity is above 0.1m/s [9]. In this study, the sliding speed near the center is about 0.16m/s, and this might bring about the influence of frictional temperature on the wear process, reduce the yield strength of surface layer material and result in more plastic flow of the matrix material as compared with that at the end.

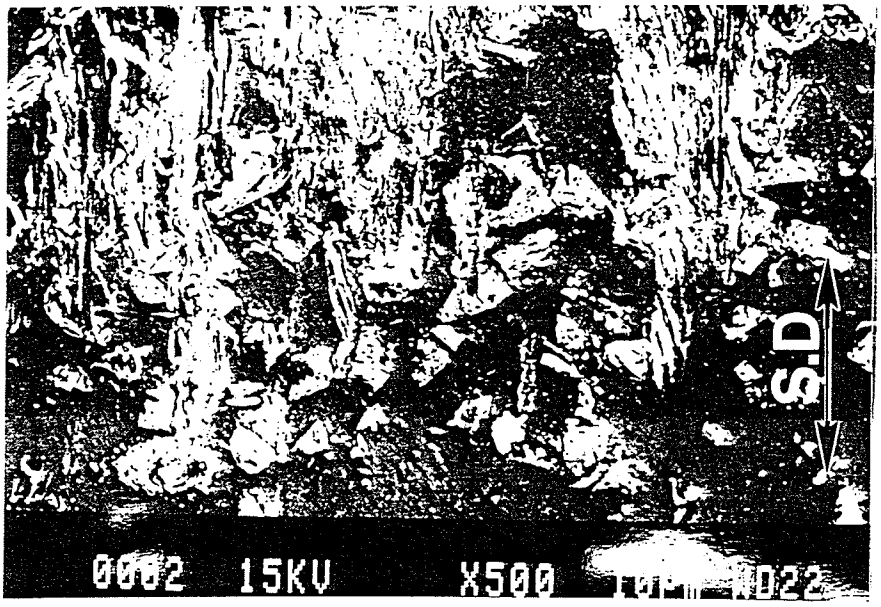

Fig 4.19 The wear track end surface after sliding 50 cycles

During this early stage, SiC particles are either crushed and wrapped by deformed matrix or pushed in to matrix, and very little lose debris exists on the track surface. This has resulted in no collection of debris at the end of the track.

Intermediate number of wear cycles (500-10,000)

When the number of wear cycles increases further, as illustrated by Fig 4.20 corresponding to the wear cycles of 3000, the wear track becomes wider and more plastic flow (overlapping) of the matrix appears both inside the track and at the edge of the track end (Fig 4.20 (a)). The configuration of the out-edge at the end of this track is nearly a semicircle, which suggests that the original asperities (SiC particles sticking out of the surface) have worn out and the slider has come in full contact with the matrix through the deformation of the matrix.

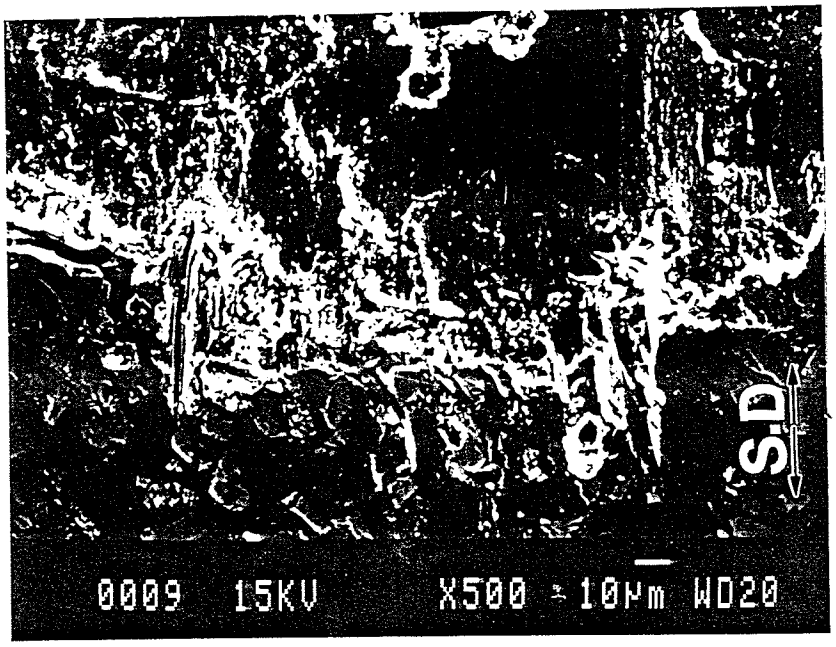

Fig 4.20 The wear track end surface after sliding 3000 cycles

Wear debris starts to accumulate at this stage at the end and pieces of broken SiC particles are wrapped in the plastically deformed matrix, but its amount is very limited. Most of the debris at this duration are flake-type-chips. Ploughing is still an important wearing mechanism at the end. Some weight loss of the composite specimen is noted.

High number of wear cycles (>10,000)

Above 10,000 wear cycles, sliding wear process appears to be smooth and in a steady state manner. A typical feature of the worn surface at the end of the wear track is shown in Fig 4.21. The edge of the track ends turns out to be a more even semicircle. No significant plastic flow seems to have occurred on the out-side edge as compared with that which has occurred during intermediate cycles. This can attributed to a comparatively low contact stress during high cycles.

With respect to Fig 4.21, the track-ends appear to include four zones, which are shown in Fig 4.22.

Zone I is characterized by ploughing or grooving induced by particles produced at lower cycles. Some debris of large particles with deformed matrix surface is located in this zone. The morphology of this zone, together with the deformed particles is very similar to that of the track at intermediate cycles (Fig. 4.20).

Zone II is a white band zone in the Fig 4.21 (b). It is noted that the width of this band is not even. It reaches its maximum at the tip (marked A) of the end, and becomes smaller towards the side of the track, and finally disappears at B and C.

Fig 4.23 (a) shows the track-end surface appearance in Zone II in more detail. It consists of clusters of very small particles (powder) with some large particles dispersed in them. The result of an energy dispersive (EDS) X-ray spot analysis at B for the small particles is shown in Fig 4.23 (b). Aluminum, silicon, iron and oxygen are present. The debris produced between 20,000 and 50,000 cycles was collected., and the morphology of the debris is shown in Fig 4.24 (a).This debris appear to be granular in shape and 1-3μm in diameter. The large particles in Fig 4.24 are actually the clusters of many very small granular particles. This gives rather different results from the experimental results obtained by [54].The chemical composition was obtained by EDS and shown in Fig 4.24 (b). From Fig 4.23 and Fig 4.24, it can be seen that the cluster of the small particles and the wear debris produced during 20,000 and 50,000 cycles are approximately of the same

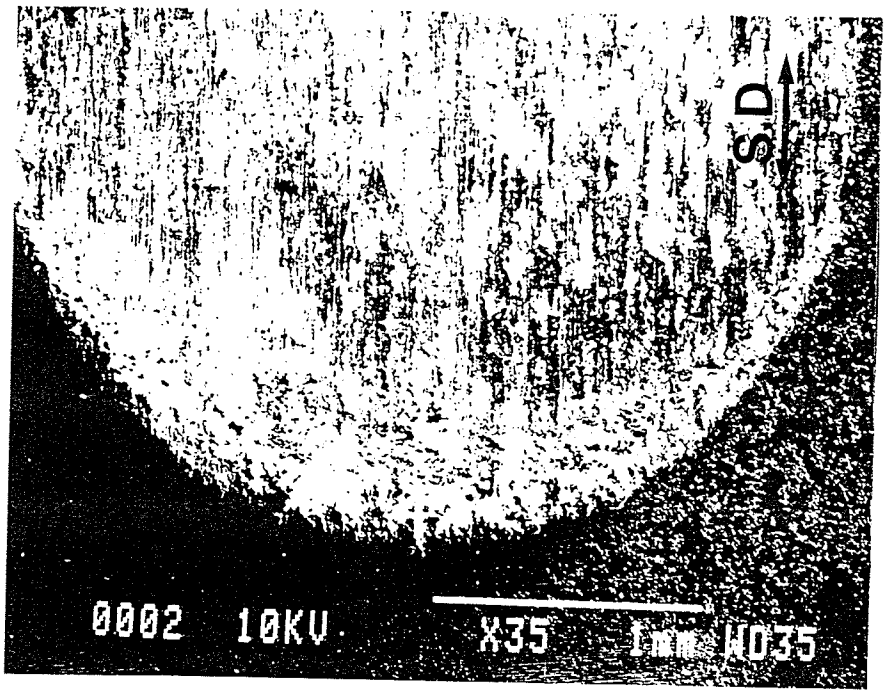

(a)

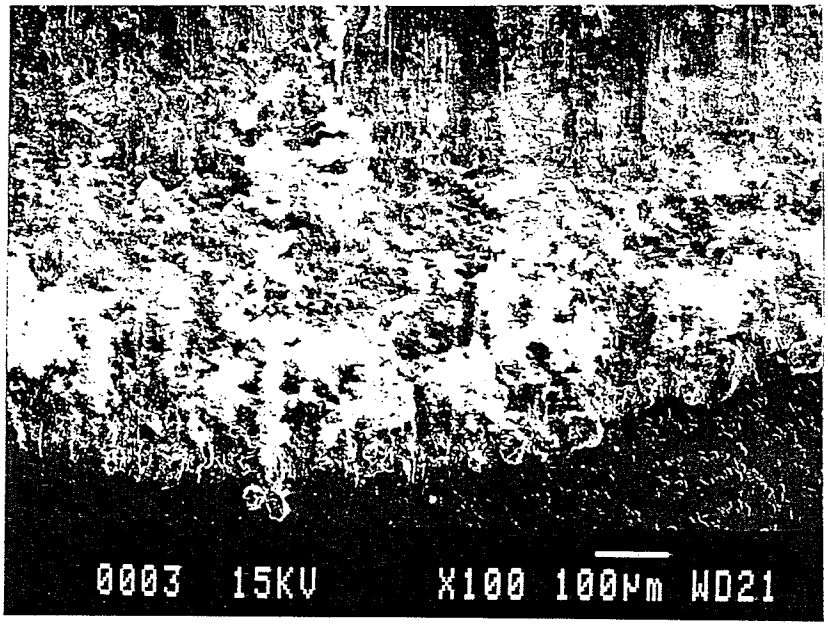

(b)

Fig 4.21 The wear track end at the wear cycles of 50,000 in a dry sliding wear (load-1kg)

(a) ×35 (b) ×100

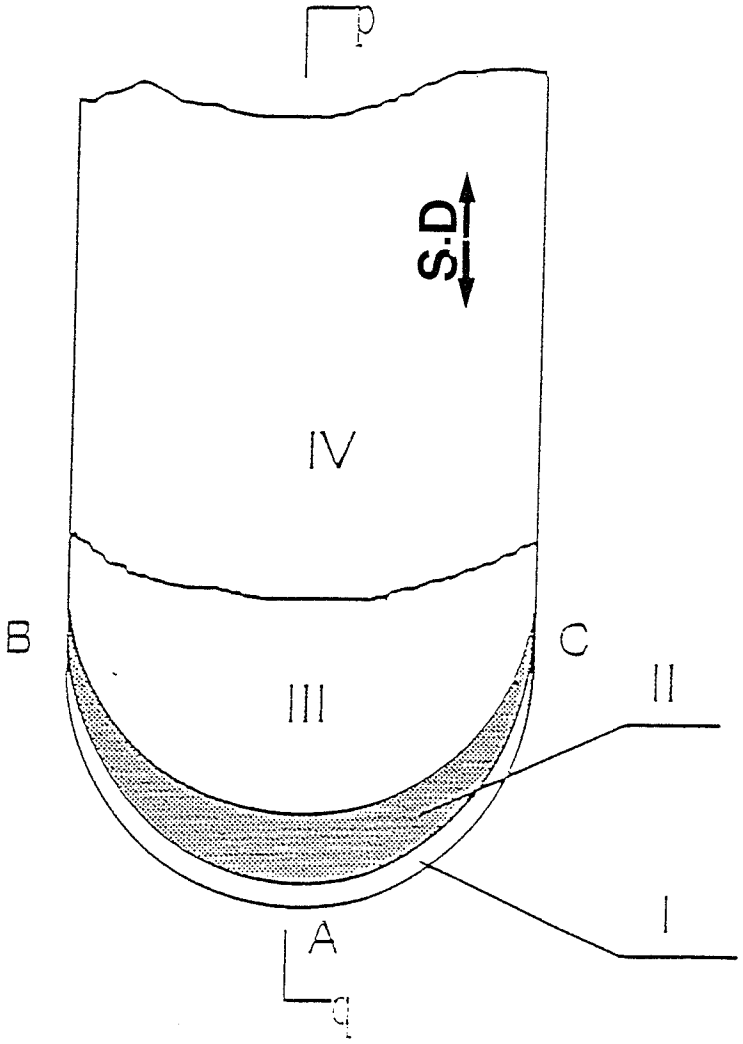

Fig 4.22 Four zones at the end of a dry wear track corresponding to 50,000 wear cycles (load-1kg)

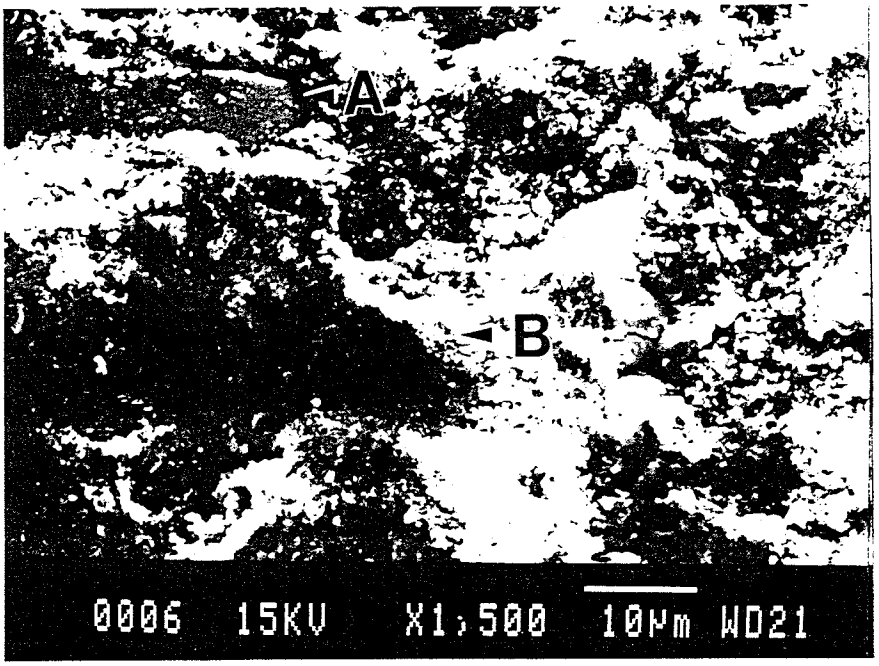

(a)

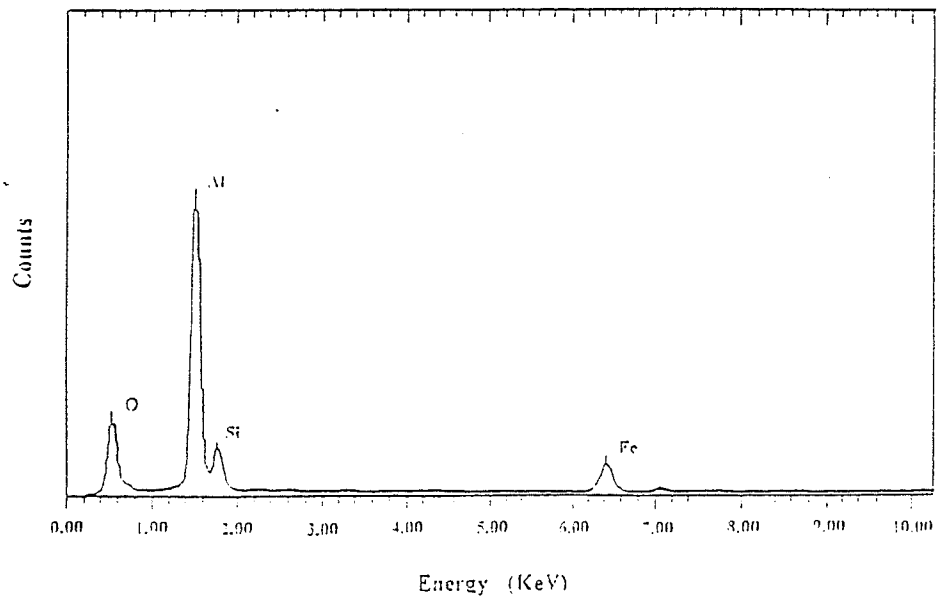

(b)

Fig 4.23 The zone II in Fig 4.22 and the result of EDS
(a) The wear debris accumulated at the track end
(A-SiC particles, B-impacted wear debris)
(b) EDS of the impacted wear debris at B

(a)

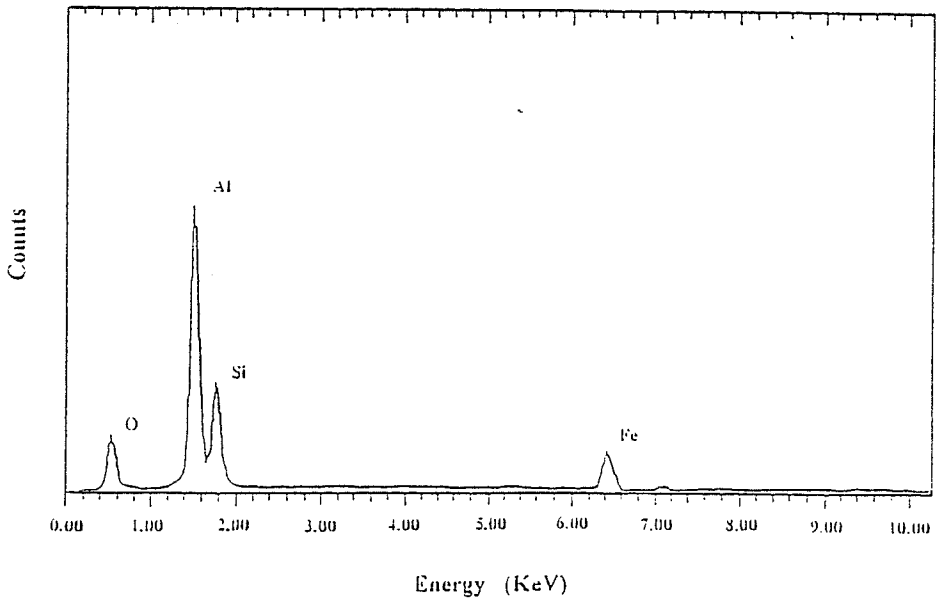

(b)

Fig 4.24 The wear debris collected in between the sliding cycles of 20,000 and 50,000 in a dry sliding test

(a) Clusters of wear debris ×200 (b) EDS of the wear debris

constituents. In other words, the white band is mainly the accumulation of wear debris at the end of the wear track. The amount of oxygen in the debris is more than that noted on the composite surface. This indicates that oxidation of the debris has occurred during the wear process. The temperature increase due to local friction heating may also contribute to the oxidation process [59]. It might be the increase in surface area of the composite and iron in debris that created more contacting surfaces with atmosphere and produced more oxidation. The large particles (Marked A) hiding in the debris are verified as SiC by EDS analysis.

Fig 4.25 Representative surface morphology in the zone III
(a) ×1000 (A - Abrasive wear of matrix, B - Fractured SiC particles) (b) ×4000

Representative surface morphology of a typical area zone III is shown in Fig 4.25. The features indicate an abrasive nature of wear. Both matrix and SiC particles have been fragmented and crushed into a finer size material which is acting as an abrasive. Because of low stress levels, plastic deformation is not predominant. Again, in this area of the track end slider velocity is low, and some debris is collected. A SiC particle was crushed in to several small pieces, and the plastic flow of matrix can not cover and wrap

the fragmented SiC particles. The fractured SiC particles acted as abrasives and caused further abrasive wear between the mating surfaces. At the same time, these abrasives were ground in between the mating surfaces.

In zone IV (same as Fig 4.14 (a)), the SiC particles are well crushed and rounded in the voids. There are many areas (white patches) which show features similar to Figure 4.25 (a). These areas are predominantly rich with many small and large SiC particles, and it appears that due to high strain rate fatigue (reciprocating action of slider) delamination or debris creation has occurred. Black areas are much smaller and polished. Unlike low number of wear cycles, it is abrasive wear rather than plastic deformation that is the predominant wear mechanism for the matrix. Another dominant wear mechanism is delamination wear due to accumulation of fatigue strain reaching the damage limit of surface layer material.

During the wear at high number of wear cycles, since contact stress is low (Fig 2), it is not possible for the matrix to plastically flow or wrap the fragmented SiC particles. Thus, the front of slider comes in direct contact with some SiC particles. Consequently, these particles are fragmented and ground into a powder in between the mating surfaces as the wear process proceeds. The debris produced by previous sliding strokes is pushed to the ends by later strokes. The more strokes we have, the more the debris is collected at the end. However, in each stroke, because the ball moves to a definite position at its end, there should be no room at the end of a stroke for the debris to stay freely in between the track surface and the ball, and the only way for the debris to reside there is to be compacted into the matrix, in spite of zero sliding speed of the ball at the very end of a stroke. As shown by A in Fig 4.22, This will result in impacting the matrix and causing some SiC particles collected in the end surface to be squeezed out of the matrix in the original size and even to be fractured. Thus, a non-uniform mechanically mixed layer of compacted debris and SiC particles, which attaches firmly to the end surface, is formed at the ends of a wear track.

The longitudinal section of this wear track along the line P-Q in Fig 4.22 was also examined by SEM (Fig 4.26). In the longitudinal section, energy dispersive analysis confirmed the presence of the accumulated debris. This debris did not distribute itself uniformly on the surface, in fact, it is compacted to the matrix as flakes. The thickness in some locations reached 10-20μm. After polishing, some of the debris tended to be detached from the base material.

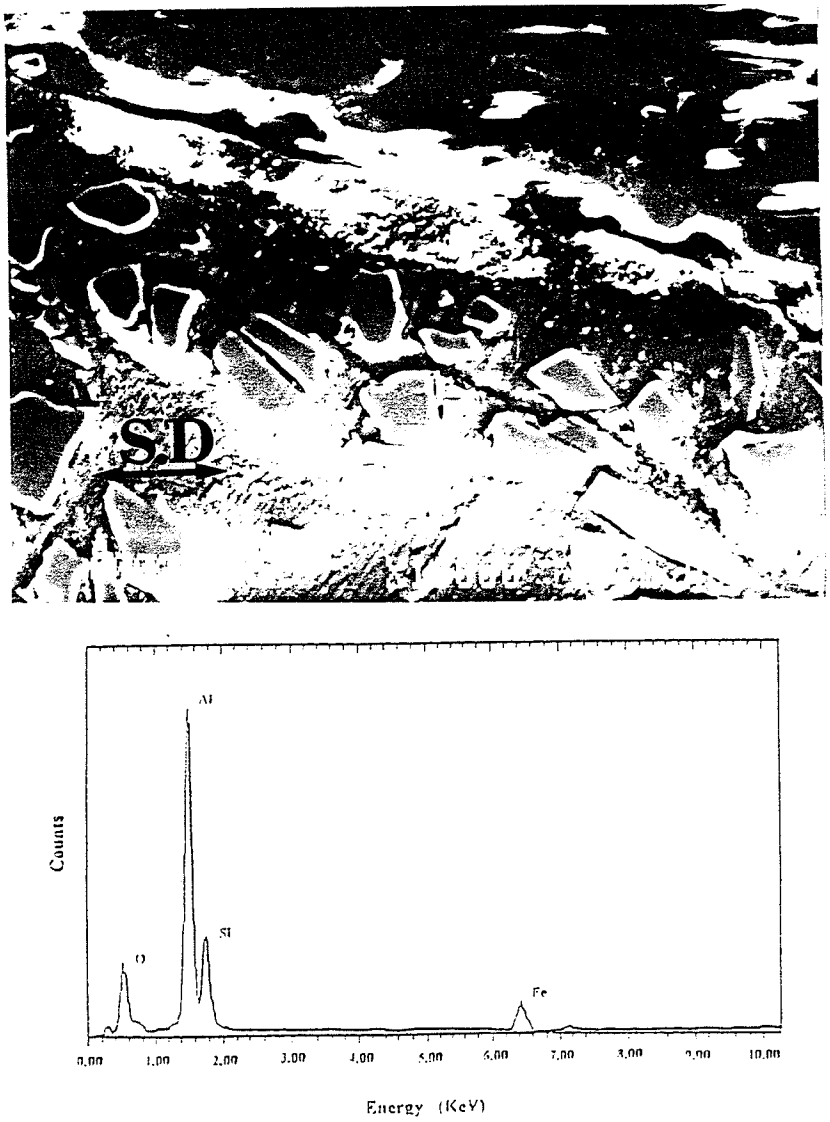

Fig 4.26 The longitudinal section P-Q in the wear track end of 50,000 wear cycles
(a) The accumulated wear debris in the longitudinal section
(b) EDS of the accumulated wear debris in (a)
(Note - The white band along the boundary of the composite and the mounting material is the result of electrically discharging)

4.2.4 Surface Mixed Layer and SiC particle Behavior

4.2.4.1 Appearance of surface mixed layer

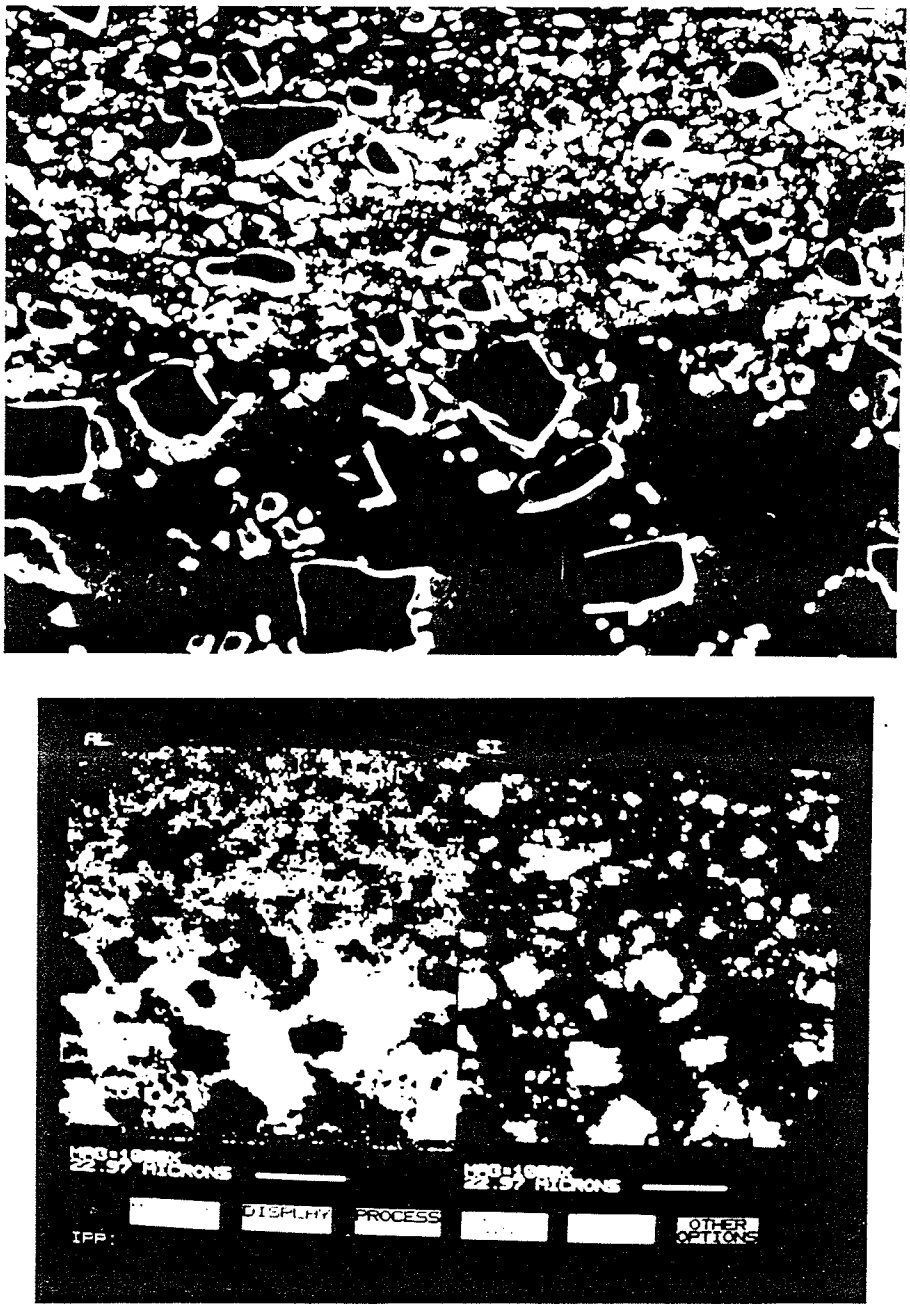

Fig 4.27 The boundary between SML and matrix

(a) SEM image (b) X-ray mapping of Al and Si

In order to determine the behavior of SiC particles during the wear process, the cross sections of wear tracks were carefully investigated using an optical microscope and a SEM. It was found that the SiC particles, size and distribution changed with the increase of wear cycles under a constant load (9.8N). A special layer, called surface-mixed-layer (SML) (Fig 4.27, and Fig 4.16) was observed after a certain number of wear cycles. The SML included heavily deformed Al-Si alloy matrix interspersed with smashed SiC particles. The depth of the SML was not uniform along the width of the cross section. It reached its maximum at the center of the track. SEM image and X-ray mapping of Si in the SML are shown in Fig 4.27 (b). A clear boundary exists between the original matrix and the SML. The distribution of SiC particles in the original matrix and the SML are plotted (as shown in Fig 4.28). A Leitz-TASIC image analyzer was used to produce these data. It is noticed that the average size of the SiC particles in the matrix (approx. 10μm) has been reduced to an average size of approx. 2μm. Moreover, the distribution range of small particles of SiC has also narrowed down significantly. This shows that the SiC particles in SML have been well crushed.

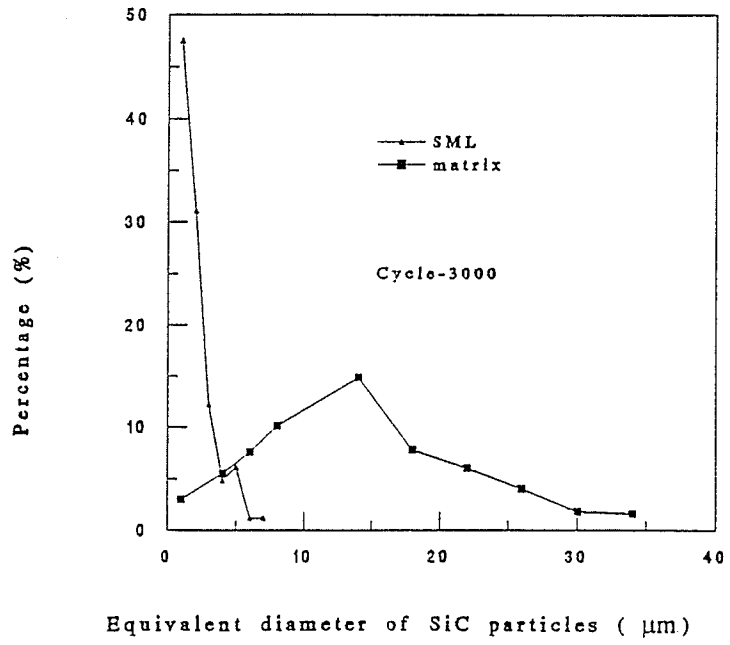

Fig 4.28 Distribution of SiC particles in SML and matrix

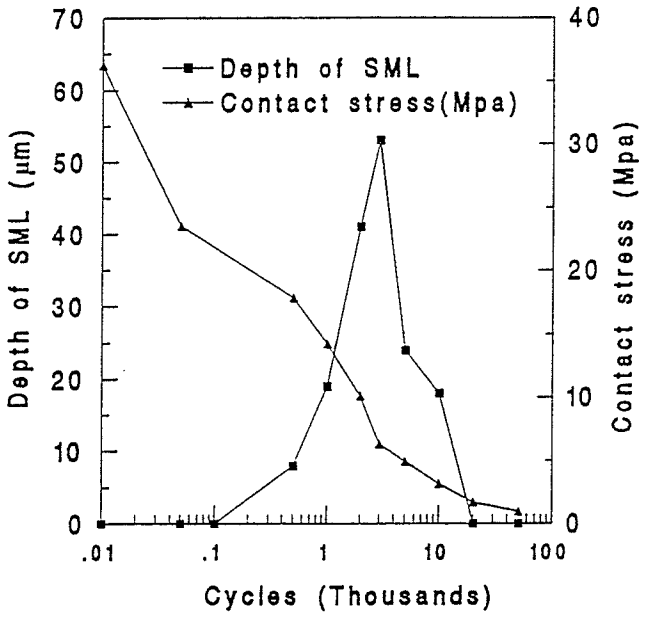

Fig 4.29 Change of SML depth and contact stress with wear cycles (load-9.8N)

Fig 4.29 shows the influence of wear cycles on the depth of the SML (at the center of the track) under a load of 9.8N. In the first 100 sliding cycles, no SML is found. However, SML starts to appear at about 500 cycles, its depth reaches a maximum of 50-55μm at a sliding cycle of about 2000-3000. As the wear cycles increase above 20,000, no SML is visible. Fig 4.29 also illustrates that the contact stress decreases with the increase in wear cycles. The contact stress is the applied normal load divided by the contact area between a slider and the composite specimen. At initial stages (cycles<500), the contact area between the steel ball and the specimen, which is the area of the wear scar on the steel ball, is very small and the contact stress generated is very high. Thus, low wear cycles are not able to create significant plastic deformation of the matrix and fragmentation of SiC particles. At high number of sliding cycles (>10,000), the steel ball contacts with the specimen in a much larger area, causing the contact stress become much smaller. SML dose not appear at this stage due to the absence of both plastic flow of both the matrix Al-Si alloy and the fragmentation of SiC particles. Beyond this stage, pure

abrasion occurs where both the ball and MMC are worn away. These observations suggest that the existence of a SML is due to a unique combination of contact stress and number of cycles. In the present test conditions, the SML exists from 100 cycles to 20,000 cycles with maximum depth occurring at 2000~3000 cycles and at a contact stress level of approximately 10MPa. During these cycles, plastic deformation of the matrix occurs together with the fragmentation of SiC particles, and therefore SML is developed. As the wear track widens, the contact stress drops, and the SML is not sustained and gets abraded away.

4.2.5 Effect of Contact Stress on Wear Mechanism

From the above experimental results, it is evident that contact stress acting on the counterfaces plays a the vital role in deciding the wear mechanism in the reciprocal sliding wear of the MMC against bearing steel balls. Fig 4.30 shows that the normalized wear rate (weight loss per unit sliding distance per unit contact area) of the composite specimen increases almost linearly through the entire contact stress range. However, from the change of surface topography with a variation in contact stress, different "wear regimes" could be identified. From the curve of the normalized wear rate vs contact stress of the steel ball bearing, two different "wear rate regimes" can be identified. Between 1 and 3 MPa, the wear rate of ball decreases with an increase in the contact stress, and the wear rate is noted to be below than 6×10^{-7}mg·mm^{-2}·mm^{-1}. Above 5MPa, defined as regime II, the wear rate increases almost linearly with the contact stress. Between regime I and regime II, there exists a transition region (3 to 4 MPa) where specimen exhibits characteristics of a mixture of both types of wear.

4.2.5.1 Wear mechanism in regime I (low contact stress)

The wear mechanism in regime I (low contact stress) is shown schematically in Fig 4.31. The wear mechanism for bearing steel ball is dominated by abrasive grooving or

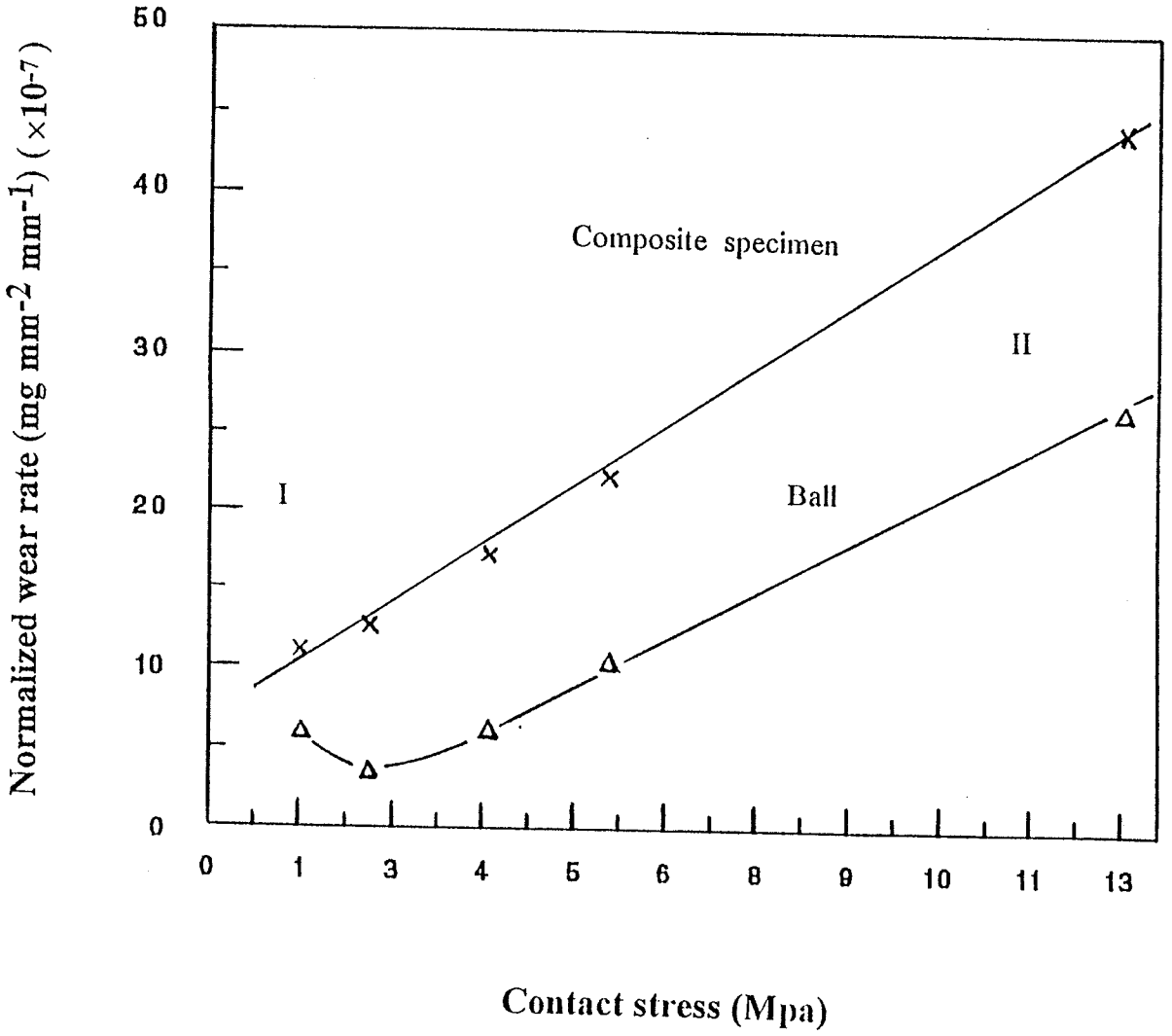

Fig 4.30 The effect of contact stress on the specific wear rate of the composite and steel balls in dry tests (load-1kg)

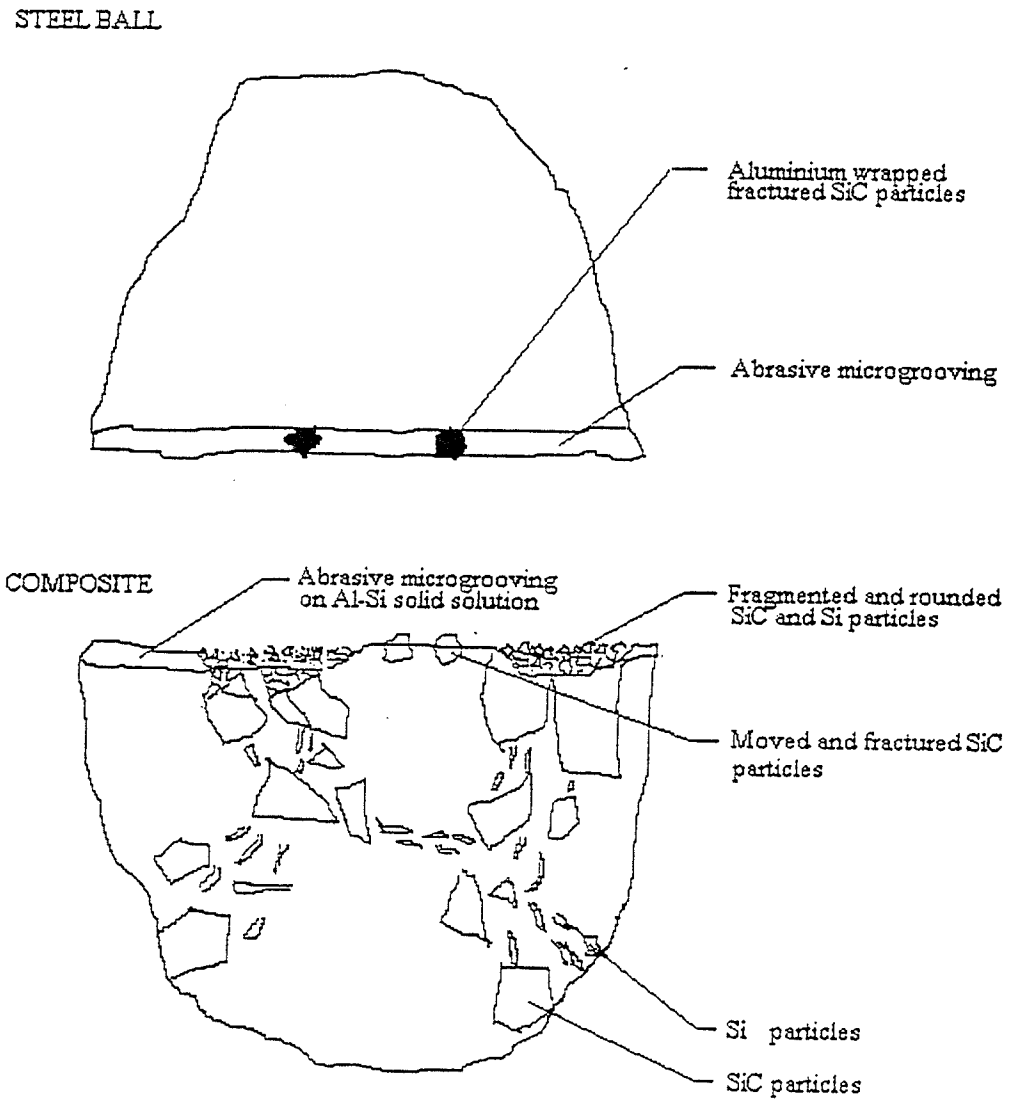

Fig 4.31 Schematic diagram of mild wear regime I

scouring. Abrading particles mainly came from the fragmentation of SiC particles in the composite material during sliding. When these abrading particles cause abrasive wear on the surface of the Al/Si matrix in the composite, deformed matrix gets attached to the SiC surface, resulting in wrapping of the abrading particles with aluminum (Fig 4.15). Because contact stress is low in this regime, no material transfer is observed from composite material to the steel counterface. However, a few abrading SiC particles have moved across the sliding direction and have made on the steel surface.

On the surface of the composite specimen, SiC particles generally protrude out of the polished surface and the particle protrusions can be as high as 5μm after final polishing [83]. During the initial sliding wear process, an impact of a slider onto SiC particles will take place, and abrasives particles will therefore be created. The broken hard abrasive particles entrapped between the counterfaces act as third body abraders. These abraders are responsible for the development of longitudinal grooves on the worn surface area of Al-Si matrix on the composite [65, 83].

As the abrasives hit the surface area of Al-Si eutectic in which SiC particles reside, these abrasives would further interact with the bulk SiC particles and cause them to fracture. The average diameter of these cavities is in the order of 50-100μm, which correlates well with the cell size in the eutectic structure in the composite. The production of the cavities on the worn surface of the composite could be attributed to this type of chain reaction between the hard abrading SiC particles and the near-surface untouched SiC particles and the eutectic network in the composite. These cavities then provide abrasives. during the wear process. In fact, the wear process in regime I is a grinding process. When sliding proceeds further, fractured SiC particles get smashed into even smaller pieces and their reaction with SiC particles in the composite further accelerates this process. Therefore, the equiaxed debris which has a granular form and a dimension of 1~3μm, is produced (Fig 4.32). EDS analysis shows that aluminum, silicon, iron and oxygen are present in the debris which is dark in color.

(a)

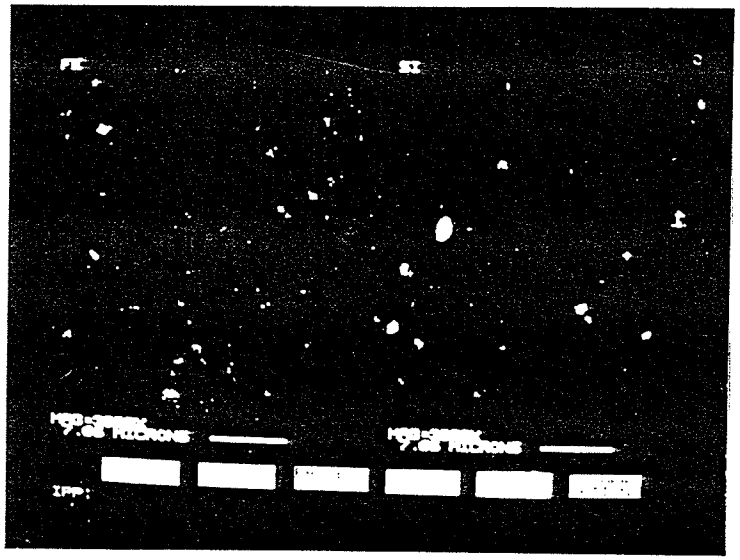

(b)

Fig 4.32 Debris collected at the wear strokes of 20,000-50,000

(a) SEM image of the debris ×3000

(b) X-ray mapping of debris for elements Fe and Si

Observation of a decrease in the wear rate of the steel ball, when contact stress increased from 1MPa to 3MPa can be the result of a competition between the plastic deformation of Al-Si matrix in the composite and abrasive wear of this plastically flowed matrix. The higher the contact stress is, the more plastic deformation occurs, which causes more eutectic network containing SiC particles to be covered or smeared by the deformed Al-Si matrix. Consequently, less SiC particles in the composite would be exposed to the counterface and less amount of abrasives are produced. Although this change did not alter wear rate of the composite significantly, the wear rate of steel balls was reduced. It is believed that the composite surface at this stage is covered with a "transferred layer" - a mixture of iron and its oxides[93], which have a low coefficient of friction and create an in situ lubrication effect. Therefore, a reverse trend of wear rate for the steel sliders is developed.

In summary, abrasive microgrooving is the dominant mechanism for the wear of both of the composite and the steel balls at low stresses. The plastic deformation which increases with the contact stress does not affect the wear rate of the composite as much as that of steel balls.

4.2.5.2 Transition region from regime I to regime II (intermediate contact stress)

As contact stress increases above 3MPa, Fig 4.30, the wear rate increases linearly. Because of the higher contact stress, more severe micro-grooving occurs both on the surface of the composite and on the counterface, and comparatively larger area on the surface of the composite is covered by the deformed Al-Si matrix and less wear cavities are produced (as seen in Fig 4.13). On the other hand, some deformed Al-Si matrix together with fractured SiC particles is transferred to the counterface. This type of wear has been often referred to as galling or scuffing [94]. Although more plastic flow of Al-Si matrix took place and some MMC material got transferred to the ball surface, the wear

rates for both composite specimen and the bearing steel balls have increased due to the increasing contact stress.

As shown in Fig 4.33, the wear debris in this regime is a mixture of small diameter equiaxed granular particles (1~3μm) (marked A) and plate-like particles (marked B). As described earlier in Regime I, abrasive wear mechanism is responsible for the creation of these granular debris. The plate-like debris might have come from subsurface delamination process of the SML at high contact stress[54, 70] (to be described in 4.2.5.3). So, the wear of the composite in this regime is dominated by the mixture of presence of a subsurface delamination and abrasive microgrooving. It should, however, be noted that their relative contributions to the wear process is not yet clear.

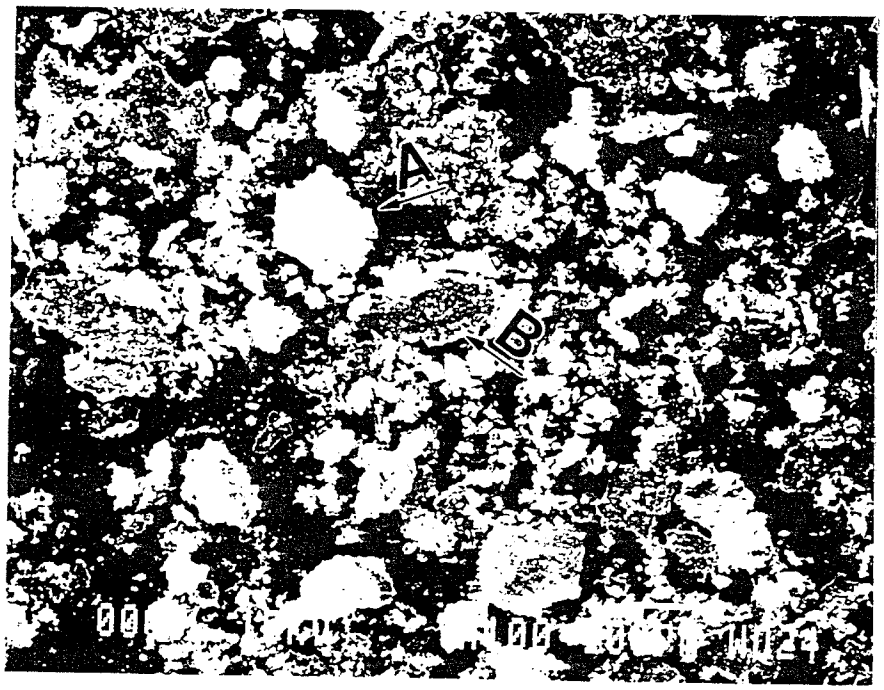

Fig 4.33 Debris produced in the transition region from regime I to regime II (intermediate stress level of 3-5MPa)

4.2.5.3 Wear mechanism in regime III (high contact stress)

In regime III, the wear proceeds by severe surface damage and involves greater MMC material transfer to the steel counterface (Fig 4.12). The surface of the composite is severely damaged (shown in Fig 4.11). The wear mechanism for regime III (contact stress P>5MPa) is schematically shown in Fig 4.34, which is basically a combination of deformation and delamination processes. The deformation here is much more severe than that present in regime II. Moreover, part of the aluminum matrix and fragmented SiC particles on the wear surface get transferred to the counterface (Fig 4.9). SEM examination of the wear surface on the counterface reveal that a pattern of "shear wedges" is formed. These "shear wedges" are found to move roughly 10-15μm along the sliding direction of the last stroke. Fractured SiC particles get dispersed in these transferred layers. At this stage, no SML with a significant depth is formed because of the low number of sliding cycles. As sliding cycles (or sliding distance) increase, more and more SiC particles become fractured, and the depth of SML increase. Finally, an equilibrium is achieved and SiC particles got fragmented and fractured to a mean size of approx. 2μm, which is about one-fifth of the original SiC size in the composite. The fractured SiC particles and severely deformed Al-Si matrix together form the SML, surface mixed layer (Fig 4.16). SEM examination of the worn surfaces of the composite reveal that part of these surface mixed layers are transferred to the surface of the steel ball. The transfer of SML layers could be attributed to the development of adhesive forces between the SML and the steel counterface. As the reciprocal sliding wear proceeds, some parts of the transferred SML on the counterface peel off to form debris or go back to composite surface and get mixed with the SML again. In other words, wear in this period is accompanied by transfer and re-transfer processes of these SML layers. This is a mechanical blending process which results in further fragmentation of SiC particles in the SML.

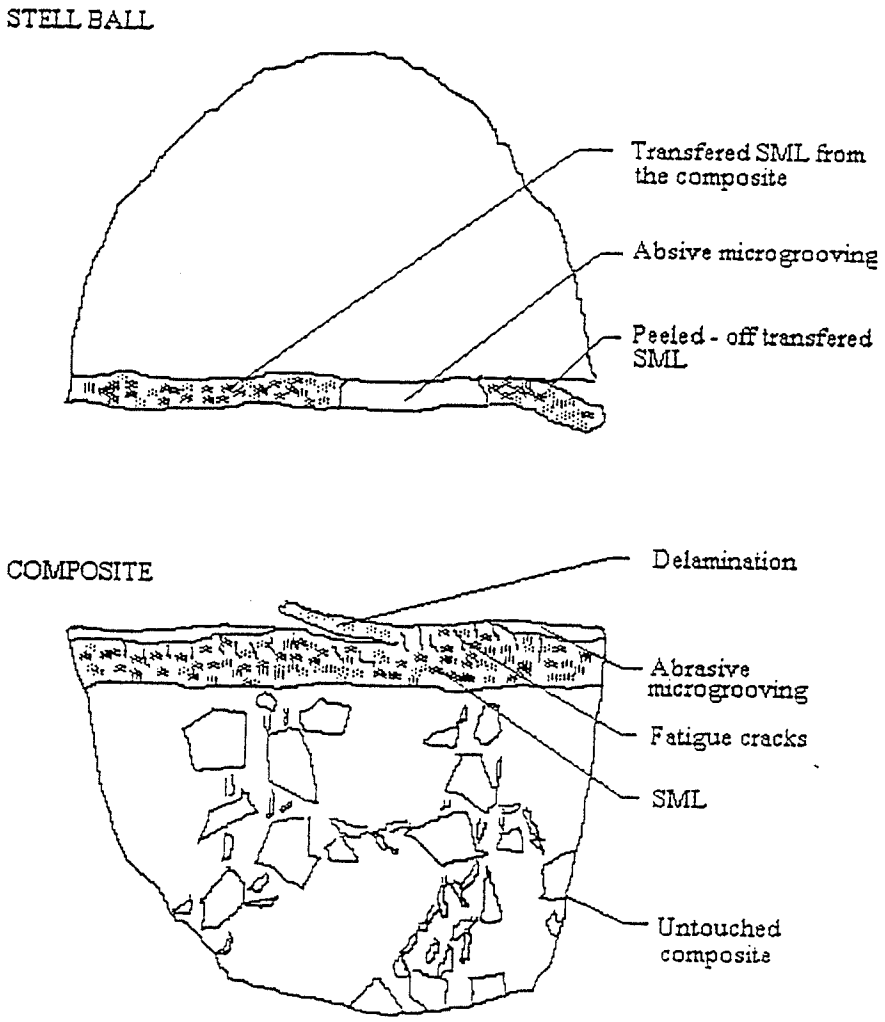

Fig 4.34 Schematic diagram of server wear regime II

For the bearing steel sliders, abrasive action of the fractured SiC carbide and Si particles, which lead to microgrooving, is the major mechanism responsible for the material loss. As shown in Fig 4.12, some broken SiC particles act as third-body abrading particles embedded on the counterface, they serve as an "anchor", and aluminum matrix will then build up on top of them. After the formation of the SML, it will then be work hardened by further deformation. Above certain number of sliding cycles (>3000), surface fatigue cracks which are perpendicular to the sliding direction are created (Fig 4.11 (b)). The occurrence of these cracks can be attributed to the cyclical stress and strain, from the reciprocating action of the sliding. During wear process, the propagation and linking of these fatigue cracks will lead to the formation of delamination, and a plate-like wear debris is thus formed (as shown in Fig 4.33). The proportion of these plate-like particles in the debris increase with the contact stress. Almost all the debris is composed of the plate-like particles when contact stress is higher than 15MPa. Therefore, it is reasonable to assume that the shear deformation and material transfer are the dominant rate-controlling mechanisms at the initial stages. However, with increasing contact stress, the SML delamination became predominant.

4.3 Reciprocal Lubricated Wear Tests

4.3.1 Weight loss in the composite specimens and steel ball

In lubricated wear tests, applied load used was 9.8N, 19.6N, 39.2N and 78.4N. Other testing parameters have already been described in section 3.3.3.

Even after sliding 500,000 wear cycles under a load of 78.4N, weight loss of the composite block specimen was so small that it could hardly been measured by the electronic scale used in this research. In other words, the weight loss for the lubricated sliding wear test was insignificant. Volume loss method did not work for the evaluation of the composite specimen either because the wear track was very shallow, and it was

difficult to get a surface profile by the instrument. For some wear tracks, such as those from 9.8N ×20, 50, 100, 1000 cycles, one could not see if there was any wear track. Therefore, instead of weighting the specimens for weight loss quantitatively, the degree of wear tracks were evaluated qualitatively by SEM, as described later.

The weight loss for steel balls was very small as well. After sliding wear at the load of 78.4N for half of a million cycles, it was less than 1.0mg. An optical microscope was used to examine the wear scars on the balls. Nearly all the wear scars were circular in configuration and their surface was quite flat.

As shown in Fig 4.35, the volume loss on a ball can be calculated through the following formulas:

$$V = \frac{1}{3}\pi h^2(3R - h) \tag{4-1}$$

Where V is the volume loss on a ball. R is the ball radius, h is the segment height, which is

$$h = R - \sqrt{R^2 - R'^2} \tag{4-2}$$

R' is the radius of a wear scar on a ball (or the width of a wear track on the composite). Then we have the weight loss,

$$W = \frac{1}{3}\pi h^2(3R - h)\cdot\rho \tag{4-3}$$

Where ρ is the steel ball density.

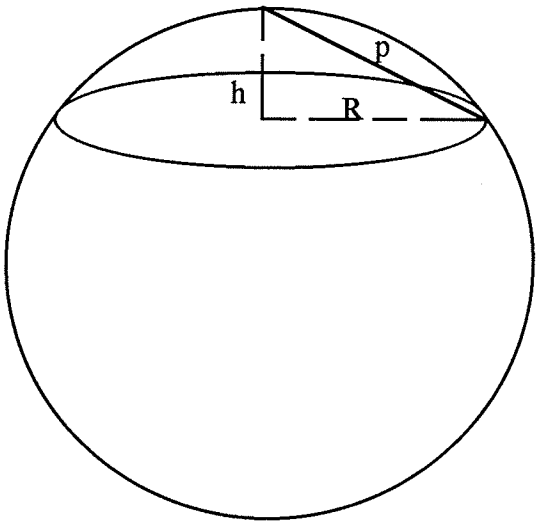

Fig 4.35 Worn segment on a ball slider

The weight loss from the worn surfaces of steel balls was thus determined as a function of sliding cycles. Representative weight loss versus sliding cycles curves for the sliders are plotted in fig 4.36.

Fig 4.36 shows that in general the weight loss increases with the sliding cycles. However, in the initial period (cycles<100,000), ball weight loss increase rapidly. After that, the wear process slows down, and the rate of weight loss gradually decrease with the wear cycles increased. For a given number of wear cycles, the lighter the load, the more the weight loss for balls occurred. The contact stress between the composite specimens and sliders is illustrated in Fig 4.37. The contact stress shows the opposite trend as compared with that of weight loss. At higher number of wear cycles, larger contact area is produced. This will in turn result in a less contact stress because of the constant load applied. At a given number of sliding cycles, a higher applied load causes higher contact stress. However, the differences in contact stresses at different applied loads become less as the number of wear cycles is increased.

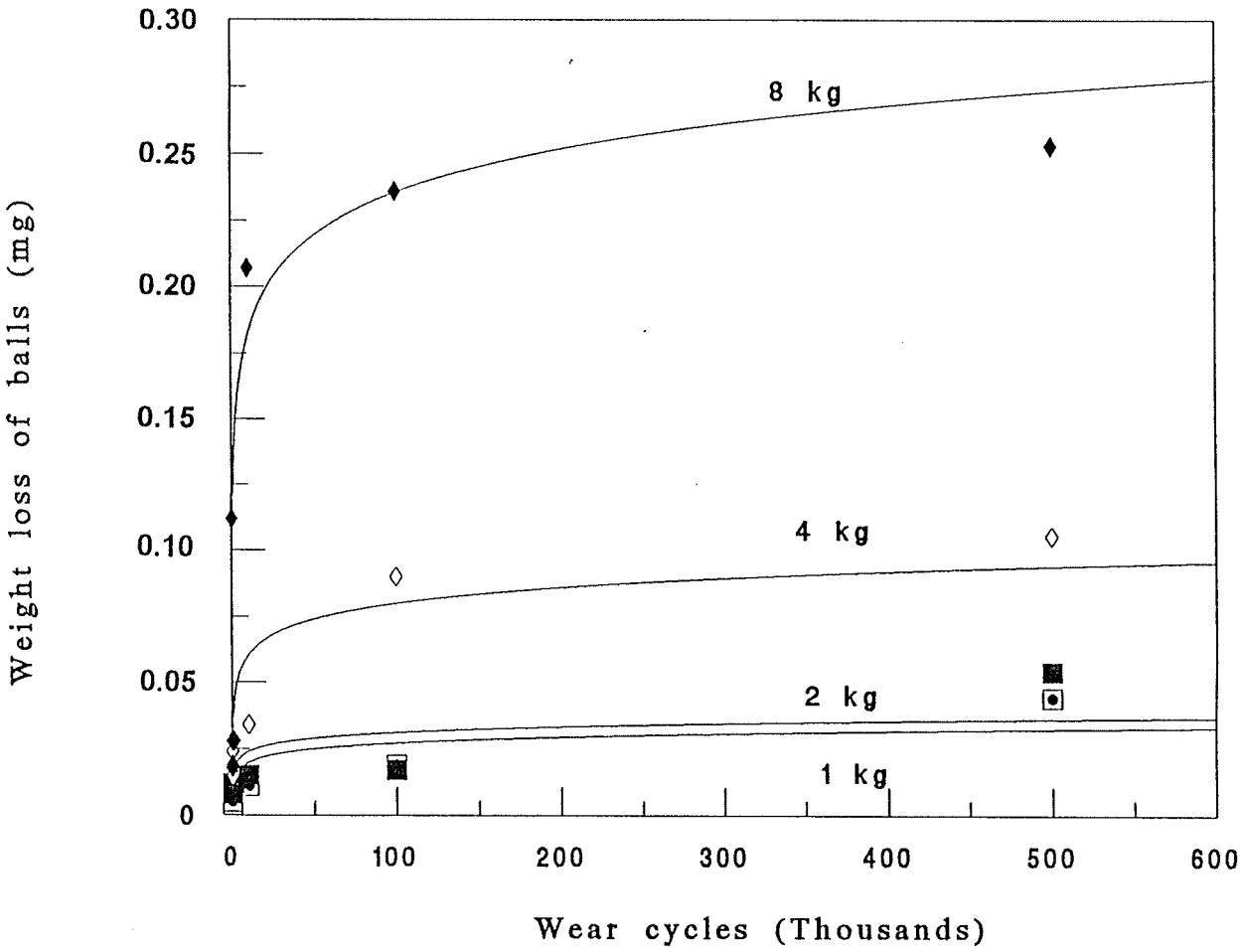

Fig 4.36 Weight loss of steel balls with the change of load and sliding cycles, lubricated test

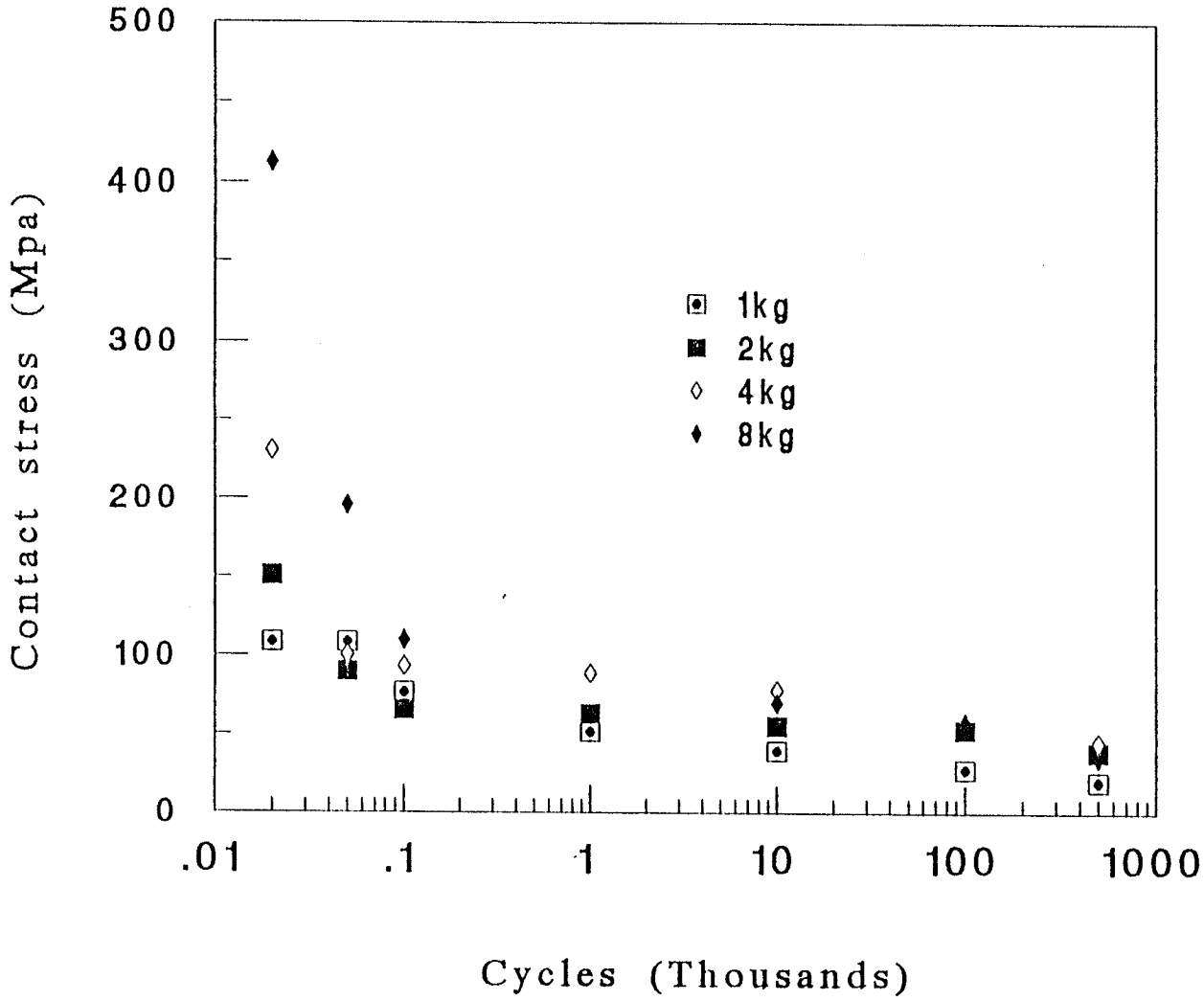

Fig 4.37 The change of contact stress with sliding cycles

4.3.2 The Effect of Contact Stress on Normalized Wear Rate

The data in Fig 4.36 and the data of worn surface areas on steel balls were used to construct normalized wear rate versus contact stress curves, which are defined as the weight loss per unit area per unit sliding distance ($mg/mm^2 \cdot mm$). Fig 4.38 shows the effect of contact stress on the normalized wear rate. It is clear that the contact stress plays a vital role in determining of the specific wear rate. The wear rate of the sliders does not increase monotonically through out the whole contact stress range. Three different regimes can be identified from Fig 4.38, and they are named P, Q and R respectively.

4.3.2.1 Wear regime P (low contact stress/high cycles of wear)

P zone is corresponding to the regime of a contact stress below 30MPa. In this regime, the normalized wear rate of the ball, the lowest among the three zones, is about 10^{-9}~10^{-8} ($mg/mm^2 \cdot mm$). The representative morphology of the worn surface on composite specimen is shown in Fig 4.39. At lower cycles, some of the SiC particles were pushed into the matrix and covered by a very thin layer of deformed matrix alloy (Fig 4.39 (a)). At a higher number of wear cycles, the relative area of deformed matrix became larger, and more SiC particles were covered by flowed matrix (EDS analysis in Fig 4.39 (c)). Very few iron particles were found on the worn surface of the composite for both low and high number of wear cycles. SiC particles were bonded well to the Al/Si alloy matrix and they were neither separated from the matrix nor pulled out from the base to serve as abrasive particles. The surface of a slider in this regime is shown in Fig 4.40. It has a quite flat surface. The wear process is mild in this regime for both the composite material and for the ball.

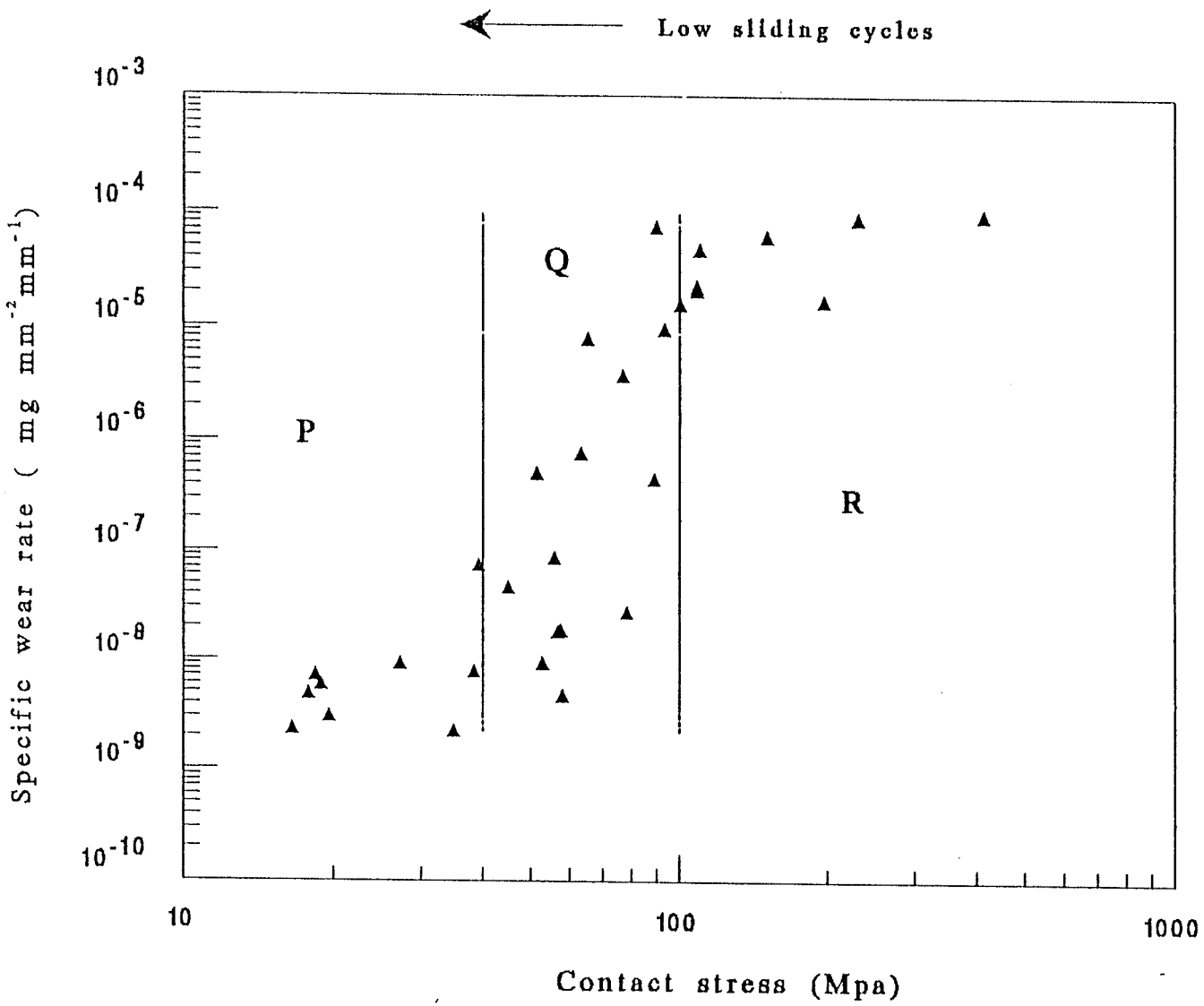

Fig 4.38 The effect of contact stress on the normalized wear rate of steel balls in lubricated wear tests

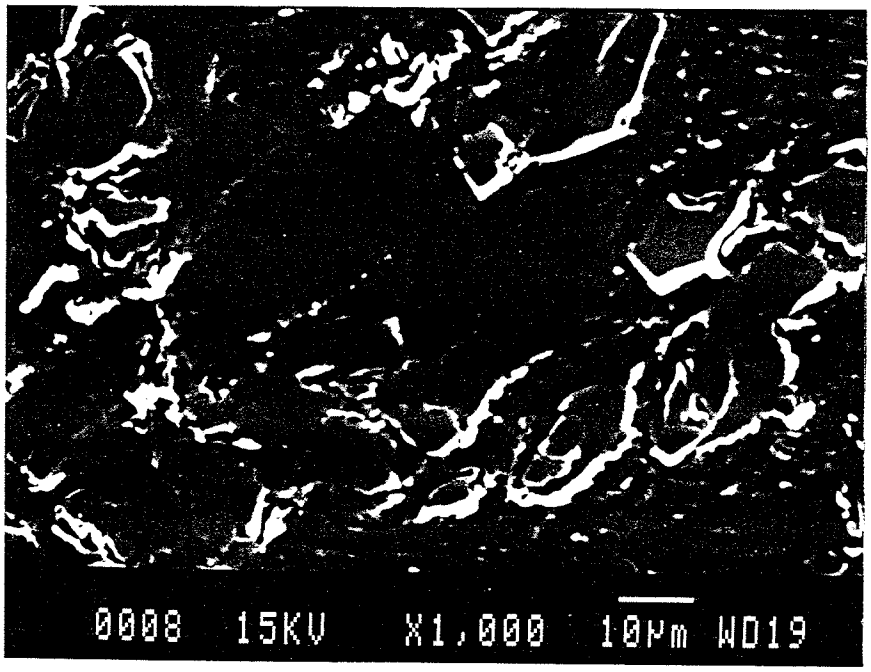

(a)

S.D

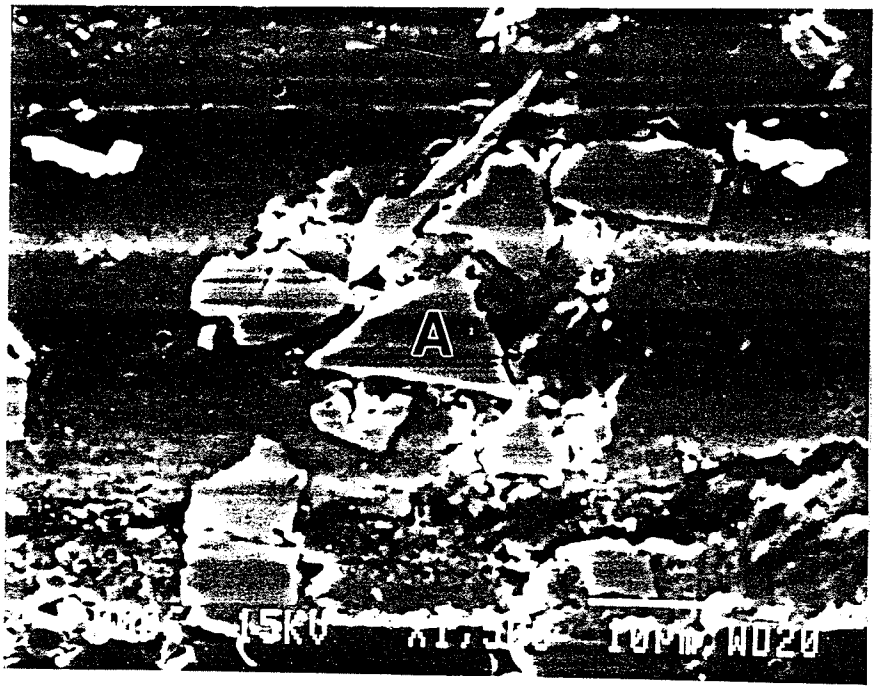

(b)

(See next page for figure caption)

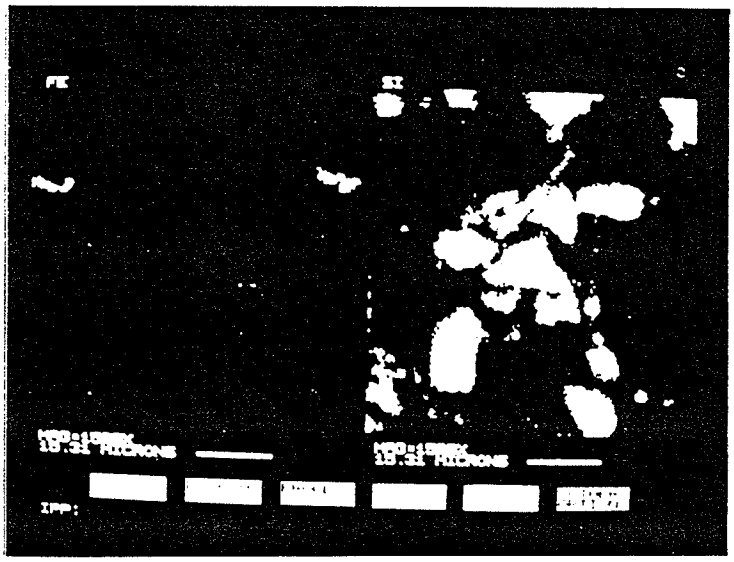

(c)

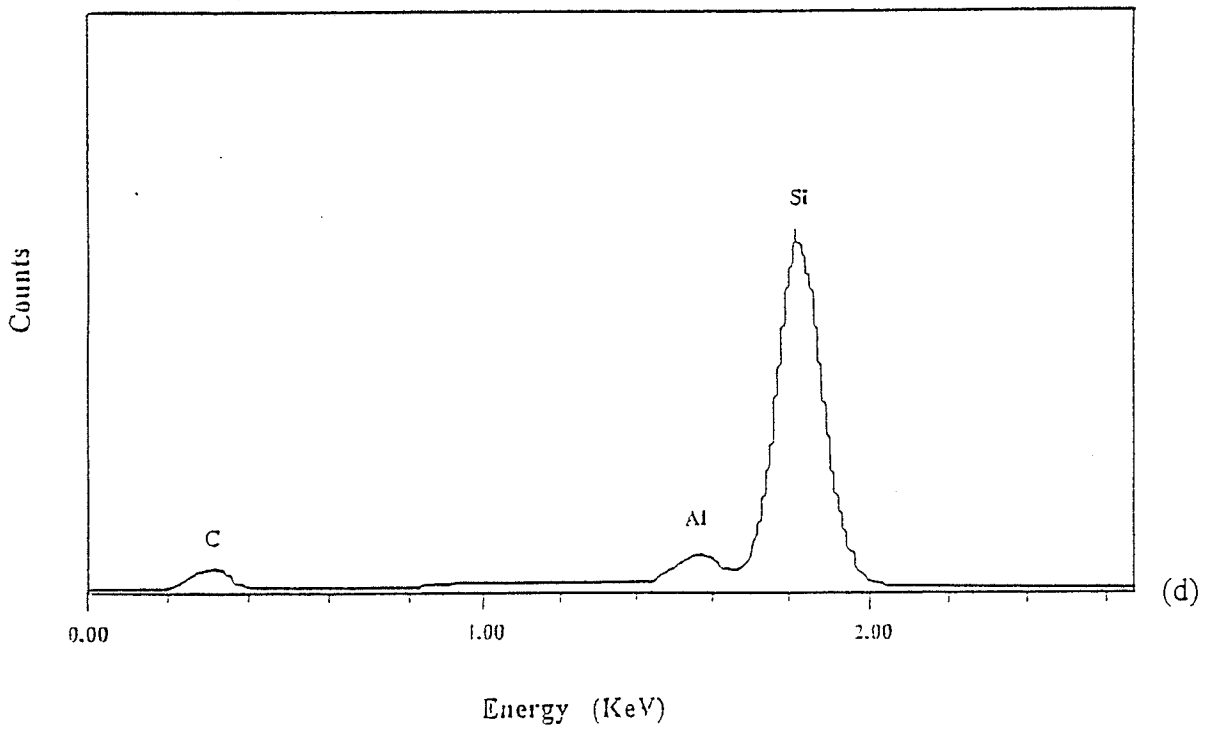

(d)

Fig 4.39 Surface of the composite after wear at low contact stress (Regime P)
(a) low sliding cycles (b) high sliding cycles
(c) EDS X-ray mapping of the surface area in (b)
(d) EDS spot analysis of marked A in (b)

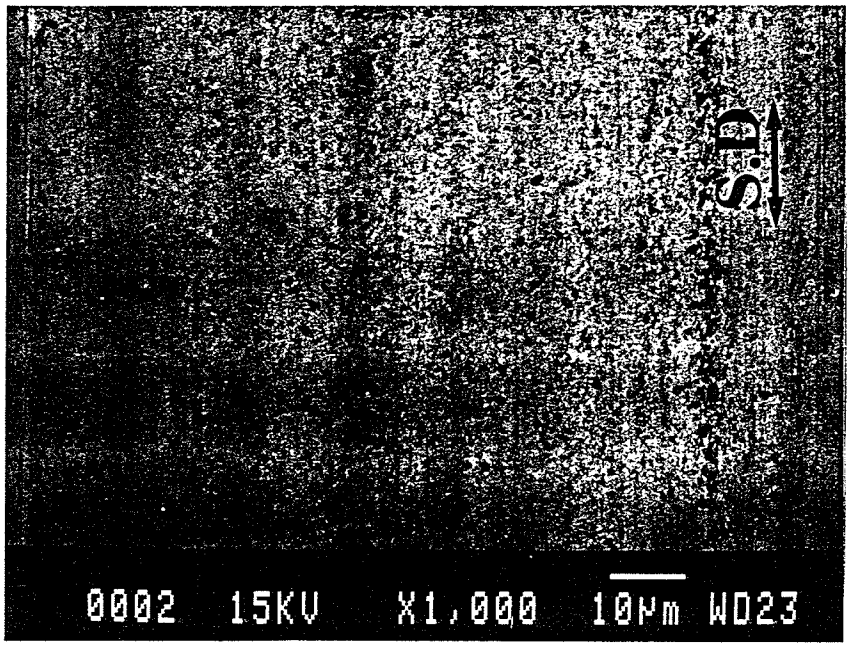

Fig 4.40 Surface morphology of a steel ball in regime P

4.3.2.2 Wear regime R (high stress level/low cycles)

When the contact stress increases above 100MPa, the normalized wear rate for the steel balls becomes stable again. Its value is about 10^{-5}~10^{-4} ($mg/mm^2 \cdot mm$). As compared with low contact stress zone P, the normalized wear rate in regime R is observed to accelerate by 3-4 orders of magnitude. For the composite specimen, the typical wear surface appearance for this regimes is shown in Fig 4.41. At low number of sliding cycles (Fig 4.41 (a)), even though plastic flow of the matrix took place as that in regime I of low contact stress, it failed to cover most of the SiC particles, and severe abrasive wear existed at the same time. Some SiC particles were fractured and pulled out from the matrix (marked A in Fig 4.41 (a)). Others were disbonded from the matrix and acted as abrasives to cause micro-cutting of the slider. A number of iron chips were present on the worn surface. At high number of sliding cycles, more abrasive wear or

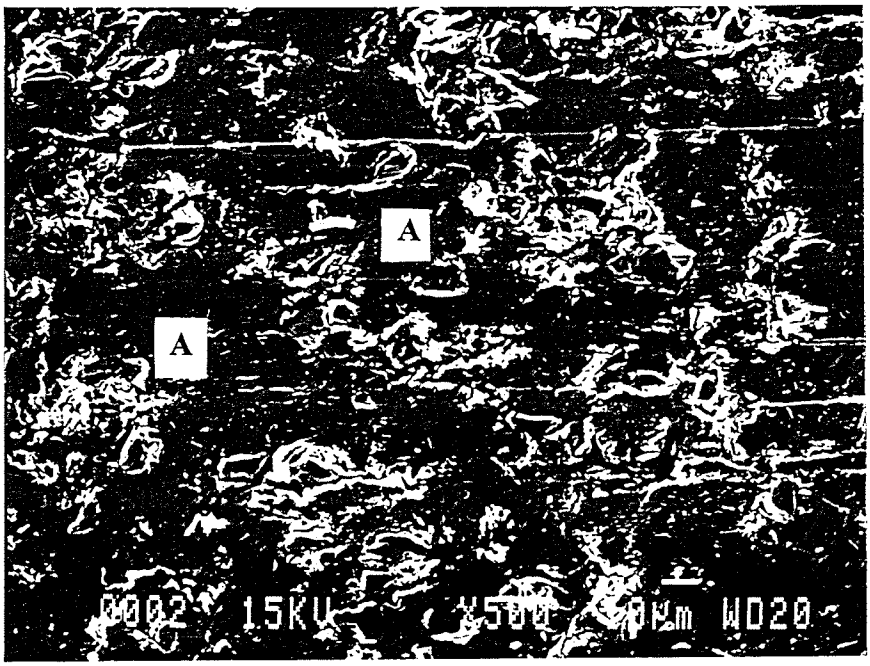

(a)

S.D

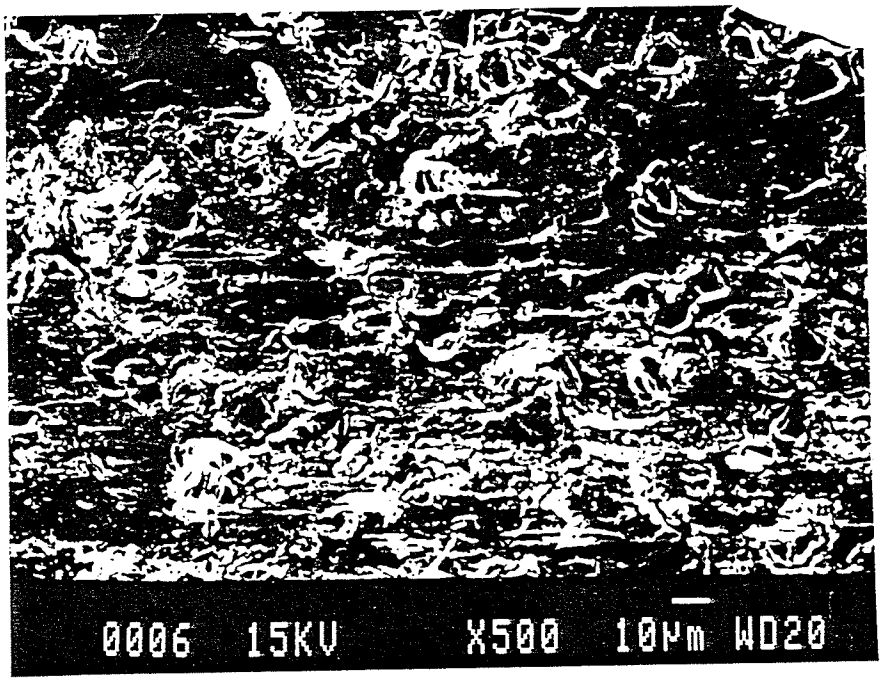

(b)

(See next page for figure caption)

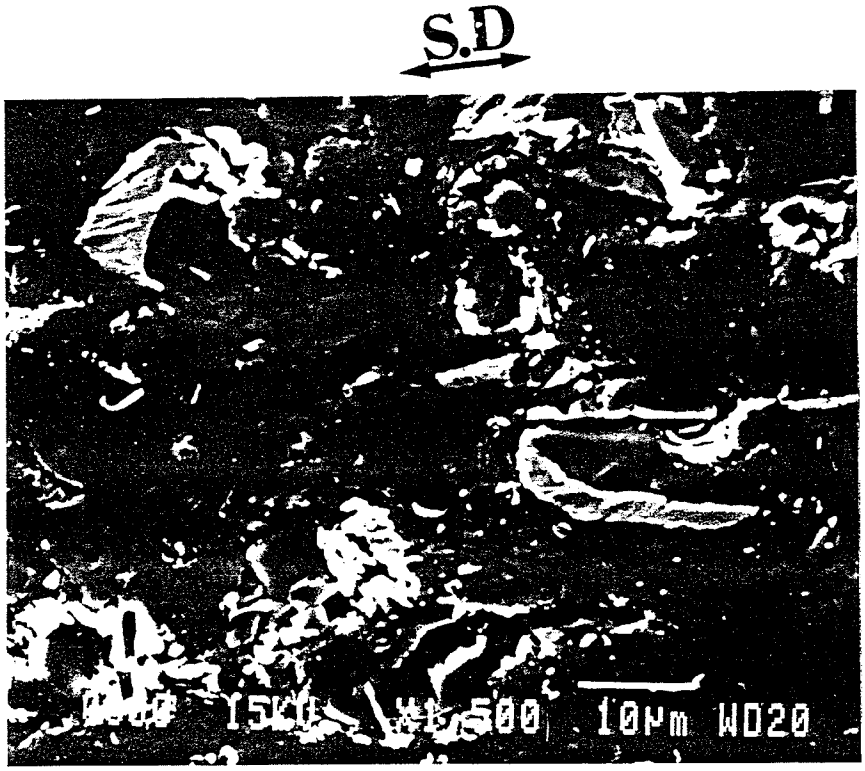

(c)

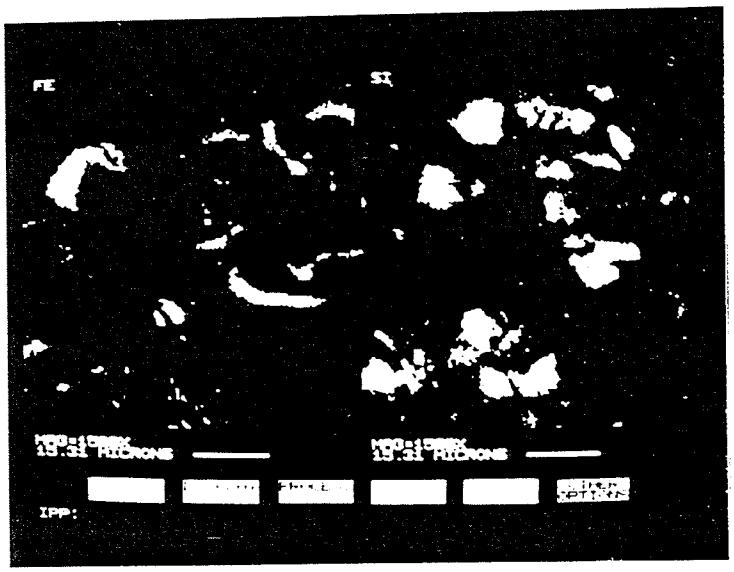

(d)

Fig 4.41 Surface of the composite after lubricated sliding wear at high contact stresses (Regime R)
(a) Initial wear (b) Steady-state wear
(c) Iron chips at steady state wear
(d) X-ray mapping of Si and Fe for (c)

scouring occurred, and more accumulation of cut iron chips was formed occurred. Fig 4.41 (c) and (d) clearly show the fracture of SiC particles and their separation form the matrix. Residual iron chips can also be seen at the tips of "micro-cutters". The surface of a worn ball is shown in Fig 4.42. It is characterized by severe microgrooving. So in this regime, material loss is severe for both the composite and the sliders.

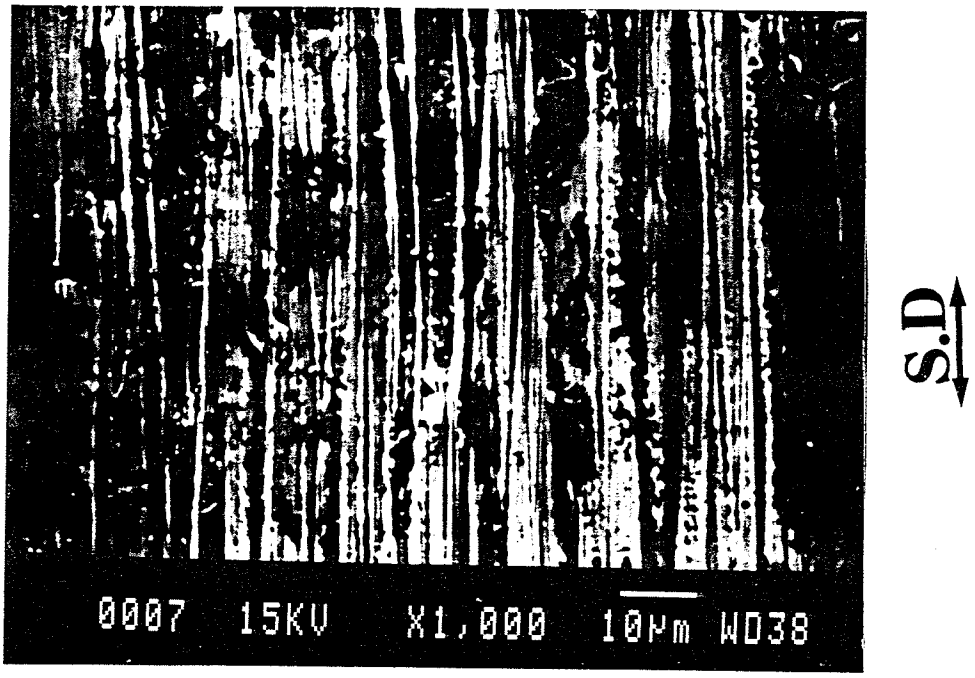

Fig 4.42 Surface morphology of a steel ball in regime R

4.3.2.3 Wear regime Q

In the intermediate zone Q, the contact stress is in between 30MPa to 100MPa. The data of the specific wear rate for the sliders is quite scattered and in between 10^{-9}~10^{-4} ($mg/mm^2 \cdot mm$). The trend appears to be a steady increase in the wear rate with an increase in the contact stress. It is a transition zone from mild abrasive wear to sever wear. Observations made on surface morphologies of these worn tracks on both steel balls and the composite specimens indicated that the wear mechanism for this regime was featured by a mixture of regime P and R.

4.3.3 The Influence of Contact Stress on Wear Mechanism

4.3.3.1 Wear Mechanism in Regime P (high stress level/low cycle)

The lower wear rate in regime P can be attributed to the formation of a special layer as a result of tribochemical reaction between the surface material of the composite and the lubricant (Fig 4.43). The development of this special layer involved a slight plastic deformation of aluminum alloy in the composite and its reaction with the lubricant. At the beginning of the wear process in this regime because of low local contact stresses which are lower than the fracture strength of SiC particles and the interfacial bonding strength between SiC particles and aluminum matrix, SiC particles can maintain their structural integrity and act as effective stress-bearing elements. Thus, the slider would ride on SiC particles rather than break them or pull them out. With the increasing number of sliding cycles, the parts of SiC protrusions get worn out, and a direct contact between the aluminum matrix and the slider occurs at a few locations. Plastic deformation of the aluminum matrix starts occurring. However, this plastic deformation is limited to a very low level, since most of the load is transferred onto SiC particles. Although the existence of this thin layer was confirmed by EDS analysis (Fig 4.39), its structure, chemical composition and the mechanism for its formation are yet to be understood.

Almost no material loss was observed for the composite specimen. For the ball sliders, most of the abrasive grooves on the counterface and the corresponding weight loss might have been produced during the initial wear against the protruded SiC particles. Microcutting is the dominant mechanism responsible for the weight loss in the sliders. When the special surface layer is established, most of SiC particles are smeared by this layer and wear rate is effectively reduced.

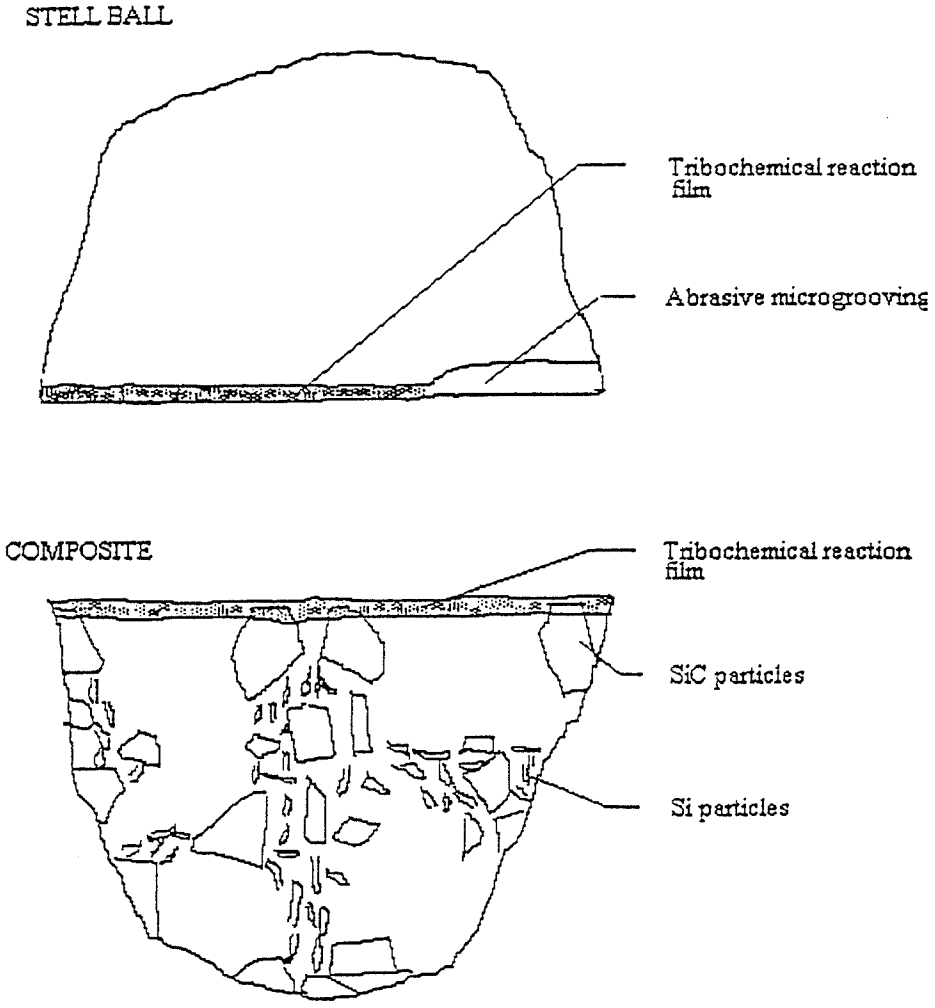

Fig 4.43 Schematic diagram of wear regime P for lubricated wear tests

As shown in Fig 4.39, an examination of the slider surfaces reveal no transfer of composite material to the counterface. That can be due to the effect of lubricant which reduces the friction coefficient and consequently presents adhesion. Further more, the existence of a lubricant between the tribosurfaces can reduce the local contact stress on asperities by distributing the normal force more uniformly along the contact surface.

4.3.3.2 Wear Mechanism in Regime R

Above a certain contact stress, which is roughly 100MPa, the wear rate increases to 10^{-5}~10^{-4}mg·mm^{-2}·m^{-1}, which is about 4 orders more than that in the mild wear regime I. The wear mechanism is schematically shown in Fig 4.44. In this regime, the local stresses generated beneath the ball are greater than the decohesion stress of the interface between SiC particles and aluminum matrix. Most SiC particles are disbonded, and some of them are fractured and pull out to act as abrasives (Fig 4.41). These abrasives cause galling on the matrix, and further decohesion and fracture of SiC particle occurs. On the other hand, plastic deformation of aluminum matrix also takes place. This process tends to cover and smear SiC particles and form a low friction coefficient tribochemical layer. The final surface topography depends upon the competition between these two processes. In this regime, because of the high contact stress, ploughing and scouring is prevalent, it is difficult for the tribochemical layer to form on most parts of the wear surface, resulting in severe wear of the composite. Thus, ploughing is the dominate mechanism for the material loss of the composite.

Since most of the wear surface is not covered by the tribochemical layer, the counterface on the slider is exposed directly to the loose and fractured SiC particles in the composite during sliding wear process. These SiC particles serve as micro-cutters and lead to a wear of the steel balls. Consequently, a lot of steel chips are left on the wear surface of the composite. Unlike low contact stress regime P, SiC decohesion, fracture and pulling out occur through out this wear process. Therefore, micro cutting is the major mechanism

causing material removal from the steel balls. In addition to microcutting, three-body abrasive wear is another wear mechanism present. It is induced by the movement of the fractured SiC particles which are pulled out of the composite.

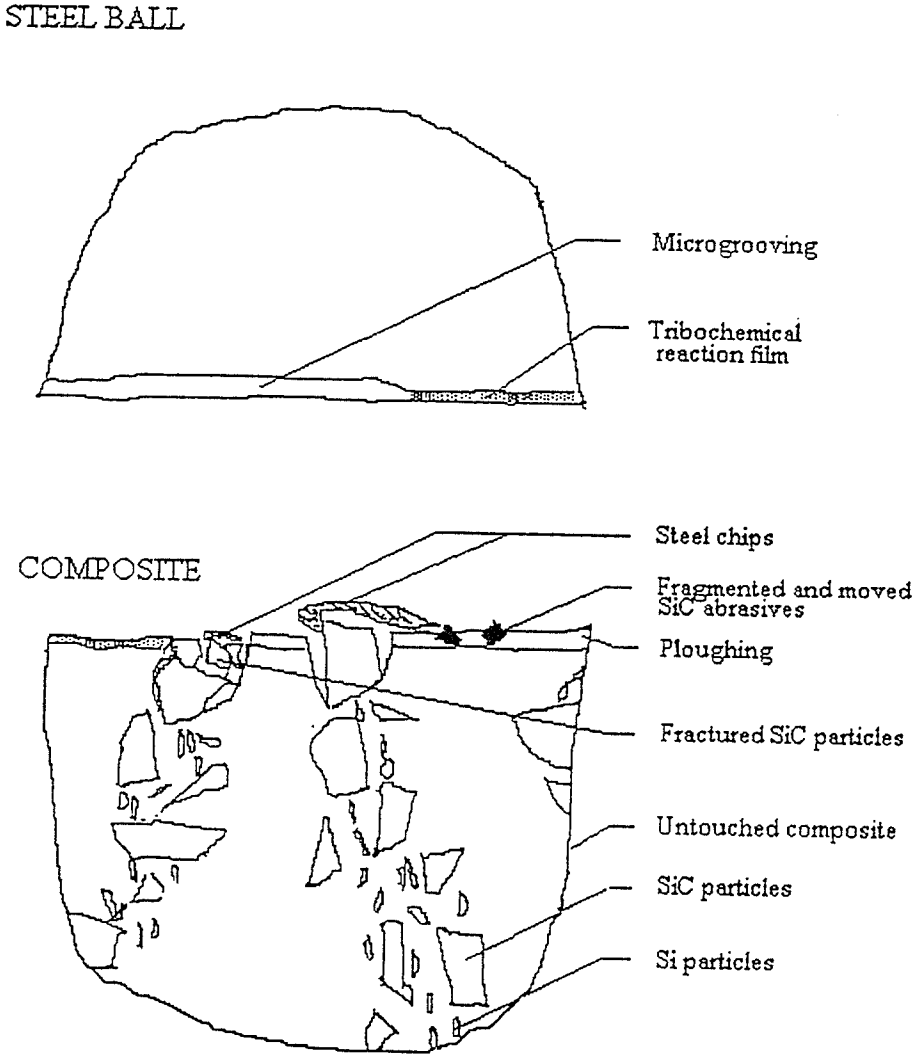

Fig 4.44 Schematic diagram in regime R for lubricated wear tests

4.4 Comparison of Dry Wear And Lubricated Wear

4.4.1 Weight loss

The weight losses for lubricated and unlubricated sliding wear in both the composite specimens and the balls are shown in Table 4.2. It is evident that the application of a lubricant has greatly reduced the weight loss for this wear couple. For instance, under a load of 9.8N at 10,000 cycles, the weight loss of the slider in lubricated wear is only 0.011mg. Compared to 0.9 mg in unlubricated wear. The former is about two orders of magnitude smaller than the latter. Unfortunately, the weight loss of the composite material in lubricated test could hardly be measured or even calculated. After sliding half a million cycles under a load of 9.8N, most of the original polished surface did not contact with the slider. This means that the wear track depth did not exceed the protruded height of the SiC particles on the polished surface. Actually, almost no wear track could be observed either by the naked eye or by optical microscope at this wear condition. Only by using the SEM the small plastic deformation of the matrix could be seen. Therefore, it is reasonable to suggest that the weight loss of the composite is less than the weight of the SiC particle that has been worn away. Based on this assumption, the weight loss of the composite should be no more than 0.13mg after the wear of half million cycles under the load of 9.8N, which is even smaller than the weight loss of the composite occurring at 3000 cycles in dry condition. After sliding half million cycles under a load of 78.4N in lubricated condition, the slider weight loss is comparable to that created at 3000 sliding cycles under a load of 9.8N in an unlubricated wear test. Therefore, the life expectancy for both of the composite and the slider can be prolonged by more than thousands times with the introduction of a lubricant.

Table 4.2 Comparison of dry and lubricated sliding wear in weight loss (mg)

sliding cycles (×1000)			1	3	5	10	20	50	100	500
Dry	load 9.8N	MMC		0.5	0.9	2.7	6.1	19.3	-	-
		ball		0.3	0.5	0.9	1.7	7.5	-	-
Lubricated	load 9.8N	MMC								<<0.13
		ball	0.005	-	-	0.011	-	-	0.019	0.044
	load 78.4N	ball	0.0112	-	-	0.207	-	-	0.236	0.375

4.4.2 Normalized Wear Rate

For the brevity of description, both of the wear rates of lubricated wear and unlubricated wear are plotted against contact stress in Fig 4.45. Considering the low contact stress range, which is the low wear rate regime P for sliders in lubricated wear, the wear rate in lubricated wear is 2 to 3 orders magnitude smaller than that during the dry wear test. This means that the lubricant can effectively enhance wear resistance of the composite material and the steel bearing sliders. In the high contact stress range (30-100 MPa), severe wear - seizure took place for dry wear test. Although dry wear behavior of the composite in seizure regime was not studied systematically in the present research because of the limitation of the wear rig, its wear rate would be definitely much greater than that of lubricated wear. No seizure has been observed in lubricated wear even when contact stress was increased to 130 MPa. Therefore, the presence of lubricant can significantly improve wear resistance through two different effects (Fig 4.45):

(a) A reduction of the normalized wear rate by a magnitude of $\Delta\mu=10^{-2}$-10^{-3} ($mg/mm^2 \cdot mm$);

(b) An increase in the stress-carrying capacity by an amount of $\Delta\sigma \geq 20$ MPa.

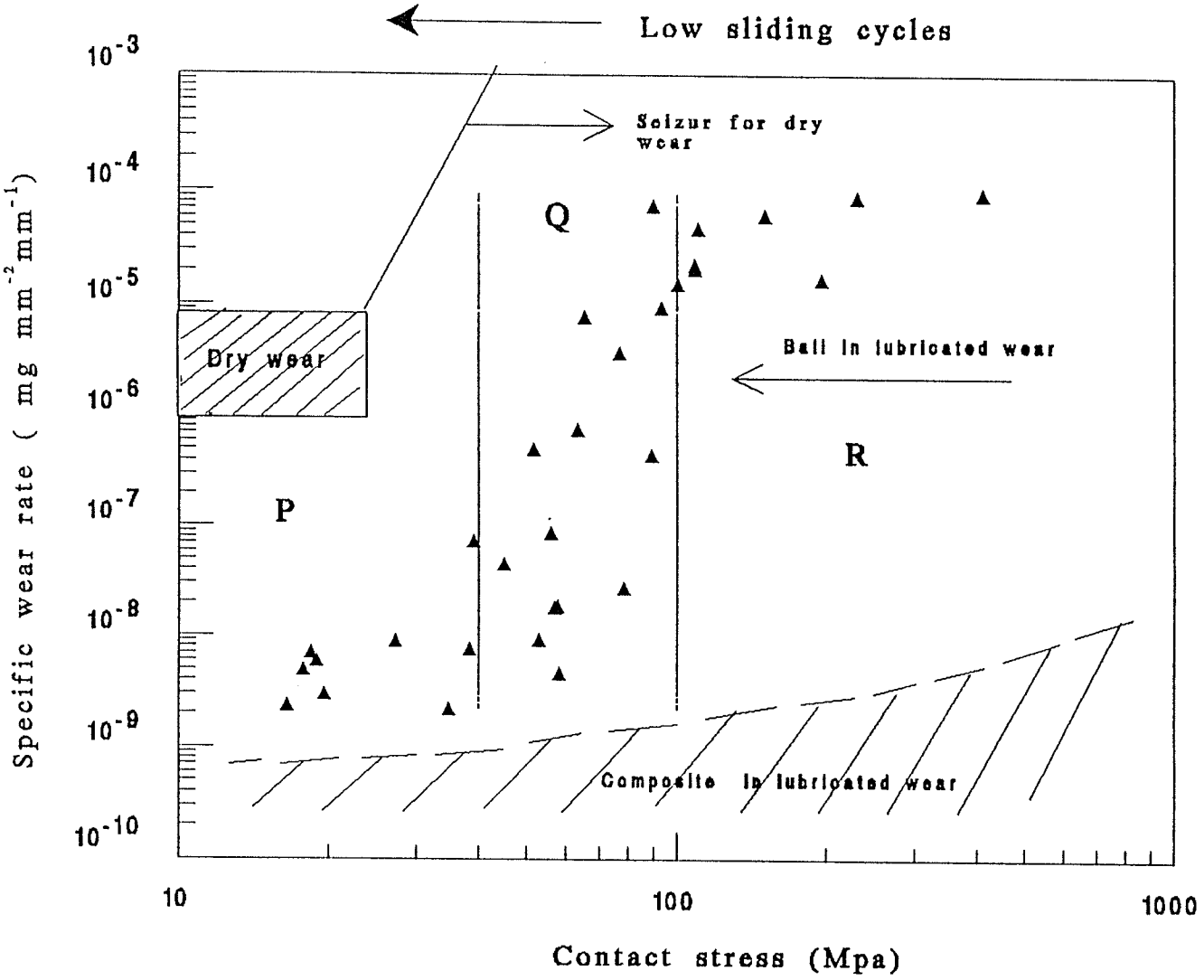

Fig 4.45 The effect of contact stress on the normalized wear rate of sliders for both dry and lubricated (reciprocal sliding wear) and the MMC

4.4.3 SiC Particle Behavior and Wear Mechanism

The wear behavior of the composite and counterface is summarized in Table 4.3. In unlubricated wear tests, SiC particles were fractured even at a very low contact stress (<1MPa) due to the impact of the sliders on to the protruding SiC particles and the grinding reaction between abrasive SiC particles and near-surface SiC particles in the composite. At high contact stress (>5MPa), SiC particles, in the form of surface mixed layer, are further fragmented. However, in lubricated sliding wear, because of the presence of lubricant, SiC particles are kept intact as contact stress is increased to 30-100 MPa, and this is the reason that make it possible for the SiC particles to bear more load and to result in lower wear rates. Consequently, the different behavior of SiC particles in dry and lubricated wear tests causes the composite having different wear mechanisms. During lubricated wear under a low stress, since SiC particles are not crushed or pulled out from the matrix, abrasive wear or microgrooving on a very small scale has occurred for the wear couple. On the contrary, during dry sliding wear, the fractured SiC particles serve as abrasives along the wear surface and cause abrasive grooving for both composite and steel sliders. Moreover, the formation for SML by the mechanical mixture of severely deformed matrix and fractured SiC particles bring about the delamination mechanism and relatively high wear rates. The influence of lubricant on SiC particle behavior and the wear mechanism of the composite can be generally rationalized by the Stribeck curve in Fig 2.6 [21].

For wear of the composite against steel sliders apart from two metal surfaces, there are SiC particles distributed in one of the metal surface (aluminum matrix). In this case, if the generalized Sommerfeld Number $\eta v/F_N$ is great enough [21] (At high sliding speed, high fluid viscosity or very low load), a thick lubricant film (h>>R) can be established (Fig 4.46). The existence of SiC particles will have no effect on wear process, since no direct physical contact between the SiC particles and the counterface occurs. morphology in low contact stress (regime P in Fig 4.38) indicates that this type of wear is

Table 4.3 Comprehensive summary of SiC behavior and wear mechanism in both lubricated and unlubricated wear

contact stress (MPa)			<1	1-5	5-13	13-30	30-100	>100
dry	SiC		fractured and serve as abrasives	fractured and serve as abrasives	form SML	----	----	----
	wear mechanism	composite	abrasive microgrooving	abrasive + plastic deformation	delamination of SML + plastic deformation	seizure	seizure	seizure
		ball	abrasive grooving					
lubricated	SiC		kept integrity and covered by a thin tribochemical reaction layer				transition	decohesion with matrix fractured and pulled out to act as abrasives
	wear mechanism	composite	very small amount of adhesive wear					abrasive scoring + boundary lubrication
		ball	small scale microcutting at beginning and adhesive wear for normal part				transition	server microcutting + abrading + boundary lubrication

obviously not possible in this regime, and it should belong to the mixed or boundary lubrication regime. As contact stress increases, the Sommerfeld Number becomes smaller, and lubricant film get "thinner" (Fig 4.46(b)). Then, the contact interaction between SiC particles and the counterface takes place. This is the turning point for the following wear mechanisms. The load can be written as the sum of that at asperity peaks (SiC particles) and that at the voids,:

$$W = A\,\alpha_w p^* + A(1-\alpha_w)p_{hydro}$$
$$= A[\alpha_w p^* + (1-\alpha_w)p_{hydro}] \qquad (4\text{-}4)$$

Where α_w is the area fraction of SiC particles in the composite, A is the total area of the contact surface, p^* is the pressure (contact stress) on SiC particles and p_{hydro} is the hydrodynamic pressure generated between SiC particles. The friction force should be the sum of the solid friction at SiC particle and the liquid friction in the voids:

$$F = A\,\alpha_w p^* f_{solid} + A(1-\alpha_w) f_{liquid} p_{hydro} \qquad (4\text{-}5)$$

Where f_{solid} and f_{liquid} are the friction coefficient for SiC and the lubricant respectively. Therefore, the friction stress on particle should be:

$$\sigma_f = p^* f_{solid} \qquad (4\text{-}6)$$

It is noted that P_{hydro} is only slightly less than P^*, so it is reasonable to define the average pressure P such that $P^*>P>P_{hydro}$, then eqn.(4-6) can be written as,

$$\sigma_f = p f_{solid} \qquad (4\text{-}7)$$

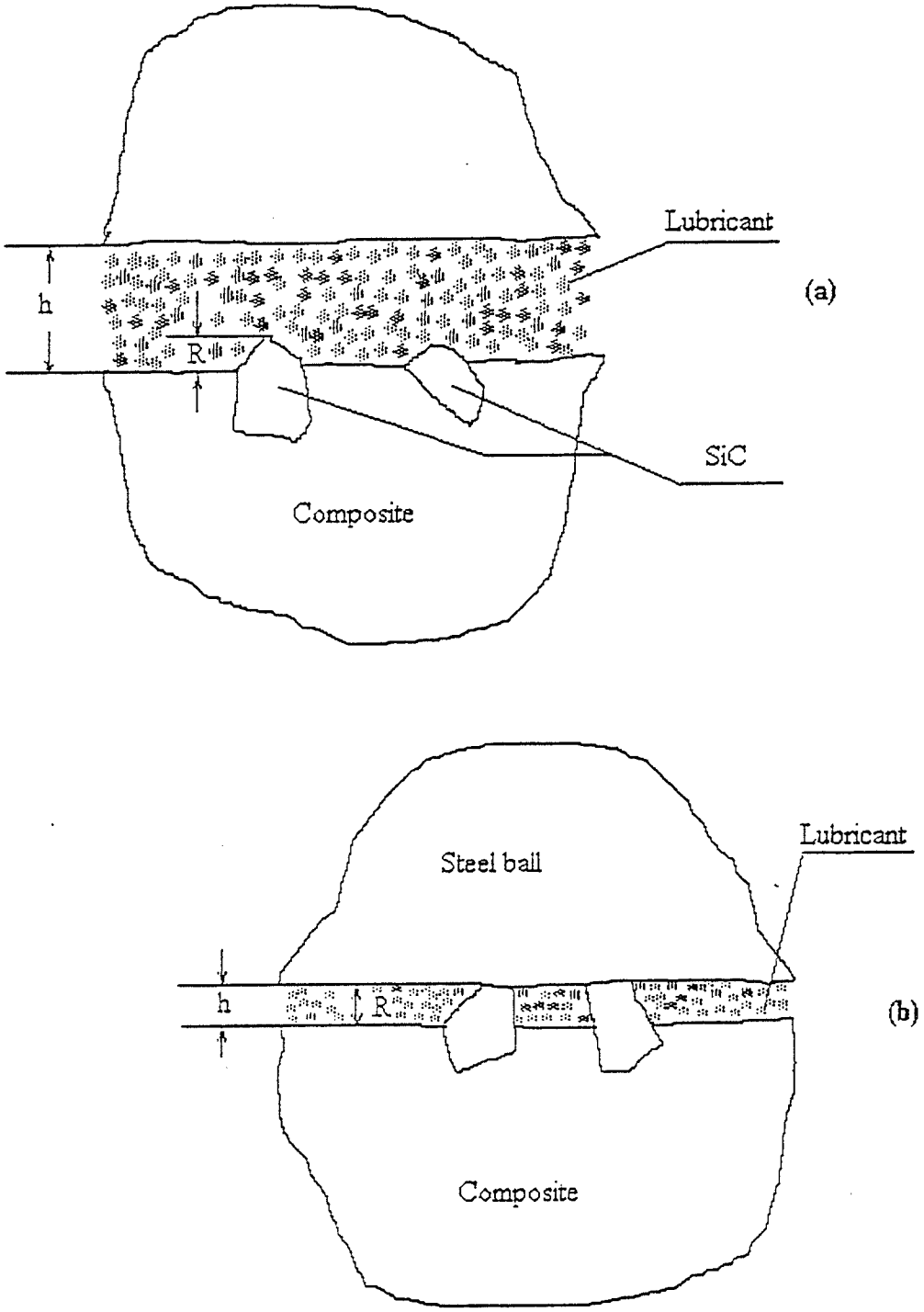

Fig 4.46 Schematic diagram for lubrication wear

(a) Hydrodynamic lubrication

(b) Boundary lubrication with SiC asperities

If P is great enough such that $\sigma_f > \sigma_{disb}$ (decohesion stress between the SiC particles and the matrix), SiC particles would be pulled out of the matrix and would be fractured. These would act as abrasives causing more wear than that in the boundary lubrication. This wear process (R regime in Fig 4.38) involves a mixture of abrasive grooving and boundary lubrication for the composite, and abrading, microcutting and boundary lubrication for the slider. As contact stress P increases, the fraction $A(1-\alpha_w)$ will be reduced, the wear process will then be accelerated.

If $\sigma_f < \sigma_{disb}$, the protruding part of SiC particles will be worn away gradually. After "wear in " period, the entire wear surface will be covered by a thin tribochemical reaction film, and a boundary lubrication state can be achieved (P regime in Fig 4.38). Therefore, it might be reasonable to add region IV to Stribeck curve (Fig 4.47) for the description of the composite wear behavior in lubricant , which is corresponding to the server wear regime R in Fig 4.38. It is the result of the decohesion and fragmentation of SiC particles in the composite and might be considered as the upper limit of the wear life for the composite against steel sliders.

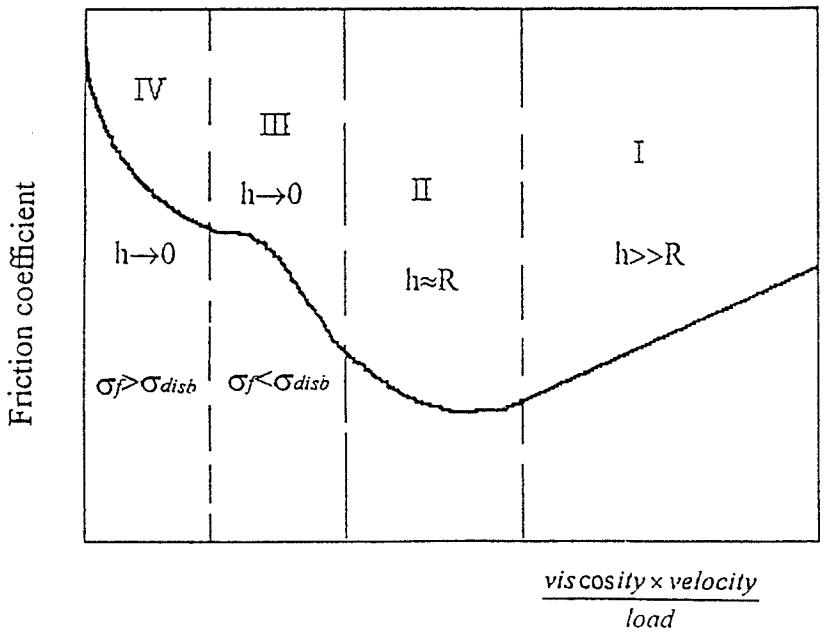

Fig 4.47 Modified Stribeck curve for friction of composite material

It should be pointed out that the effect of boundary lubrication on wear of the composite against the composite steel balls is beyond the scope of this research. In order to better understand the wear mechanism of this wearing couple, and the effects of sliding speed, lubricant temperature and the microstructure of the tribochemical reaction film, more research work needs to be done.

CHAPTER 5 CONCLUSIONS

Through the systematic study of the wear behavior of SiC particulate reinforced A356 aluminum composite in both dry and lubricated reciprocal sliding conditions, the following conclusions can be drawn:

1. In both dry and lubricated reciprocal sliding wear, the contact stress between the composite and the slider played a vital role in deciding the behavior of SiC particles and the wear mechanism of the composite and its counterface.

2. Two wear regimes were revealed for this composite in dry reciprocal sliding wear according to the change of normalized wear rate and wear surface morphology. At low contact stresses (<3MPa), abrasive microgrooving was the dominant mechanism for the material loss of both the composite and its counterface. Near surface SiC particles in the composite were fractured and acted as abrasives causing three body abrasive wear. The small granular debris (1-3μm) came from the intergrinding action of these SiC particles. With an increase in the contact stress, the normalized wear rate of the composite increased linearly. However, the normalized wear rate decreased at the beginning (1-3MPa) and then increased linearly for the slider. The reason for this decrease was the occurrence of a layer of deformed aluminum matrix which could prevent the further fragmentation of the SiC particles in the matrix. At high contact stresses (>5MPa), a surface mixed layer (SML), which was composed of fragmented SiC particles and severely deformed aluminum matrix, was formed. Consequently, in this regime, material removal for the composite was dominated by the delamination of this SML, and the normalized wear rate of the composite and the steel balls continuously increased with the contact stress.

3. In lubricated reciprocal sliding wear of the SiC particle A356 aluminum alloy, three regimes were present depending on the contact stress. Mild wear regime corresponded to low contact stresses (<30MPa). In this regime, SiC particles were kept

thus integrity and were covered by a thin tribochemical reaction layer. The weight loss in the composite resulted from the wearing of the portion of SiC particles that protruded out of the matrix after polishing. The weight loss for the ball counterface came from initial microcutting of its surface by the protruding SiC particles. Boundary lubrication dominated the normal wear process and the normalized wear rates for the balls were in the range of 10^{-9}-10^{-8}mg·mm^{-2}·mm^{-1}. As contact stress increased above 100MPa, a second regime, the server wear regime, occurred. The normalized wear rate for the counterface increased dramatically to 10^{-5}-10^{-4}mg·mm^{-2}·mm^{-1}. SiC particles were either fractured or pulled out from the matrix to act as abrasives. Decohesion took place between SiC particles and the matrix. Abrasive scouring and micro-cutting were the main mechanisms for the wear of the composite and the sliders respectively.

4. As compared with dry sliding wear, the wear resistance of this wear couple was dramatically improved through the application of lubricant; 1) reducing the normalized wear rate of the slider by the magnitude of 10^{-2}-10^{-3} (mg·mm^{-2}·mm^{-1}), and 2) increasing the contact stress bearing capacity of the ball by 20MPa.

5. In dry sliding wear, the surface morphology at the track ends was found to change dramatically with the increase in wear cycles. The accumulation of significant amounts of wear debris was a major feature for the dry sliding wear at high number of wear cycles (10,000-50,000).

CHAPTER 6 RECOMMENDATIONS FOR FURTHER STUDY

Based on the present work in this thesis, some suggestions for further study can be made.

The surface mixed layer (SML), which occurred during the wear of SiC particulate reinforced A356 aluminum composite, is very important for the reciprocal wear behavior of this composite at high contact stress. Even though it is clear that the SML is a mixture of severely deformed aluminum alloy and fractured SiC particles, the microstructure of it is far more understood. It would be interesting to identify the crystal structural changes if the SiC particles and the matrix in SML and to study the changes in dislocation distribution and dislocation densities. This may lead to a more fully understanding the wear mechanism of the SML - subsurface delamination.

In lubricated wear condition, the upper limit of contact stress for the application of this composite should be 30MPa below which SiC particle can keep integrity and boundary lubrication can exist. What is not really known is the nature of the tribological reaction film. Moreover, many factors can affect the formation of the tribochemical reaction film apart from contact stress, such as temperature, sliding speed, lubrication rate and type of the lubricant. In order to study the influences of these factors on the tribochemical film quantitatively, a wear testing setup with constant contact area is preferred.

REFERENCES

1. "Glossary of Terms and Definitions in the Field of Friction, Wear and Lubrication (Tribology)"., Research Group on Wear of Engineering Materials, Organization for Economic Cooperation and Development (OECO), Paris, (1969).
2. A. R. Lansdown and A. L. Price., "Materials to Resist Wear"., (1986).
3. D. A. Rigney, Scripta Met., No. 5, 24 (1990) 799.
4. J. Halling., "Introduction to Tribology"., London and Winchester, (1976).
5. D. A. Regney and W. A. Glaeser., American Society for Metals, Metals Park, Ohio 44073, (1976).
6. "Standard Terminology Relating to Wear and Erosion", Annual Book of Standards, ASTM, 03.02 (1987) 243-250.
7. T. S. Eyre., Tribology International., Oct. 9 (1976).
8. K. C. Ludema., ASM Handbook, "Friction, Lubrication and Wear Technology"., (1992).
9. S. C. Lim, M. F. Ashby., Acta Metall., 35 (1987) 1-24.
10. S. C. Lim, M. F. Ashby, and J. H. Bruton., Wear., 35 (1987) 1343-1348.
11. E. Rabinowicz., Wear, 25 (1973) 357.
12. W. R. D. Wilson., Tans. ASME, J. Lub. Tech., 22 (1976) 98.
13. B. Kehl, E. Siebel, Archs Eisenhutt., 9 (1936) 563.
14. K. Nakajima, Y. Mizutani., Wear., 13 (1969) 283.
15. J. F. Archard., J. appl. Phys., 24 (1953) 981.
16. G. Yoshimoto, T. Tsukizoe., Wear., 1 (1957/58) 472.
17. J. Halling, Trans., ASME., J. Lub. Tech., 105 (1983) 212.
18. E. F. Finkin., Wear., 47 (1978) 107.

19. S. Hogmark, S. Jacobson, etal., "Surface Damage", ASM Handbook, "Friction, Lubrication and Wear Technology"., (1992)

20. K. H. Z. Gahr., Tribology Series, 10, (1987).

21. Horst Czichos., "Tribology"., Elsevier Scientific Publishing Company, Oxford, New York, (1978).

22. ASTM Standard G99-90.

23. ASTM Standard G83-89.

24. ASTM Standard G77-83.

25. G. C. Barber, K. C., Luderma, Wear., 118, (1987), 57.

26. C. M. Li, K. N. Tandon., J. Mater & Sci., 29 (1994) 1462-1497.

27. H. Czichos, S. Becker, and J. Lexow, Wear., 135 (1989), 171.

28. H. Czichos., Wear., 41 (1977) 45-55.

29. "Standard Practice for Conducting an Inter-laboratory Study to Determine the Precision of a Test Method"., E691, Annual Book of ASTM Standards, ASTM. (1990).

30. "Precision of Test Methods - Determination of Repeatability and Reproducibility for a Standard Test Method by Inter-laboratory Tests"., Standard 5725, International Organization for Standardization, Geneva, (1986).

31. L. M. Hutchings., Mater. Sci & Eng., A184 (1994) 185-195.

32. P. K. Rohatgi, Y. Liu, and R. Asthana., ASM International., P. K. Rohatgi, P. Blau, and C. Yust, Ed., (1990) 69.

33. F. M. Hosking, F. Folgar Portillo, and R. Wunderlin., J. Mater. Sci., 17 (1982) 477-498.

34. M. Kobashi, T. Choh., J. Mater. Sci., 28 (1993) 684-690.

35. S. J. Harris Mater. Sci. and Tech., 4 (1988) 231-239.

36. B. Zantout, A. A. Das, and J. R. Franklin, The Metallurgy of Light Alloys Spring Residential Conf., The Inst. of Metallurgists, 20 (1983).

37. I. Sngishita, J. Jap. Foundrymen's Soc., 57 (1985) 2.

38. R. T. Peper, and R. A. Penty., J. Composite Mater., 8 (1974) 29.

39. R. Mehrabian, R. G. Riek, and M. C. Flemings, Met. Trans., 5 (1974) 1899-1905.

40. M. Hasegawa, K. Takeshita, Met. Trans., 9B (1978) 383-388.

41. A. Richard., U. K. Patent 2115014A, (1983).

42. J. V. Wood, J. L. F. Kellie, and P. Davies., Trans. Inst. Metall. A101 (1992) 187.

43. S. Ray., J. Mater. & Sci., 28 (1993) 5397-5413.

44. Adv. Mater. Proc., June, (1993) 20.

45 "Composite Material Handbook". EASIAP. Institute for Technological Development, University of Manitoba, (1993)

46. S. V. Pradad, T. H. Kosel., Proc. of Int. Conf. on Wear of Materials, Apr. 14-18, 1985, Vancouver, K. C. Ludema, ed., ASME, 59-66.

47. S. V. Prasad, P. K. Rohatgi, and T. H. Kosel., Mater. Sci. Eng., 80 (1986) 213-220.

48. K. J. Bhansali, R. Mehrabian., J. Metals., 32 (1982).

49. P. K. Rohatgi, Y. Liu, M. Yin, and T. L. Barr., Mater. Sci. Eng., A213 (1990) 213.

50. S. V. Prasad, P. K. Rohatgi., Proc. Int. Conf. on Aluminum (INCAL-85), N. Delhi, Nov.- Dec, (1985) 561-567.

51 P K. Rohatgi, Y. Liu, and S. Ray., "Friction and wear of metal matrix composites". ASM Handbook, Friction, lubrication and technology, (1992) 801-810.

52. S. V. Parasad, P. K. Rohatgi., J. Metals., November, (1987) 22-26.

53. A. T. Alpas, J. D. Embury., Wear of Materials., ASME, (1991)

54. A. T. Alpas, J. D. Embury., Scrip. Metall., 24 (1990) 931-935

55. S. Bhattacharrya, F. C. Bock., Wear., 46 (1978) 1.

56. T. P. Murali, S. V. Prasad, M. K. Surappa and P. K. Rohatgi., Wear., 80 (1982) 149.

57. A. Sato, D. Mehrabian., Metall. Trans., 713B (1976), 443.

58. L. B. Johnson, D. K. Wilsdorf., Mater. Sci. Eng., 58 (1981) PL1.

59. J. D. Ayers, T. R. Tucker, and R. C. Bowers., Scr. Metall., 14 (1980) 549.

60. D. Nath, S. K. Biswas, and P. K. Rohatgi., Wear., 60, (1980) 61.

61 A. Somi Reddy, B. N. Bai, K. S. S. Murthy, and S. K Biswas., Wear., 171 (1994) 115-127

62. P. R. Gibson, A. J. Clegg, and A. A. DAS., Wear., 95 (1984), 193.

63. H. Tokisue, G. J. Abbaschian., Mater. Sci. Eng., 34 (1978) 75.

64. P. K. Rohatgi, S. Ray, and Y. Liu., Int. Mater. Rev., 37 (1992) 129.

65. P. K. Rohatgi, Y. Liu, M. Yn, and T. L. Barr., Mater. Sci. Eng., A123 (1990), 213.

66. A. Sato, D. Mehrabian., Metall. Trans., 713B (1976) 443.

67. M. Suwa, K. Komuro, and K. Soeno., J. Jpn. Inst. Met., 40 (1976) 1074.

68. M. A. Martinez, A. Martin, and J. Llorca., Scripta Metallurgic et Materialia., 28 (1993) 207-212.

69. A. K. Jha, S. V. Prasad, and G. S. Upadhyaya., Wear., 133 (1989) 163.

70. A. T. Alpas, J. Zhang., Scripta. Metall., 26 (1992) 505-509.

71. E. Yuasa, T. Morooka, and F. Hayama., J. Jpn Inst. Met., 50 (1986) 1032.

72. S. Mohan, V. Agarwala, and S. Ray., Wear., 140, (1990), 83.

73. F. Rana, D. M. Stefanescu., "Friction Properties of Al-1.4 Pct Mg/SiC Particulate Metal-Matrix Composites". (1984).

74. J. Yng, D. D. L. Chung., Wear., 13 (1989) 53.

75. A. Wang, H. J. Rck., Mater. Sci. Eng., A147 (1991) 211-224.

76. B. N. Keshavaram, P. K. Rohatgi, R. Asthana, and K. G. Sathyanaragana., P. K. Rohatgi, P. Blau, and C. Yust. Ed., ASM International., (1990) 133.

77 J. L. Johnson, J. Schreurs., Wear., 78 (1982) 219.

78. B. P. Kirshnan, N. Raman, K. Narayanaswamy, and P. K. Rohatgi., Tribol. Int., (1983) 239.

79. P. K. Rohatgi, B. C. Pai., Wear., 59 (1980) 323.

80. J. Zhang, A. T. Alpas., Mater. Sci. Eng., A160 (1993) 25-35.

81. C. P. You, N. T. Donlan, and J. M. Boileau., "Tribology of Composite Materials"., P. K. Rohatgi, P. J. Blau, and C. S. Yust Ed., ASM International., (1990) 157.

82. K. Kuniya, H. Arakawa, and T. Namekawa., Trans. Jpn. Inst. Met., 128 (1987) 238.

83. L. Cao, Y. Wang, and C. K. Yao., Wear., 140 (1990), 273.

84. Z. Eliezer, V. D. Khanna, and M. F. Amateau., Wear., 51 (1978) 169.

85. Y. Tsuya., Jpn. Inst. Compos., 11 (1985) 127.

86. N. Saka, D. P. Karalekas., Wear of Materials., (1985) 7864.

87. S. Bhattacharrya, F. C. Bock., Wear., 135 (1989) 53.

88. J. Yang , D. D. L. Chung., Wear., 135 (1989) 53.

89. S. Usmani., MSc thesis (1992), Mechanical and Industrial Engineering Department, University of Manitoba.

90. D. R. Uhlmann, B. Chalmers, and K. A. Jackson., J. Appl. Phys., 35 (1964) 2986.

91. S. N. Omenyi, A. W. Neumann., J. Appl. Phy., 47 (1976) 3956.

92. A. T. Alpas, J. Zhang., Metall. Materials Trans. A., 25A (1994) 969-983.

93. E. Rabinowicz., "Compatibility criteria for metals in friction and lubrication in metal processing", F. F. Ling, R. L. Whitely, P. M. Kn, and M. B. Peterson, eds., ASME, New York, NY, (1966) 90-102.

94. K. C. Ludema., Wear., 100 (1984) 315-318.